**Title**
Testing a Proposed Driver of the End-Permian Biotic Crisis



**Author**
Benca, Jeffrey Paul

**Publication Date**
2018

Peer reviewed|Thesis/dissertation

# Testing a Proposed Driver of the End-Permian Biotic Crisis

By

Jeffrey P. Benca

A dissertation submitted in partial satisfaction of the

requirements for the degree of

Doctor of Philosophy

in

Integrative Biology

in the

Graduate Division

of the

University of California, Berkeley

Committee in charge:

Professor Cindy V. Looy, Chair
Professor Ivo A. P. Duijnstee
Professor Robert C. Rhew
Professor Todd E. Dawson

Fall 2018

Abstract

Testing a Proposed Driver of the End-Permian Biotic Crisis

by

Jeffrey P. Benca

Doctor of Philosophy in Integrative Biology

University of California, Berkeley

Professor Cindy V. Looy, Chair

The end-Permian biotic crisis, occurring ~252 million years ago (Ma), was the largest extinction event in Earth history and serves as an important case study for understanding how biodiversity crises unfold. During this event, palynological sections across the planet feature abundant pollen and spore abnormalities coinciding with decline of arborescent seed plants and insurgencies of spore-bearing lycopsid-dominated floras. These fossil trends are hypothesized to signal deteriorating atmospheric conditions—specifically elevated solar ultraviolet B [UV-B] radiation exposure resulting from volcanogenic deterioration of the stratospheric ozone layer. This body of work integrates three experimental and observational studies of modern plants to determine whether historic ozone weakening events could have induced end-Permian palynomorph abnormalities and vegetation turnovers.

Chapter one investigates whether pollen malformations and forest recessions in the end-Permian fossil record could result from past ozone weakening events. Many of the seed plant lineages affected by the crisis produced the same 'winged' (saccate) pollen type as some modern conifer groups, such as pines. However, the effects of elevated UV-B exposure on pollen development, survival and reproductive capacity in modern conifers are not understood. This chapter experimentally evaluates whether end-Permian modeled UV-B regimes induce pollen malformations, heightened mortality and/or reduced fitness in the modern pine, *Pinus mugo* 'Columnaris.' The results of this study demonstrate that elevated UV-B exposure not only induces the same types of pollen malformations seen in the end-Permian fossil record, but also could have played a role in causing forest recessions by causing premature death of seed cones—rather than killing—ancient seed plants.

Chapter two examines whether the lycopsid lineage [isoetaleans] that dominated end-Permian and early Triassic crisis assemblages may have had a competitive advantage over seed plants under an ozone weakening scenario. Modern quillworts, *Isoëtes*, represent the closest living relatives and functional counterparts to Late Paleozoic isoetaleans, however the effects of elevated UV-B exposure on their survival and growth are unknown. This chapter experimentally tests whether *Isoëtes howellii* could survive, grow, and produce spores under end-Permian

modeled UV-B regimes. Although irradiated *I. howellii* survived and were stunted, they produced mature spores that were potentially viable. Despite experiencing more adverse impacts to their vegetative growth, modern isoetaleans may therefore have a fitness advantage over conifers under ozone weakening scenarios.

Chapter three evaluates how frequently saccate pollen malformations are produced by modern conifers under 'non-stressed' growth conditions to better interpret malformations in palynological assemblages. Saccate pollen types are produced by members of two living conifer families—Pinaceae and Podocarpaceae. Although prior studies suggest that malformation frequencies of >3% in fossil yields indicate environmental stress, the variability in their expression amongst 'non-stressed' extant conifer lineages is not well understood. This chapter serves as a baseline comparison of the frequency and variability in saccate malformation expression in pollen yields of fourteen conifer genera in cultivation spanning Pinaceae and Podocarpaceae. Malformed grains represent <3% of pollen yields in twelve of the fourteen genera studied and no discernable phylogenetic pattern in malformation expression was detected. These results demonstrate that pollen malformations are rarely produced in 'unstressed' conifers, specifically lineages with bisaccate grains. Therefore, malformation frequencies exceeding 3% of bisaccate yields in palynomorph assemblages likely indicate a historical environmental stress

TABLE OF CONTENTS

## DEDICATION

This work is dedicated in memory of my father, Paul J. Benca, who was an incredible role model of diligence and integrity for me while growing up. His enthusiastic support and encouragement to take the road less travelled has been a central influence on my work and career as a whole.

## ACKNOWLEDGEMENTS

This body of work would not have been possible without the support, mentorship and encouragement of many incredible individuals and institutions, for which I am immensely grateful. Here I attempt to give credit where it is due, however this list cannot do justice to all that have helped me reach this milestone.

First, I am indebted to my dissertation advisors, Cindy Looy and Ivo Duijnstee. Ever since the first time we corresponded from afar during my early undergraduate years, Cindy and Ivo have been immensely supportive of my development and vision as an aspiring scientist. I am especially grateful for how firmly they have stood by me when deviating from traditional approaches to address research questions in Paleobotany. Thanks also go out to my other dissertation committee members, Todd Dawson and Robert Rhew for their advice, critical feedback and faith in my abilities throughout the course of this work.

I am incredibly grateful to Caroline Strömberg for her mentorship and support during the planning stages of this work at the University of Washington [UW], and for introducing me to the field of Paleobotany. Doug Ewing at the UW Botany Greenhouse and Chad Husby of Fairchild Tropical Botanic Garden served as my horticultural mentors as I developed the cultivation techniques used in chapters 1 and 2. Also when I was and undergraduate at UW, Brooks Miner taught me the ultraviolet-B [UV-B] experimental techniques that later served as a framework for the experimental design of chapters 1 and 2. Others that were instrumental in shaping the development of ideas and methodologies of this work include Henk Visscher, Barry Lomax, Benjamin Black, Henrik Svensen, Stephen Self, Andrew Leslie, Estella Leopold, Seth Finnegan, Bill Clemens, Patricia Holroyd, Charles Marshall and William DiMichele. I also thank the entire UC Museum of Paleontology [UCMP] community and its invited speakers for immersing me in rich educational experiences and providing critical feedback throughout my graduate years.

Thanks go to Clinton Foster for graciously allowing me to use photographs from his prior study in chapter 1. I thank Paul Halladin for recommending *Pinus mugo* 'Columnaris' as an experimental system and supplying well-established dwarf conifer specimens for chapter 1, John Game for locating an exceptional source population of *Isoëtes howellii* specimens in Marin County, CA for chapter 2, and Bill Kuhn for providing research permit access to that *I. howellii* population. Cindy Looy, Ivo Duijnstee and Julie Carrasco assisted in collecting the *I. howellii* specimens. Thanks also go to Paul Halladin, Keith Possee, Marc Frank, Arthur Lee Jacobson, Erik Fredrickson and Chad Husby for their assistance in pollen cone collection for chapter 3. Mihai Tomescu and Holly Forbes also graciously permitting pollen cone collection at Humboldt State University and the University of California Botanical Garden respectively. I also thank Diane Erwin for her continued guidance in accessioning and housing research specimens from this work archivally in the UCMP collections.

I am immensely grateful to Todd Dawson for providing access and supporting my usage of environmentally-controlled growth chambers and greenhouse spaces in the Valley Life Sciences Building [VLSB]. I also thank Christina Wistrom and Jacob Shogren for providing growth chamber facilities and technical support for the chapter 2 experiment at Oxford Tract, as well as Joseph Yon for providing access to an outdoor growth space on campus for housing experimental specimens. I am indebted to Adam Doban and Derek Apodaca for providing

critical support for all growth facilities in VLSB. Dwight Springthorpe helped design and construct the circuitry for UV-B lamps in the experimental chambers and Jay Silverman conducted critical spectral output and reading tests for our UV-B lamps, radiometer and sensor respectively at Solar Light Company, Inc. Several graduate and undergraduate students provided helped me conduct the experiments for chapters 1 and 2. Specifically, Renske Kirchholtes, Seth Kauppinen, Cameron Williams, Elizabeth Rico, Katie Shin, Ryan Tang, Emily Hall and Julie Carrasco assisted in daily plant rotations.

I owe immense gratitude to my friends and family who helped me keep moving forward throughout the planning and execution of this project, specifically my partner, Julie Carrasco, my late father, Paul Benca, my uncle, Jose Quintans, as well as John Game, Tim Ho, Susan Fawcett, Seth Kauppinen, Jun Ying Lim, Adam Huttenlocker, Patricia Holroyd, Thien-Y Le and Bob Dannenhold. Major thanks go to my incredible labmates Renske Kirchholtes, Dori Contreras, Benjamin Muddiman and Nicholas Spano. I also thank Raymond and Gail Damazo for opening their doors to Julie and me while working on the final stages of this dissertation remotely in Washington state, and Ron Gagliardo for generously making accommodations to ensure I could complete this dissertation while continuing to work in the Amazon Spheres Horticulture Program.

This research was made possible through generous support and contributions of the following institutions and funding sources: National Science Foundation Graduate Research Fellowship 1000135655 to Jeffrey Benca, the Research Council of Norway through its Centres of Excellence funding scheme to Centre of Earth Evolution and Dynamics, project number 223272.L. to Cindy Looy, National Science Foundation Division of Environmental Biology grant 1457846 to Cindy Looy, Paleontological Society Richard Bambach Award to Jeffrey Benca, UCMP Clair Englander Student Prize to Jeffrey Benca, UCMP Graduate Fellowship to Jeffrey Benca, and the UCMP George D. Louderback Award in Paleontology to Jeffrey Benca.

# CHAPTER 1

## UV-B-induced forest sterility: Implications of ozone shield failure in Earth's largest extinction[1]


## ABSTRACT

While Siberian Trap volcanism is considered a primary driver of the largest extinction in Earth history, the end-Permian crisis, the relationship between these events remains unclear. However, malformations in fossilized gymnosperm pollen from the extinction interval suggest biological stress coinciding with pulsed forest decline. These grains are hypothesized to have been caused by enhanced ultraviolet-B (UV-B) irradiation from volcanism-induced ozone shield deterioration. We tested this proposed mechanism by observing effects of inferred end-Permian UV-B regimes on pollen development and reproductive success in living conifers. We find pollen malformation frequencies increase fivefold under high UV-B intensities. Surprisingly, all trees survived, but were sterilized under enhanced UV-B. These results not only support the hypothesis that heightened UV-B stress could have contributed to pollen malformation production, but also deforestation during Permian-Triassic crisis intervals. By reducing fertility of several widespread gymnosperm lineages, pulsed ozone shield weakening could have induced repeated terrestrial biosphere destabilization and food web collapse without exerting a direct "kill" mechanism on land plants or animals. These findings challenge the paradigm that mass extinctions require kill mechanisms and suggest modern conifer forests may be considerably more vulnerable to anthropogenic ozone layer depletion than expected.



[1]Benca, J. P., I. A. P. Duijnstee and C. V. Looy. 2018. UV-B–induced forest sterility: Implications of ozone shield failure in Earth's largest extinction. *Science advances* 4: p.e1700618. DOI: 10.1126/sciadv.1700618

## INTRODUCTION

The end-Permian crisis (~251.9 Ma) (Burgess et al. 2014), the largest mass extinction in Earth history, initiated a series of floral destabilization-recovery episodes that continued ~500 kyr into the succeeding Triassic Period (Looy *et al*. 2001, Hochuli et al. 2016). Massive volcanism associated with formation of the Siberian Traps igneous province is considered a likely driver behind these events (Burgess and Bowring, 2015). Although many Traps-related kill mechanisms have been proposed, the proximal causes of ecosystem-scale disturbance are unclear. Among the few inferred direct clues of biological stress in the fossil record are malformed bisaccate pollen grains (Fig. 1, B to H, Foster and Afonin, 2005). Bisaccate pollen are wind-dispersed grains that normally consist of a central body with two symmetric, bladder-like appendages called sacci. Sacci are inflated regions of the outermost pollen wall that function to increase the buoyancy of pollen grains, enabling their flotation against gravity through downward-facing liquid pollination drops associated with the inverted (upside-down-facing) ovules of several conifer and seed fern groups (Salter et al. 2002, Leslie, 2010). This pollen form is produced abundantly by certain gymnosperm lineages and has remained a conspicuous element of palynomorph assemblages since the Pennsylvanian (Millay and Taylor, 1974). Bisaccate pollen malformations are likely products of meiotic disruption, as they have asymmetric sacci, more or less than two sacci, and are occasionally fused or unseparated (Fig. 1, B to H) (Foster and Afonin, 2005).

In end-Permian fossil pollen assemblages studied for abnormalities, 3–6% of two bisaccate pollen types, *Klausipollenites schaubergeri* and *Alisporites* sp., appear malformed in coeval, but geographically distant sediments of the Northern Paleohemisphere (Russia and China; Foster and Afonin, 2005). Malformations also occur in *Klausipollenites,* multitaeniate bisaccates*,* and non-saccate *Ephedripites* pollen of end-Permian assemblages from offshore Norway (Hochuli et al. 2017). Similar abnormalities have been reported from distant end-Permian localities of the Southern Paleohemisphere: in South Africa (*K. schaubergeri* and *Alisporites* sp.; Prevec et al. 2010) and in central Gondwanan India (*Klausipollenites* sp*.* and *Hamiapollenites insolatus*; Mishra et al. 2018). *Alisporites* type grains have been found *in situ* within pollen organs of peltasperm and corystosperm seed ferns (Srivastava, 1983; Osborn and Taylor, 1993) and pollen cones of conifers (Florin et al. 1944; Potonié, 1962; Grauvogel-Stamm, 1978). Multitaeniate bisaccate grains in the Northern Hemisphere are associated with late Permian peltasperms and conifers (Clement-Westerhof, 1974; Balme, 1995; Zavialova and Karasev, 2015). *Ephedripites* pollen have been isolated from late Permian gnetalean pollen cones (Wang, 2004). *Klausipollenites* and *Hamiapollenites* were also produced by gymnosperms, but their exact botanical affinities are unknown. Some affected pollen types, such as *Alisporites* spp. (Foster and Afonin, 2005*,* Peng et al. 2006; Schneebeli-Hermann et al. 2015; Eshet et al. 1995; Orlowska-Zwolinska, 1984; Lindström and McLoughlin, 2007; Cirilli et al. 1998) and *Klausipollenites* spp. (Foster and Afonin, 2005, Schneebeli-Hermann et al. 2015; Eshet et al. 1995; Orlowska-Zwolinska, 1984; Lindström and McLoughlin, 2007; Cirilli et al. 1998; Bercovici et al. 2015), occur from near the paleoequator through mid and high latitudes of both hemispheres. It is therefore likely that several common, widely-distributed conifer, seed fern and gnetalean lineages were affected. These malformations were deposited amidst (and during, Hochuli et al. 2017; Mishra et al. 2017) forest recession episodes across the planet and massive perturbations in the global carbon cycle (Fig. 2) (Foster and Afonin, 2005; Hochuli et al. 2017; Schneebeli-Hermann et al. 2015).

Heightened malformed pollen frequencies are hypothesized to be an indication of enhanced ultraviolet-B radiation (UV-B; 280–315 nm) exposure during the end-Permian (Foster and Afonin, 2005). This increase in UV-B and associated radiative stress in the flora has been attributed to pulsed release of ozone-depleting halocarbons by Siberian Traps magmatism (Foster and Afonin, 2005), coeval with the crisis (Burgess and Bowring, 2015; Visscher et al. 2004; Svensen et al. 2009). Geophysical evidence supports this hypothesis—the Traps formed amidst enormous (up to 2.5 km thick) Cambrian evaporite sequences, samples of which still emit high concentrations of ozone-deteriorating methyl chloride ($CH_3Cl$) and methyl bromide ($CH_3Br$) in heating experiments (Svensen et al. 2009). Additionally, global atmospheric circulation models infer moderate depletion to near-total collapse of Earth's ozone layer if metamorphic Siberian Trap emissions entered the stratosphere (Black et al. 2014).

While this hypothesis has gained support and also been extrapolated using other lines of paleobotanical evidence (Visscher et al. 2004), the effects of enhanced UV-B radiation on the reproductive biology of gymnosperms remains untested. Members of several living conifer genera produce pollen similar in size, proportionality and bisaccate architecture as those of affected Permian-Triassic conifers and seed ferns, suggesting their grains function in the same manner (Leslie et al. 2008). Among living conifers, pines produce a phenotypically similar range of malformations to end-Permian forms (Foster and Afonin, 2005). Pines therefore provide a functionally and developmentally relevant system for evaluating UV-B influences on the reproductive biology of affected Permian-Triassic conifers, peltasperms, corystosperms and potentially other gymnosperm lineages. Using the dwarf pine, *Pinus mugo* Turra 'Columnaris,' we directly tested in growth chambers whether UV-B regimes modeled for the end-Permian induce pollen malformations, tree death, and/or reduced fertility. We therefore experimentally evaluated a proposed mechanistic link between Siberian Traps volcanism and end-Permian floral turnover.

## METHODS

### Experimental Design

In January, 2013, sixty *Pinus mugo* 'Columnaris' specimens were established outdoors, fully exposed to sun on a rooftop of the Valley Life Sciences Building, University of California, Berkeley, CA, US (37° 52' 17.2" N, 122° 15' 44.2" W). Trees were purchased from Iseli Nursery (Boring, OR, US) and grown outdoors under ambient UV-B exposure until March, 2014 to minimize unusual stress responses to acute UV-B dosages during the experiment (Hectors et al. 2007). These trees were a reproductively mature dwarf pine variant, measuring 42–49 cm in height, cultured in 19 cm tall × 20.95 cm diameter terra cotta pots (100043015, NorCal Pottery Products Inc.; Richmond, CA, US). Thus, canopy apices of trees grown in pots were 61–68 cm in height from the ground. Terra Cotta pots were used in place of conventional plastic, and specimen labels were buried in the substrate to avoid UV-induced degradation and potential volatile release into enclosed growth chambers. Plants were grown and acclimatized to full sunlight outdoors in a predominately mineral substrate consisting of 3:2:1 pumice, sandy loam, and peat (American Soil and Stone, Richmond, CA, US). This substrate simulated qualities of low-nutrient sediments associated with many natural conifer habitats in the Northern Hemisphere (Lavola et al. 2003) and served to reduce susceptibility of *P. mugo* specimens to heightened UV-

B (Hunt and McNeil, 1998). In each pot, the substrate surface was covered by a disk of 100% opaque, biodegradable, cellulose weed barrier (WeedGuardPlus®; Sunshine Paper Co., Aurora, CO, US). This layer of weed barrier was used to prevent UV-B mediated changes to below-ground microbial communities that could adversely impact plant health in confined pots (Klironomos and Allen, 1995). Plants outdoors were watered three times weekly overhead via hose with industrial tap water (pH 8.4–8.9). Fertilizer was not supplemented to plants the year prior to, or throughout the experimental duration to prevent artificially heightened UV-B sensitivity associated with increased substrate phosphorus and nitrogen availability (Hunt and McNeil, 1998; Murali and Teramura, 1985).

While all tree specimens were assigned accession numbers (PM01–60) in January, 2013, thirty were selected for study. These specimens were chosen as they yielded the highest numbers of pollen and ovulate cones of the group in 2013. All were outwardly robust and healthy prior to the experiment. Six specimens remained outdoors for baseline comparisons of ovulate cone production. The remaining 24 were transferred into growth chambers (E15; Conviron®, Winnipeg, MB, CA). Throughout growth chamber culture and the experiment, trees in each treatment were watered three times weekly with 1.6 liters (l) of industrial tap water (pH 8.4–8.9) overhead via plastic watering can (204787CP: Fiscars®, Helsinki, FI). Photosynthetically active radiation (PAR) was administered in chambers via sixteen cool, white 160 W fluorescent tubes (F72T12/CW/VHO, Sylvania; Mississauga, ON, CA). Relative humidity in chambers was set to 50% for both day and night.

From 7–31 March 2014, plants were acclimated to 14.0 ˚C-day, 8.0 ˚C-night temperatures and a 12.5-hour photoperiod; (approximate mean values for Berkeley, CA, US for March–April, 2013) (Table S5). Specimens were divided into four groups of six trees and redistributed into four growth chambers on 1 April 2014. In the four chambers, trees were acclimated to 16.0 ˚C-day, 10.0 ˚C-night temperatures and 14-hour photoperiod (approximate mean values for Berkeley, CA, US in May 2013) (Table S6).

One of the four chambers served as a control, (no supplemental UV-B source); the other three housed two 120 V fluorescent UV-B lamps; each containing two broadband bulbs with a 312 nm emission peak and 281–405 nm spectral output (XX-15B; Spectronics Corporation, Westbury, NY, US). The emitting surfaces of these lamps were suspended 79.7 cm above each chamber floor (18.7–11.7 cm above tree apices) from frames constructed of bolted stainless steel L-beams. Each end-Permian treatment chamber housed one of three enhanced biologically effective (BE) UV-B regimes; 54, 75 and 93 (kJ $m^{-2}d^{-1})_{BE}$. These treatments correspond with 40–60 to 50–100 (kJ $m^{-2}d^{-1})_{BE}$ UV-B fluxes inferred from modeled scenarios in which net Siberian Trap halocarbon emissions were released over a 400 to <200 kyr interval (Fig. 6) (Beerling et al. 2007). These fluxes were recorded from the height of the tallest tree specimen (68 cm above the chamber floor, 11.7 cm from the UV-B-emitting lamp surface). UV-B measurements were conducted using a UV-B sensor and handheld radiometer calibrated before the experiment in winter, 2014 (SKU 430; Apollo Display Meter; Skye Instruments Ltd., UK). The UV-B-emitting surface of each lamp was covered by a 0.003 mm-thick fresh sheet of clear, cellulose acetate (Grafix™; OH, US) to intercept UV wavelengths shorter than the spectrum reaching Earth's surface (< ~295 nm) (Williamson et al. 2001). These filters were replaced every 7 days, due to UV-induced degradation of the cellulose acetate. UV-B intensity was attenuated in the 54 and 75 (kJ $m^{-2}d^{-1})_{BE}$ treatments by covering emitting surfaces of lamps with aluminum mesh screen (1.5 $mm^2$ mesh size) (Phifer Inc., Alabama, US). Two sheets of mesh were stacked offset for the 54

(kJ $m^{-2}d^{-1})_{BE}$ treatment, and one sheet for the 75 (kJ $m^{-2}d^{-1})_{BE}$ treatment. Lamps in the 93 (kJ $m^{-2}d^{-1})_{BE}$ treatment therefore were only shielded by cellulose acetate.

Treatment groups were exposed to heightened UV-B regimes for 57 photoperiods [15 April through 10 June 2014]. This interval encompassed pollen development and dispersal, ovulate cone development, and pollination– for trees in which ovulate cones reached receptivity, Stages 4L–5L (Fig. 4, A). Plants in all growth chambers received PAR for 14 hours each day. UV-B lamps emitted radiation 12 hours per day in each treatment chamber. UV-B treatments commenced 1 hour following the start of each PAR photoperiod and ceased 1 hour prior to darkness. This cycle simulated attenuated UV-B exposure during low-angle sunlight hours of mornings and evenings outdoors. Throughout the treatment, potted plants were manually shifted 3 times daily: once every 4 hours during each 12-hour UV-B photoperiod. Plants were shifted within rows of three, in the same order and direction daily. This rotation pattern ensured uniform UV-B dosage for all trees per treatment group and reduced chamber effects. Moreover, this practice guaranteed each tree experienced acute UV-B dosage [highest under the lamp center] at the same timeslot per photoperiod. Plants in the control chamber were also shifted in this manner on the same schedule for comparability. During all rotations, potted plants were shifted slowly and steadily to prevent shaking-induced ethylene stress responses (Biddington, 1986). Trees were removed from all chambers after the last pollen cone was collected on 10 June 2014. Following the experiment, trees were placed back into the space where they were grown outdoors, exposed to full sunlight, and watered three times weekly.

**Applied biologically effective dosages of UV-B**

The goal for this experiment was to expose developing pollen and ovulate cones of conifers to biologically effective (BE) UV-B fluxes in the same range as modeled for the end-Permian (*33*). To verify accuracy of the measurements, evaluations of irradiance for the UV-B lamps (Spectronics XX-15B) and spectral sensitivity of our UV-B detector (SKYE meter SKA 400 43638 + SKYE detector SKU 430) were conducted at testing facilities of Solar Light Co. (Glenside, PA, US). There, spectral irradiance curves were generated at four distances from our UV-B lamps, which were comparable to readings of our UV-B sensor at those same distances in growth chambers. To estimate BE UV-B flux, the wavelength-specific fluxes (measured for 2 nm bins) were multiplied by the corresponding wavelength-specific Relative Photon Effectiveness (see Fig. 3 in Caldwell, 1971). The integral of the resulting multiplied curve yields the BE UV-B flux at a specific distance from the lamp (Fig. 6). For the end-Permian, various model-reconstructed scenarios of volcanism-enhanced BE UV-B irradiation are reported: with the lowest scenario having UV-B fluxes of 30–60 (kJ $m^{-2}d^{-1})_{BE}$ and the highest reaching 50–100 (kJ $m^{-2}d^{-1})_{BE}$ (Fig. 6) (Beerling et al. 2007).

The tops of tree canopies in the enhanced UV-B treatment chambers (on average, 15.2 cm from the UV-B lamps) experienced UV-B fluxes of 54, 75 and 93 (kJ $m^{-2}d^{-1})_{BE}$ for the minimum, medium and maximum treatment levels, respectively. This range is similar to maximum values in the lowest and highest flux scenarios (i.e. 60 and 100 (kJ $m^{-2}d^{-1})_{BE}$) modeled for the end-Permian (Beerling et al. 2007). The elevation range of pollen cones selected for this study was further in distance (between 30.2 and 37.8 cm) away from the lamps. This elevation range therefore experienced more attenuated UV-B fluxes; 26–31, 36–43 and 45–54 (kJ $m^{-2}d^{-1})_{BE}$ for

the minimum, medium and maximum treatment levels, respectively (Fig. 6). The range in these values roughly corresponds with the minimum values in the lowest and highest flux scenarios (i.e. 30 and 50 (kJ $m^{-2}d^{-1})_{BE}$) modeled for the end-Permian (Beerling et al. 2007).

While we were unable to monitor UV-B dosage experienced by outdoor trees, they likely experienced an average flux of 7.2 (kJ $m^{-2}d^{-1})_{BE}$, based on Caldwell-adjusted sum estimates for 300, 305, 311, 317, 325, 332, and 368 nm for the University of California, Berkeley campus [37° 52' 17.2" N, 122° 15' 44.2" W] generated by the Tropospheric UV model (TUV) using data assimilated from NASA TOMS/OMI and MODIS satellites and NCEP NARR surface datasets (UVMRP). We were also unable to supplement growth chamber control and treatment groups with enhanced UV-A (315–400 nm) and photosynthetically active radiation (PAR, 400 –1700 nm) due to spatial constrains. Heightened exposure to these forms of solar radiation would also accompany ozone-weakening events. Though lower doses of UV-A radiation facilitate repair of UV-B-incurred DNA damage in pine seedlings, higher doses have been found to impose additive effects to UV-B (Fernbach and Mohr, 1992). Therefore, while our experimental conditions deviated in some respects with ozone weakening events in nature, the results of this study may not have been considerably altered by proportionately increased UV-A and PAR.

**Pollen cone collection**

Altogether, 114 pollen cones (from 15 branches), 212 pollen cones (from 33 branches), 137 pollen cones (from 11 branches), and 298 pollen cones (from 34 branches) were collected from the control and 54, 75, and 93 (kJ $m^{-2}d^{-1})_{BE}$ treatment growth chambers respectively. Entire pollen cones produced in each tree were individually collected using stainless steel forceps just prior or after opening (indicated by cone yellowing, expansion and elongation). Pollen cones separated from the parent plant were immediately placed in plastic 1.7 mL microcentrifuge tubes (C2170, Denville Scientific Inc.; Holliston, MA, US) containing a solution of 95% ethanol solution ($C_2H_6O$; CAS# 64-17-5) for preservation. Cones were placed directly into ethanol rather than conventionally dried to minimize contamination, sample loss, and desiccation-induced grain distortion (Traverse, 2007). Each pollen cone was accessioned with collection date, branch height, and relative degree of shading from overhanging branches [full shade, partial shade, or exposed].

Since UV-B dosage decreases with distance from the lamps (Fig. 6) and malformation production rates may vary throughout a season, comparability of samples between trees and treatments was maximized by subsampling pollen collections on the basis of cone height and collection date. Specifically, we limited our comparison to cones collected in the shortest time interval within the smallest height range yielding 8 non-shaded (one exception, see note below) cones per tree, in three trees per treatment (Fig. 7). This resulted in the selection of 96 cones [4 treatments × 3 trees × 8 cones per tree] (table S4) that matured between 20 and 26 days after the start of the treatment (5–11 May 2014). These pollen cones developed on the trees between 41.9 and 49.5 cm in height from the growth chamber floor (i.e. 37.8 and 30.2 cm below UV-B-emitting lamp surfaces). For corresponding UV-B dosages in this zone, see (Fig. 6). Note: Cones sampled from specimen PM52 within this elevation range and timeframe were partially shaded. Nevertheless, its cones yielded the highest mean malformation frequency in the 75 (kJ $m^{-2}d^{-1})_{BE}$

treatment: 9.5%, compared to 7.1% and 8.2% for specimens PM38 and PM54, respectively (Fig. 3 and table 8).

**Pollen sample size determination**

A subsample size of 600 pollen grains was used to enumerate the proportion of malformations within pollen cones harvested during the experiment. This number was based on *in silico* simulations (Fig. 8) investigating the effect of pollen subsample size on accurately recognizing background frequencies of malformed pollen (i.e. the chance of each sampled pollen grain exhibiting malformation = 0.02). This revealed that subsample sizes exceeding 600 pollen grains do not produce markedly smaller interquartile ranges (IQRs) relative to the increase in effort their analysis would require (Fig. 8). Thus, 600 pollen grains were morphotyped from each of the 96 cones, yielding a comparison of 57,600 grains.

**Pollen processing procedure**

All pollen samples were exposed to alcohol-soluble (but water insoluble) resin acids exuded from associated cone tissues during storage in 95% ethanol solution. As a result, processing steps immersing resin-contaminated pollen in deionized water during initial processing tests resulted in clumping and adherence of grains to tube walls during centrifuging. To minimize pollen loss during decanting cycles, we developed a simplified rendition of a clearing and staining protocol for extant spores and pollen (Traverse, 2007). Specifically, our protocol substitutes use of deionized water in decanting steps with 95% ethanol. Here we provide this protocol in detail.

Microcentrifuge tubes containing individual cones and their dispersed pollen were manually shaken to encourage grain suspension. A disposable soda-lime glass pasteur pipette and 3 mL rubber dropper bulb (13-678-6A, 03-448-26; Fisherbrand™, Pittsburgh, PA, US) were used to extract and transfer a small subsample of pollen-containing ethanol solution to empty microcentrifuge tubes. The transferred samples were topped with 95% ethanol solution, manually shaken, and centrifuged at 3,800 rotations per minute (rpm) for 30 seconds in a microcentrifuge (5415 D, Eppendorf; Hamburg, DE). The ethanol solution was removed using the same pipette, the tube filled to 75% volume with 10% Potassium hydroxide solution (KOH; CAS# 1310-58-3), and placed into wells of a 110 W dry block heater (12621-104, VWR® International; Radnor, PA, US) set to 130.8 ˚C for 6 minutes [on high heat, with both low and high dials set to “7”]. Temperature was measured from the bottom center of wells by a K-type thermocouple sensor probe attached to an LCD instant-read digital thermometer (HYELEC MS6501; CN). During the KOH hot-bath, tubes were removed from wells with a toothpick every 45 seconds, uncapped to release pressure, manually shaken, and placed back in the well. This 10% KOH cooking step served to hydrolyze cellulose and lyse protoplasts, leaving the exine of pollen grains (i.e. the sporopollenin outer layer retained in fossilized palynomorphs) intact, but transparent (Traverse, 2007).

Following heating, the tubes were vented and recapped to relieve pressure, manually shaken, centrifuged, decanted, and filled with 95% ethanol solution. After three further

centrifuge/decanting cycles with 95% ethanol solution, two drops Safranin O dye ($C_{20}H_{19}N_4Cl$; CAS# 447-73-6) were added, and the tube topped with 95% ethanol solution, manually shaken, and centrifuged. 85–90% volume of the dye solution was then decanted via pipette, leaving behind a solution highly concentrated in dyed pollen. One drop glycerol ($C_3H_8O_3$; CAS# 56-81-5) was added, then mixed with the sample using a flat toothpick (Diamond®, Jardin Corp.; Fishers, IN, US).

Small pollen subsamples were extracted using glass pipette/dropper bulb and transferred to the centers of standard microscope slides on a slide warmer set to 56 ˚C (XH-2002, Premiere®, C&A Scientific Co., Inc.; Manassas, VA, US). Pollen solution subsamples were left exposed on the slide warmer in a fume hood for approximately five minutes to evaporate residual ethanol and ensure the residue contained predominately stained pollen and glycerol. On each slide, the pollen grain-containing solution was gently mixed with one small (2–3 mm dia.) melted cube of glycerin jelly (7.63% Gelatin, 53.4% Glycerin, 0.76% Phenol) using a flat toothpick, then enclosed by a 22 × 30 × 0.16 mm cover glass (12-544-A, Fisherbrand™, Pittsburgh, PA, US). Mounted slides were left for 30 minutes on the slide warmer (set to 56 ˚C) to encourage spread of sample/medium under the cover glass. Slides remained in a fume hood at ~22 ˚C for two days after mounting to off-gas residual water and ethanol vapor from under the cover glass. Cover glasses were then sealed either by paraffin-embedding or clear nail polish. Five to eight slides were prepared from each pollen cone so that 600 grains were counted.

**Pollen microscopy analyses**

Pollen grains were morphotyped using a Leica DM2500 microscope fitted with a Differential Interference Contrast system (to render contrast in transparent grains) using a 20 × Objective lens (506503, Leica Microsystems, Inc; Wetzlar, DE). All grains were morphotyped by one individual [J.P.B.], to minimize deviations in protocol. Data pertaining to treatment group, cone elevation, and shading were omitted from all sample slide labels to ensure blind comparison. Malformed grains were categorized into subgroups using a 40 × Objective lens (506144, Leica Microsystems Inc.; Wetzlar, DE). Grains bearing two sacci were counted as phenotypically normal while those having more or less than two sacci were scored as malformations (Fig. 1, J to P and table 8). Normal and malformed grains were tallied using a two-key desktop laboratory counter (Clay Adams, Becton, Dickinson and Co.; Parsippany, NJ, US). Malformation categories were tallied using a 24-key desktop laboratory counter (Vary-Tally, Veeder-Root Inc.; Hartford, CT, US). Exemplary normal and malformed grains were imaged through the view of a Plan Apo 63 × Oil Objective lens (506187; Leica Microsystems Inc.; Wetzlar, DE) for the highest degree of Apochromatic and Flat Field correction. Grains were imaged with a Nikon Digital Sight DS-Fi1 camera with live feed into a Nikon DS-L2 control unit (Nikon Corp., JP). Extended depth of field (EDF) images were generated using CombineZP. Images were compiled as jpegs (2560 × 1920 pixels; 300 dpi).

**UV-B impacts on whole plant reproduction**

Whole plant fitness across treatments was assessed by morphological assessment of *in vivo* ovulate cone survivorship throughout canopies of all growth chamber and outdoor specimens. We used stage 6 (Fig. 4, A) as a proxy for pollination success rather than *in vitro* pollen germination because successful pollination is required to reach this stage (Williams, 2009) and even pollen with lethally-irradiated nuclei in some plants can germinate, produce pollen tubes and penetrate ovules *in vitro* (Pandey et al. 1990). For each ovulate cone, accession number and elevation were written on a 1.5 × 1.0 cm label cut from water-repellent paper (978-1-932149-89-0; Rite in the Rain®, JL Darling LLC. Tacoma, WA, US) using no. 2 pencil. These labels were threaded through stainless steel 38 × 0.25 mm insect pins (#000; Ento Sphynx®, Černá za Bory, CZ) taped to pine needles in fascicles adjacent to each ovulate cone using label tape (L-3000-3, GeneMate; VWR® International, Radnor, PA, US).

We categorized ovulate cone survivorship using developmental stages described for controlled pollination of *Pinus* by the US Department of Agriculture (Cumming and Righter, 1948; Bramlett and O'Gwynn, 1980; Bramlett and O'Gwynn, 1981) with subdivisions of stages 4 and 5 (Fig. 4, A) (Williams, 2009, Owens et al. 1981). Ovulate cones emerged from buds between 20–26 April (Stage 3) (Fig. 4, A). During this time, pollen grains were found adhered to exposed surfaces throughout each growth chamber. Pollen was therefore available in all growth chambers to ovulate cones reaching the stages of receptivity (4L–5L) (Fig. 4, A). Survivorship of all ovulate cones was morphologically assessed based on photographs taken of each cone ~70–76 days after emergence [5−11 July 2014] with scale. By this point, ovules pollinated with successfully germinating pollen had reached stage 6 (Fig. 4, A) (Williams, 2009). Cones that appeared un-pollinated expanded until nearly completing stage 5L (Fig. 4, A, Williams, 2009), when their ovuliferous scales ceased growth and hardened as the cone desiccated.

**RESULTS**

Five populations of *P. mugo* (n=6 clones) were grown for 56 days during pollen and ovulate cone development. One population was grown outdoors under ambient UV-B conditions in Berkeley, CA, US as a reference group for both the control and treatment groups in growth chambers. This outdoor tree population experienced an estimated biologically effective (BE) UV-B flux of 7.2 (kJ $m^{-2}d^{-1}$)$_{BE}$ (UVMRP). The other four populations were cultivated in growth chambers under control (no UV-B; 0 (kJ $m^{-2}d^{-1}$)$_{BE}$) and three enhanced UV-B treatments: 54, 75 and 93 (kJ $m^{-2}d^{-1}$)$_{BE}$. These treatment values correspond with modeled near-surface increases in UV-B irradiation from a Late Permian background of 10–20 (kJ $m^{-2}d^{-1}$)$_{BE}$ to ozone depletion scenarios of 40–60 and 50–100 (kJ $m^{-2}d^{-1}$)$_{BE}$ if net emissions from the Siberian Traps and organohalogens were combined and released over 400 to <200 kyr, respectively (Fig. 6) (*33*). These fluxes represent maximum dosages received at the top of tree canopies. Morphological analysis was conducted on 600 pollen grains per pollen cone, and 24 pollen cones from each growth chamber population (Table 8). Ovulate cone survivorship was morphologically assessed at the end of the developmental season in outdoor and growth chamber populations (Table S4).

Malformations constituted <3% of pollen yields in the control and 54 (kJ $m^{-2}d^{-1}$)$_{BE}$ treatments, increasing four- to fivefold in the two highest UV-B treatments (Fig. 3 and tables 6, 7

and 8). The two highest UV-B regimes therefore induced significantly ($p < 0.05$) more pollen malformations than the control and 54 (kJ $m^{-2}d^{-1})_{BE}$ treatments in a two-mixed-factor nested ANOVA (Fig. 3; table 6, 7).

While all conifers survived our experiment, trees under all three enhanced UV-B regimes experienced catastrophic fertility reduction. Whereas 98% and 92% of ovulate cones produced in outdoor and control populations successfully reached stage 6 of cone development (n=60 per group), 100% of the ovulate cones died under all three heightened UV-B regimes (n= 48, 48 and 50 for 54, 75 and 93 (kJ $m^{-2}d^{-1})_{BE}$ treatments respectively) (Figs. 4, 5 and table S4). All ovulate cones of irradiated trees died upon or just after emergence—prior to pollination receptivity and irrespective of canopy position or degree of self-shading (stages 3–4 of cone development. Figs. 4, 5). However, the exact developmental phase and mechanism of premature ovule death requires further investigation. This period of UV-B stress did not noticeably hamper vegetative growth of *P. mugo*, nor did it permanently sterilize the trees, as irradiated specimens successfully produced ovulate cones reaching developmental stage 6 (Fig. 4, A) in years following the experiment outdoors.

## DISCUSSION

Prior studies of fossil and modern gymnosperm pollen suggest yields comprising >3% malformed grains are associated with environmental stress (Foster and Afonin, 2005). In this study, >3% malformation frequencies correspond with reproductive failure in conifers under heightened UV-B exposure (Fig. 3). Because ovulate cones in irradiated trees died prior to pollination receptivity (Figs. 4, 5), pollen fertility was inconsequential to their fitness. Pollen germination studies were therefore not pursued.

Based on our results, we propose that high frequencies in phenotypic abnormalities in bisaccate pollen can be indicative of elevated UV-B exposure among other stresses, and that periods with heightened abnormality frequencies in the Permian-Triassic fossil record could also have been characterized by widespread UV-B-induced fertility reduction. Under heightened UV-B, malformations are likely conservative indicators of reproductive stress because even in the 54 (kJ $m^{-2}d^{-1})_{BE}$ treatment, all ovulate cones died prematurely while trees yielded normal background malformation frequencies (1.6%) (Figs. 3 and 4, B and tables 6, 7 and 8). Considering fossilized pollen assemblages are time-averaged samples accumulated in depositional basins over many years, those yielding >3% abnormal grains could reflect either high-frequency (decadal) or prolonged (century or longer) ozone deterioration pulses. Infertility intervals corresponding to either scenario would culminate in steep fitness and population decline of gymnosperms. Intervals of volcanogenic deterioration of the stratospheric ozone layer could have triggered temporary population decline for several gymnosperm lineages, rather than immediate extinction. Subsequent intervals of reduced eruption and halocarbon emissions would result in rapid ozone shield repair (within ~10–20 years) ( Beerling et al. 2007; Black et al. 2014), allowing for gymnosperm recovery from existing populations.

Despite longevity and resiliency of individual trees, frequent or prolonged fertility reduction could diminish seed yields in regions with favorable climates as well as viable seed banks in those with more sporadic recruitment opportunities (e.g. periodic wildfires, rare rainy seasons). Under either circumstance, progressively fewer seeds would germinate and reduced seedling populations would be subject to background mortality rates they may not have been able to sustain. Over time, fitness reduction coupled with even modest seedling mortality could therefore have culminated in regional extirpation or even extinction of some Permian-Triassic gymnosperm lineages. Additionally, Permian-Triassic crisis intervals appear to coincide with phases of intense greenhouse climatic conditions (Romano et al. 2013), during which time a concomitant fertility crisis could have severely hampered migration of some gymnosperm lineages.

Reduced fertility of several widespread and/or common gymnosperm groups could impose severe ecological consequences consistent with patterns of vegetation turnover observed in several high-resolution fossil pollen and spore assemblages (e.g. Fig. 2 in *3*). Fluctuations in ozone column thickness may explain pulsed extirpation, recovery and delayed extinction of some gymnosperm lineages in palynomorph assemblages spanning both hemispheres from the latest Permian to 500 kyr into the Early Triassic (Fig. 2) (Hochuli et al. 2016). Concomitantly with the pulsed vegetation turnover, U-Pb dates of Siberian Trap deposits indicate the onset of flood volcanism ~300 ± 126 kyr before faunal extinctions and cessation ~500 kyr into the Early Triassic (Burgess and Bowring, 2015). Additionally, paleomagnetic studies suggest the volcanism during this interval was likely pulsed in nature (Pavlov et al. 2011). While extrusive eruptions appear concentrated into two phases, intrusive magmatism likely persisted throughout the Angaran Province during the interim, after the marine biotic crisis (Burgess and Bowring, 2015). Passive emissions of organohalogens could therefore have continued between eruptive phases via contact metamorphism of host sediments containing petroleum-bearing evaporites (Svensen et al. 2009; Burgess and Bowring, 2015).

Volcanogenic $SO_2$ aerosols would likely have contributed strongly acidic rain (Black et al. 2014) in Permian-Triassic Siberia. This, together with heavy metal pollution, is another stress associated with pollen malformations in modern conifers of industrially polluted regions ( Mičieta and Murín, 1996;  Tretyakova and Noskova, 2004) and could thus have contributed to the observed changes in Permian-Triassic palynological records as well. However, Siberian Trap-induced acid rain would have been regionally confined to the Northern Hemisphere (Beerling et al. 2007; Black et al. 2014), while malformed pollen (Prevec et al. 2010, Mishra et al. 2017) and gymnosperm turnovers (Lindström and McLoughlin, 2007; Schneebeli-Hermann et al. 2015) also occurred in the Southern Hemisphere (Fig. 2). The extent of Siberian Trap stratospheric ozone destruction, in contrast, would have encompassed the entire planet (Black et al. 2014).

Although other untested forms of environmental stress may well have contributed to localized pollen malformation production, UV-B radiation is uniquely capable of inducing globally-consistent reproductive defects in terrestrial vegetation. This possibility may be further evidenced by an increase of fossilized unseparated lycophyte spore tetrads worldwide—a hypothesized floristic stress response to enhanced UV-B (Visscher et al. 2004). While these plants are interpreted to be environmental stress-tolerators (Looy et al. 2000), further study is needed to evaluate susceptibility of crown members in this lineage to heightened UV-B and stimuli conducive to spore tetrad production.

Through decreasing fertility of several common gymnosperm lineages across latitudes, pulsed volcanogenic ozone weakening could have restructured dominance patterns in global vegetation repeatedly. Widespread switchovers in the Permian-Triassic fossil record from taxonomically diverse gymnosperm-dominated assemblages to diversity-impoverished lycophyte/pteridosperm floras (Hochuli et al. 2016) constitute drastic reorganizations of the terrestrial food web base. Such changes could have triggered food web collapse and extinction cascades within terrestrial animal communities without contribution of an abiotic kill mechanism. Similarly, models of probabilistic trophic networks predict Late Permian terrestrial vertebrate communities were likely prone to collapse via primary productivity disruption (Angielczyk et al. 2005).

We have demonstrated that enhanced UV-B does not kill conifer trees outright, but inhibits their reproduction. If late Paleozoic putative relatives of modern conifers (e.g. Volziales) as well as peltasperms, corystosperms and gnetaleans were similarly sensitive to UV-B, their ovules would have been considerably more vulnerable to its impacts. Unlike modern pines, which shield their ovules with heavily-reinforced, overlapping bracts and ovuliferous scales, early conifers and seed ferns bore their ovules on sparsely-foliated shoots (Schweitzer, 1996; Looy, 2007; DiMichele et al. 2005) lacking structural protection from the external environment.

Furthermore, we found ovulate cones were systemically killed or aborted throughout *P. mugo* canopies regardless of location or shading. This finding indicates UV-B induces whole-plant sterility rather than acting upon individual exposed branches. As a result, self-shaded ovulate cones in the lower canopy of conifers also do not yield viable seeds under UV-B regimes modeled for the end-Permian. This observation would suggest that, under an ozone weakening scenario, understory woody plants would be less likely to experience UV-B-induced fertility reduction than canopy-dominant trees. However, this protection would have been reduced as Permian-Triassic forests transitioned to more open woodlands during crisis intervals.

The fertility crisis hypothesis we propose was prompted by unanticipated results of an exploratory, reproductive study of a single species cultivar over one growth season. Of course, constraints of our experimental system raise uncertainties when extrapolating long-term, widespread responses of several major plant lineages in the distant past. Nevertheless, using observable modern systems as proxies for historical processes is the basis of nearly all actualistic studies in paleobiology. While some uncertainties raised by this investigation may not be resolvable, several are experimentally testable. For example, while we cannot affirm that malformation-producing Paleozoic gymnosperm lineages were vulnerable to UV-B stress on the basis of *P. mugo* alone, further investigations of additional early-divergent conifer lineages and gnetophytes could determine whether UV-B-induced fertility reduction is more likely ancestral or lineage-specific within crown gymnosperms. Additionally, even if heightened UV-B was a primary contributor to Permian-Triassic gymnosperm declines, it is unclear why some seed-free vascular plant lineages were not similarly affected. Experimental studies focusing on nearest living relatives of such lineages may elucidate whether UV-B could elicit contrasting responses between major plant groups.

We found that end-Permian modeled UV-B regimes did not permanently sterilize the trees nor noticeably impact their vegetative growth. It is therefore possible that *P. mugo* may have acclimatized to these conditions if exposed for subsequent years. Similarly, previous multi-

year studies have documented acclimatization in vegetative growth of conifer seedlings to heightened UV-B, though under substantially lower regimes than this study—1×, 2× and 3× ambient modern conditions (7.7 kJ $m^{-2}d^{-1}$; Bassman et al. 2002). However, our results imply that conifer vegetative and reproductive sensitivity to UV-B may be decoupled. Consequently, even long-term studies on vegetative growth and ecophysiology of conifers could underestimate the consequences of ozone weakening events on forest health and sustainability.

Several features of our study system imply that fertility reduction may not have been easily mitigated by acclimatization under a prolonged treatment. *P. mugo* is a conservative system for interpreting UV-B responses in conifers because it is an alpine-adapted species, and should have exceptional foliar protection from UV-B (Day et al. 1992). Furthermore, our specimens were reproductively mature trees acclimatized to nutrient-poor substrates under full sunlight outdoors preceding the experiment. Oligotrophic substrates are associated with many natural conifer habitats across the Northern Hemisphere (Lavola et al. 2003) and can convey reduced UV-B sensitivity in plants (Hunt and McNeil, 1998). Moreover, somatic mutations appear to accumulate in conifers under prolonged UV-B exposure, suggesting damage symptoms may be delayed in long-lived trees (Sullivan and Teramura, 1992).

Considering the severity of response in stress-primed, alpine-adapted mature conifers to only one growth season of end-Permian modeled UV-B regimes, we caution extrapolating reproductive acclimatization on the basis of prior vegetative seedling or juvenile tree studies. While it is difficult to approximate a satisfactory cutoff for an acclimatization experiment on trees that could live centuries, further, multi-year studies will be necessary to evaluate whether UV-B-induced fertility reduction is temporary or perennial.

Our results suggest modern conifer forests may be considerably more vulnerable to anthropogenic ozone layer depletion than expected. Had the 1987 Montreal Protocol to curb anthropogenic ozone-depleting Chlorofluorocarbons not been implemented, global stratospheric models suggest a worldwide average of 67% reduction in ozone column thickness from 1980 to 2065 (Newman et al. 2009). This reduction would have been global in extent and year-round, with near total destruction of the stratospheric ozone layer in the tropics and a 550% increase in DNA-damaging UV wavelengths in Northern Hemisphere midlatitudes by 2065 (Newman et al. 2009). Given that 34% of the world's conifer species today are vulnerable or threatened with extinction (Fig. 3 in IUCN Redlist), implementation of the Montreal Protocol may have prevented widespread conifer decline and potentially extirpations. Proposals to curtail restrictions on industrial ozone-depleting pollutant emissions should therefore be treated with extreme caution.

Our experimental approach contributes biological data challenging the broadly popularized paradigm that ecosystem turnovers associated with mass extinctions result from kill mechanisms [catastrophic mortality of organisms]—rather than termination of evolutionary lineages. These findings, together with fossilized pollen records imply Permian-Triassic forests would have appeared deceptively healthy at many points amidst the crisis. By analogy, the Chernobyl exclusion zone now hosts lush, park-like forests only decades after nuclear disaster (Møller and Mousseau, 2006). However, subtle floral and faunal malformations abound throughout the region, reflecting increased mutation rates and potentially heightened selectivity (Møller and Mousseau, 2006). In such cases, fingerprints of even potent selective forces on ecosystems can be highly cryptic. Environmental disasters in the past and present (e.g. current

anthropogenic climate change) are therefore not always easily perceived as they unfold. Their consequences may instead manifest over generational to geologic timescales.

**WORKS CITED**


Aitken, G. A. 1998. *A palynological and palaeoenvironmental analysis of Permian and Triassic sediments of the Ecca and Beaufort groups, northern Karoo Basin, South Africa*. Dissertation, University of the Witwatersrand.

Angielczyk, K. D., P. D. Roopnarine and S. C. Wang. 2005. Modeling the role of primary productivity disruption in end-Permian extinctions, Karoo Basin, South Africa. *N. M. Mus.* New Mexico Museum of Natural History Bulletins 30: 16–23.

Balme, B. E. 1995. Fossil in situ spores and pollen grains: an annotated catalogue. Review of Palaeobotany and Palynology 87: 81–323.

Bassman, J. H., G. E. Edwards and R. Robberecht. 2002. Long-term exposure to enhanced UV-B radiation is not detrimental to growth and photosynthesis in Douglas-fir. New Phytologist 154: 107–120.

Beerling, D. J., M. Harfoot, B. Lomax and J. A. Pyle. 2007. The stability of the stratospheric ozone layer during the end-Permian eruption of the Siberian Traps. Philosophical Transactions of the Royal Society A 365: 1843–1866.

Bercovici, A., Y. Cui, M. B. Forel, J. Yu and V. Vajda. 2015. Terrestrial paleoenvironment characterization across the Permian–Triassic boundary in South China. Journal of Asian Earth Sciences 98: 225–246.

Biddington, N. L. 1986. The effects of mechanically-induced stress in plants—a review. Plant Growth Regulation 4: 103–123.

Black, B. A., J. F. Lamarque, C. A. Shields, L. T. Elkins-Tanton and J. T. Kiehl. 2014. Acid rain and ozone depletion from pulsed Siberian Traps magmatism. Geology 42: 67–70.

Bramlett, D. L. and C. H. O'Gwynn. 1980. *Recognizing developmental stages in southern pine flowers: the key to controlled pollination*. Gen. Tech. Rep. SE-18. Asheville, NC: USDA Forest Service, Southeastern Forest Experiment Station. SE-18.

Bramlett, D. L. and C. H. O'Gwynn. 1981. Controlled pollination. *Pollen management handbook*. USDA Forest Service, Agriculture Handbook No. 587. pp. 44–51.

Burgess, S. D., S. Bowring and S. Z. Shen. 2014. High-precision timeline for Earth's most severe extinction. Proceedings of the National Academy of Sciences of the United States of America 111: 3316–3321.

Burgess, S. D. and S. A. Bowring. 2015. High-precision geochronology confirms voluminous magmatism before, during, and after Earth's most severe extinction. Science Advances 1: e1500470–e1500470.

Caldwell, M. M. 1971. "Solar UV irradiation and the growth and development of higher plants." *Photophysiology* (pp. 131–177. Academic Press, New York, 1971).

Cirilli, S., C. Pirini Radrizzani, M. Ponton and S. Radrizzani. 1998. Stratigraphical and palaeoenvironmental analysis of the Permian-Triassic transition in the Badia Valley (Southern Alps, Italy). Palaeogeography, Palaeoclimatology, Palaeoecology 138: 85–113.

Clement-Westerhof, J. A. 1974. In situ pollen from gymnospermous cones from the Upper Permian of the Italian Alps—a preliminary account. Review of Palaeobotany and

Palynology 17: 63–73.
Cumming, W. C. and F. I. Righter. 1948. *Methods used to control pollination of pines in the Sierra Nevada of California*. USDA Circular 792.
Day, T. A., T. C. Vogelmann, E. H. DeLucia. 1992. Are some plant life forms more effective than others in screening out ultraviolet-B radiation? Oecologia 92: 513–519.
DiMichele, W. A., H. Kerp, M. Krings and D. S. Chaney. 2005. The Permian peltasperm radiation: evidence from the southwestern United States. New Mexico Museum of Natural History Bulletins 30: 67–79.
Eshet, Y., M. R. Rampino and H. Visscher. 1995. Fungal event and palynological record of ecological crisis and recovery across the Permian-Triassic boundary. Geology 23: 967–970.
Fernbach, E. and H. Mohr. 1992. Photoreactivation of the UV light effects on growth of Scots pine (*Pinus sylvestris* L.) seedlings. Trees-Structure and Function 6: 232–235.
Florin, R. 1944. Die Koniferen des Oberkarbons und des Unteren Perms. Palaeontographica Abteilung B-Palaophytologie 85: 365–456.
Foster, C. and I. Metcalfe. 2002. Carbon isotopic composition of organic matter from non-marine Permian–Triassic boundary sections at Dalongkou and Lucaogou, Xinjiang, NW China. Geol. Soc. of Australia, Abstracts No. 68, First International Palaeontological Congress (IPC2002). pp. 56–57.
Foster, C. B. and S. A. Afonin. 2005. Abnormal pollen grains: an outcome of deteriorating atmospheric conditions around the Permian–Triassic boundary. Journal of the Geological Society Geological Society of London 162: 653–659.
Galfetti, T., P. A. Hochuli, A. Brayard, H. Bucher, H. Weissert and J. O. Vigran. 2007. Smithian-Spathian boundary event: Evidence for global climatic change in the wake of the end-Permian biotic crisis. Geology 35: 291–294.
Grauvogel-Stamm, L. 1978. La flore du Grès à *Voltzia* (Buntsandstein súperieur) des Vosges du Nord (France). Morphologie, anatomie, interprétations phylogénique et paléogéographique. Université Louis-Pasteur de Strasbourg Institut de Géologie 50: 1–225.
Gutiérrez, P. R., A. M. Zavattieri and M. Ezpeleta. 2017. Palynology of the la Veteada Formation (Lopingian) at its type locality, Famatina Range, la Rioja Province, Argentina. Spores. Ameghiniana 54: 441–464.
Hadley, A. *CombineZP*. GNU public license software. http://www.hadleyweb.pwp.blueyonder.co.uk/CZP/News.htm
Hermann, E., P. A. Hochuli, H. Bucher, T. Brühwiler, M. Hautmann, D. Ware and G. Roohi. 2011. Terrestrial ecosystems on North Gondwana following the end-Permian mass extinction. Gondwana Research 20: 630–637.
Hectors, K., E. Prinsen, W. De Coen, M. A. Jansen and Y. Guisez. 2007. *Arabidopsis thaliana* plants acclimated to low dose rates of ultraviolet B radiation show specific changes in morphology and gene expression in the absence of stress symptoms. *New Phytol*. **175**, 255–270.
Hochuli, P. A., E. Hermann, J. O. Vigran, H. Bucher and H. Weissert. 2010. Rapid demise and recovery of plant ecosystems across the end-Permian extinction event. Global and Planetary Change 74: 144–155.

Hochuli, P. A., A. Sanson-Barrera, E. Schneebeli-Hermann and H. Bucher. 2016. Severest crisis overlooked–Worst disruption of terrestrial environments postdates the Permian-Triassic mass extinction. Scientific Reports 6: 28372.
Hochuli, P. A., E. Schneebeli-Hermann, G. Mangerud and H. Bucher. 2017. Evidence for atmospheric pollution across the Permian–Triassic transition. Geology 45: 1123–1126.
Hunt, J. E. and D. L. McNeil. 1998. Nitrogen status affects UV-B sensitivity of cucumber. Functional Plant Biology 25: 79–86.
IUCN Red List of Threatened Species, *Summary Statistics* (http://www.iucnredlist.org/about/summary-statistics). Accessed 10 October 2016.
Klironomos, J. N. and M. F. Allen. 1995. UV-B-mediated changes on below-ground communities associated with the roots of *Acer saccharum*. Functional Ecology 9: 923–930.
Lavola, A., P. J. Aphalo, M. Lahti and R. Julkunen-Tiitto. 2003. Nutrient availability and the effect of increasing UV-B radiation on secondary plant compounds in Scots pine. Environmental and Experimental Botany 49: 49–60.
Leslie, A. B. 2008. Interpreting the function of saccate pollen in ancient conifers and other seed plants. International Journal of Plant Sciences 169: 1038–1045.
Leslie, A. B. 2010. Flotation preferentially selects saccate pollen during conifer pollination. New Phytologist 188: 273–279.
Lindström, S. and S. McLoughlin. 2007. Synchronous palynofloristic extinction and recovery after the end-Permian event in the Prince Charles Mountains, Antarctica: Implications for palynofloristic turnover across Gondwana. Review of Palaeobotany and Palynology 145: 89–122.
Looy, C. V., J. H. A. Van Konijnenburg-Van Cittert, H. Visscher. 2000. On the ecological success of isoetalean lycopsids after the end-Permian biotic crisis. LPP Contributions Series 13: 63–70.
Looy, C. V., R. J. Twitchett, D. L. Dilcher, J. H. Van Konijnenburg-Van Cittert and H. Visscher. 2001. Life in the end-Permian dead zone. Proceedings of the National Academy of Sciences of the United States of America 98: 7879–7883.
Looy, C. V. 2007. Extending the range of derived Late Paleozoic conifers: *Lebowskia* gen. nov. (Majonicaceae). International Journal of Plant Sciences 168: 957–972.
Mičieta, K. and G. Murín. 1996. Microspore analysis for genotoxicity of a polluted environment. Environmental and Experimental Botany 36: 21–27.
Millay, M. A. and T. N. Taylor. 1974. Morphological studies of Paleozoic saccate pollen. Palaeontographica Abteilung B-Palaophytologie pp. 75–99.
Mishra, S., N. Aggarwal and N. Jha. 2018. Palaeoenvironmental change across the Permian-Triassic boundary inferred from palynomorph assemblages (Godavari Graben, south India). Palaeobiodiversity and Palaeoenvironments 98: 177–204.
Møller, A. P. and T. A. Mousseau. 2006. Biological consequences of Chernobyl: 20 years on. Trends in Ecology & Evolution 21: 200–207.
Murali, N. S. and A. H. Teramura. 1985. Effects of ultraviolet-B irradiance on soybean. VI. Influence of phosphorus nutrition on growth and flavonoid content. Physiologia Plantarum 63: 413–416.
Newman, P. A., L. D. Oman, A. R. Douglass, E. L. Fleming, S. M. Frith, M. M. Hurwitz, S. R. Kawa, C. H. Jackman, N. A. Krotkov, E. R. Nash and J. E. Nielsen. 2009. What would

have happened to the ozone layer if chlorofluorocarbons (CFCs) had not been regulated?. Atmospheric Chemistry and Physics 9: 2113–2128.
Orlowska-Zwolinska, T. 1984. Palynostratigraphy of the Buntsandstein in sections of western Poland. Acta Palaeontologica Polonica 29.
Osborn, J. M. and T. N. Taylor. 1993. Pollen morphology and ultrastructure of the Corystospermales: permineralized *in situ* grains from the Triassic of Antarctica. Review of Palaeobotany and Palynology 79: 205–219.
Owens, J. N., S. J. Simpson and M. Molder. 1981. Sexual reproduction of *Pinus contorta*. I. Pollen development, the pollination mechanism, and early ovule development. Canadian Journal of Botany 59: 1828–1843.
Pandey, K. K., L. Przywara, P. M. Sanders. 1990. Induced parthenogenesis in kiwifruit (*Actinidia deliciosa*) through the use of lethally irradiated pollen. Euphytica 51: 1–9.
Pavlov, V. E., F. Fluteau, R. V. Veselovskiy, A. M. Fetisova and A. V. Latyshev. 2011. Secular geomagnetic variations and volcanic pulses in the Permian-Triassic traps of the Norilsk and Maimecha-Kotui provinces. Izvestiya, Physics of the Solid Earth 47: 402–417.
Peng, Y., J. Yu, Y. Gao and F. Yang. 2006. Palynological assemblages of non-marine rocks at the Permian–Triassic boundary, western Guizhou and eastern Yunnan, South China. Journal of Asian Earth Sciences 28: 291–305.
Potonié, R. 1962. Synopsis der Sporae in situ. Beihefte zum Geologischen Jahrbuch 52: 1–204.
Prevec, R., R. A. Gastaldo, J. Neveling, S. B. Reid and C. V. Looy. 2010. An autochthonous glossopterid flora with latest Permian palynomorphs and its depositional setting in the Dicynodon Assemblage Zone of the southern Karoo Basin, South Africa. Palaeogeography, Palaeoclimatology, Palaeoecology 292: 391–408.
Retallack, G. J. 1995. Permian-Triassic life crisis on land. Science 267: 77–80.
Romano, C., N. Goudemand, T. W. Vennemann, D. Ware, E. Schneebeli-Hermann, P. A. Hochuli, T. Brühwiler, W. Brinkmann and H. Bucher. 2013. Climatic and biotic upheavals following the end-Permian mass extinction. Nature Geoscience 6: 57–60.
Salter, J., B. G. Murray and J. E. Braggins. 2002. Wettable and unsinkable: the hydrodynamics of saccate pollen grains in relation to the pollination mechanism in the two New Zealand species of *Prumnopitys* Phil. (Podocarpaceae). Annals of Botany 89: 133–144.
Schneebeli-Hermann, E., P. A. Hochuli, H. Bucher, N. Goudemand, T. Brühwiler and T. Galfetti. 2012. Palynology of the Lower Triassic succession of Tulong, South Tibet—Evidence for early recovery of gymnosperms. Palaeogeography, Palaeoclimatology, Palaeoecology 339–341: 12–24.
Schneebeli-Hermann, E., W. M. Kürschner, H. Kerp, B. Bomfleur, P. A. Hochuli, H. Bucher, D. Ware and G. Roohi. 2015. Vegetation history across the Permian–Triassic boundary in Pakistan (Amb section, Salt Range). Gondwana Research 27: 911–924.
Schweitzer, H. J. 1996. *Voltzia hexagona* (Bischoff) Geinitz aus dem mittleren Perm Westdeutschlands. Palaeontographica Abteilung B-Palaophytologie 29: 1–22.
Scotese, C. R. 1997. *Continental Drift* (PALEOMAP Project, Arlington, ed. 7).
Srivastava, S. C. 1983. *Lelestrobus*: A new microsporangiate organ from the Triassic of Nidpur, India. The Palaeobotanist 32: 86–90.
Sullivan, J. H. and A. H. Teramura. 1992. The effects of ultraviolet-B radiation on loblolly pine. Trees-Structure and Function 6: 115–120.
Svensen, H., S. Planke, A. G. Polozov, N. Schmidbauer, F. Corfu, Y. Y. Podladchikov and B. Jamtveit. 2009. Siberian gas venting and the end-Permian environmental crisis. Earth and

Planetary Science Letters 277: 490–500.
Traverse, A. 2007. *Paleopalynology*. Springer, Dordrecht, ed. 2.
Tretyakova, I. N. and N. E. Noskova. 2004. Scotch pine pollen under conditions of environmental stress. Russian Journal of Ecology 35: 20–26.
U.S. Climate Data. (http://www.usclimatedata.com/climate/berkeley/california/unitedstates/usca0087/2013/5). Accessed 10 February 2014.
U.S. Naval Observatory, *Berkeley, California; Rise and Set for the Sun for 2013* (http://aa.usno.navy.mil/cgibin/aa_rstablew.pl?ID=AA&year=2013&task=0&state=CA&place=Berkeley). Accessed 10 February 2014.
UVMRP, UV irradiance estimator. UV-B Monitoring and Research Program. http://uvb.nrel.colostate.edu/UVB/da_interactiveMapSums.jsf. Accessed 19 September 2017.
Visscher, H. 1971. The Permian and Triassic of the Kingscourt outlier, Ireland: A palynological investigation related to regional stratigraphical problems in the Permian and Triassic of western Europe (Geological Survey of Ireland Special Paper).
Visscher, H., C. V. Looy, M. E. Collinson, H. Brinkhuis, J. H. Van Konijnenburg-Van Cittert, W. M. Kürschner and M. A. Sephton. 2004. Environmental mutagenesis during the end-Permian ecological crisis. Proceedings of the National Academy of Sciences of the United States of America 101: 12952–12956.
Wang, Z. Q. 2004. A new Permian gnetalean cone as fossil evidence for supporting current molecular phylogeny. Annals of Botany 94: 281–288.
Williams, C. G. 2009. *Conifer Reproductive Biology*. Springer Science & Business Media.
Williamson, C. E., P. J. Neale, G. Grad, H. J. De Lange and B. R. Hargreaves. 2001. Beneficial and detrimental effects of UV on aquatic organisms: implications of spectral variation. Ecological Applications 11: 1843–1857.
Wright, R. P. and R. A. Askin. 1987. *The Permian–Triassic Boundary in the Southern Morondava Basin of Madagascar as Defined by Plant Microfossils* (American Geophysical Union, Washington, D. C., pp. 157–166. vol. 41 of Geophysical Monograph Series.
Yu, J., J. Broutin, Z. Q. Chen, X. Shi, H. Li, D. Chu and Q. Huang. 2015. Vegetation changeover across the Permian–Triassic Boundary in Southwest China. *Earth-Sci. Rev*. 149: 203–224.
Zavialova, N. and E. Karasev. 2015. Exine ultrastructure of in situ *Protohaploxypinus* from a Permian peltasperm pollen organ, Russian Platform. Review of Palaeobotany and Palynology 213: 27–41.
Zi-qiang, W. 1996. Recovery of vegetation from the terminal Permian mass extinction in North China. Review of Palaeobotany and Palynology 91: 121–142.

## CHAPTER 1 TABLES

**Table 1.** Results of a two-mixed-factor nested ANOVA of malformed pollen frequencies. Significance of treatment and tree-specific effects were tested. Listed are sum of squares (*SS*), degrees of freedom (*df*), mean sum of squares (*MS*), *F*-statistic (*F*), and *p*-value. Data consisted of 4 treatments, with 3 trees each, 8 cones per tree and 600 pollen grains per cone analyzed for malformations. In the analysis, treatment type was treated as a fixed factor; which tree within each treatment was treated as random factor.

| | *SS* | *df* | *MS* | *F* | *p*-value |
|---|---|---|---|---|---|
| Treatment (fixed factor) | 30979 | 3 | 10326 | 22.301 | 0.00031 |
| Tree; nested in treatments (random factor) | 3704 | 8 | 463.04 | 2.3617 | 0.02414 |
| Within | 16469 | 84 | 196.06 | | |
| Total | 51152 | 95 | 538.45 | | |

**Table 2.** Summary of a pairwise, two-mixed-factor nested ANOVA of malformed pollen frequencies. The *F*-statistic is shown in the supra-diagonal part of both sub-tables; *p*-values in the sub-diagonal parts. Data consisted of 4 treatments, with 3 trees each, 8 cones per tree, and 600 pollen grains per cone analyzed for malformations. In the analysis, treatment type was treated as a fixed factor; which tree within each treatment was treated as random factor. Bold values refer to either significant differences between pairs of treatments, or significant differences between the trees within pairs of treatments. Numbers in the labels of enhanced UV-B treatments refer to the dosage of biologically effective UV-B at the top of the canopy, in $(kJ\ m^{-2}d^{-1})_{BE}$.

| | Treatment (fixed factor) | | | | Tree; nested in treatments (random factor) | | | |
|---|---|---|---|---|---|---|---|---|
| | Control 0 | UV-B 54 | UV-B 75 | UV-B 93 | Control 0 | UV-B 54 | UV-B 75 | UV-B 93 |
| Control 0 | | 0.016 | **51.158** | **16.155** | | **7.187** | **2.602** | **2.829** |
| UV-B 54 | 0.9063 | | **81.503** | **19.922** | **0.0002** | | 1.590 | **2.217** |
| UV-B 75 | **0.0020** | **0.0008** | | 1.619 | **0.0495** | 0.1947 | | 2.011 |
| UV-B 93 | **0.0159** | **0.0111** | 0.2722 | | **0.0364** | **0.0835** | 0.1104 | |

**Table 3.** Pollen malformation frequencies, percentages, and index per tree. Percentages rounded to the nearest tenth.

| Chamber treatment (kJ $m^{-2}d^{-1}$)$_{ave}$ | Tree | Pollen surveyed (n) | Σ Malformation frequency | % Malformed | Malformation index· | Malformation classes | | | | |
|---|---|---|---|---|---|---|---|---|---|---|
| | | | | | | 0 Sacci | 1 Saccus | 3 Sacci | 4 Sacci | ≥ 5 Sacci |
| Control [0] | PM03 | 4800 | 58 | 1.2 | 0.8 | 0 | 0 | 49 | 7 | 2 |
| Control [0] | PM17 | 4800 | 30 | 0.6 | 0.4 | 3 | 0 | 22 | 5 | 0 |
| Control [0] | PM23 | 4800 | 131 | 2.7 | 1.8 | 1 | 0 | 116 | 12 | 2 |
| 54 | PM15 | 4800 | 98 | 2.0 | 1.3 | 5 | 0 | 90 | 2 | 1 |
| 54 | PM36 | 4800 | 64 | 1.3 | 0.9 | 3 | 0 | 58 | 3 | 0 |
| 54 | PM44 | 4800 | 69 | 1.4 | 0.9 | 11 | 0 | 50 | 4 | 4 |
| 75 | PM38 | 4800 | 339 | 7.1 | 4.6 | 4 | 0 | 328 | 5 | 2 |
| 75 | PM52 | 4800 | 456 | 9.5 | 6.3 | 0 | 0 | 438 | 16 | 2 |
| 75 | PM54 | 4800 | 395 | 8.2 | 5.4 | 0 | 1 | 371 | 22 | 1 |
| 93 | PM10 | 4800 | 384 | 8.0 | 5.3 | 3 | 0 | 371 | 10 | 0 |
| 93 | PM28 | 4800 | 354 | 7.4 | 4.9 | 4 | 0 | 334 | 14 | 2 |
| 93 | PM42 | 4800 | 213 | 4.4 | 2.9 | 2 | 0 | 205 | 6 | 0 |

**Table 4.** Ovulate cone survivorship across treatments. Survivorship indicated by cones reaching stage 6. See (Fig. 4, A) for developmental stage descriptions, and (Fig. 4, B) for images of representative cones from each treatment. Percentages rounded to the nearest tenth.

| Stage reached | Treatments ($kJ\ m^{-2}d^{-1}$)$_{BE}$ | | | | | | | | | |
|---|---|---|---|---|---|---|---|---|---|---|
| | Control [0] | | Outdoor [7.2] | | 54 | | 75 | | 93 | |
| | Count | % | Count | % | Count | % | Count | % | Count | % |
| 1 | - | - | - | - | - | - | - | - | - | - |
| 2 | - | - | - | - | - | - | - | - | - | - |
| 3 | - | - | - | - | 12 | 25 | 37 | 77.1 | 14 | 28 |
| 4 | - | - | - | - | 36 | 75 | 11 | 22.9 | 36 | 72 |
| 4L | - | - | - | - | - | - | - | - | - | - |
| 5E | - | - | - | - | - | - | - | - | - | - |
| 5L | 1 | 1.7 | 5 | 8.3 | - | - | - | - | - | - |
| 6 | 59 | 98.3 | 55 | 91.7 | - | - | - | - | - | - |
| Σ no. ovulate cones | 60 | | 60 | | 48 | | 48 | | 50 | |

**Table 5.** Temperature settings during growth chamber experiment. Temperatures based on U.S. Climate Data for Berkeley, CA, US (US Climate Data). Temperatures rounded to the nearest tenth.

| Interval, 2013 | Average high (C) $T_{HIGH}$ | Average low (C) $T_{LOW}$ | Mean (C) $T_{AVE}$ | Chamber day setting (C) $T_{AVE}$ | Chamber night setting (C) $T_{LOW}$ |
|---|---|---|---|---|---|
| March–April | 20.0 | 7.9 | 14.0 | 14.0 | 8.0 |
| May | 22.7 | 10.1 | 16.4 | 16.0 | 10.0 |

**Table 6.** Photoperiod settings during growth chamber experiment. Photoperiods based on estimations of sunrise and sunset times for Berkeley, CA, US (US Naval Observatory). Values listed in hours : minutes. Chamber photoperiod rounded to the nearest half hour.

| Interval, 2013 | Estimated photoperiod (first day of interval) | Estimated photoperiod (last day of interval) | Averaged photoperiod | Chamber photoperiod |
|---|---|---|---|---|
| March/April pooled | 11:23 | 13:45 | 12:37 | 12:30 |
| May | 13:47 | 14:36 | 14:12 | 14:00 |

## CHAPTER 1 FIGURES

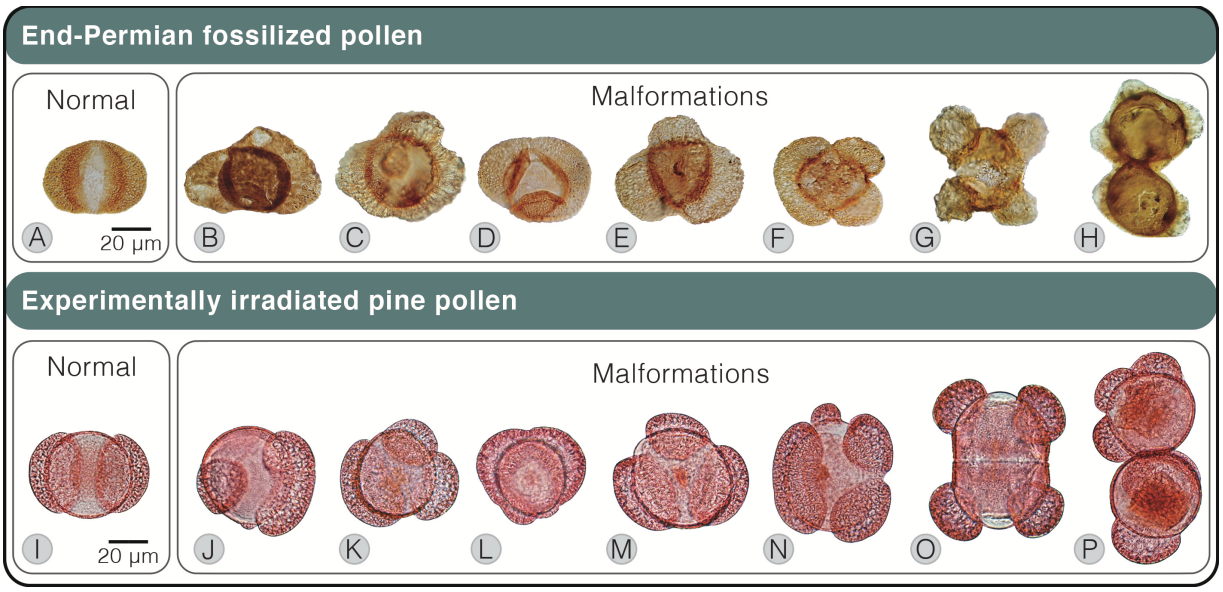


**Figure 1.** Normal and malformed bisaccate pollen. (A–H) Fossilized pollen of end-Permian gymnosperms from the Guodikeng Formation, Dalongkou section, North China (A–G) and Nedubrovo, Russia (H). (A) *Alisporites* sp., bisaccate. (B) Bisaccate indet., possibly taeniate with asymmetric sacci. (C) *Klausipollenites* sp., trisaccate. (D–F) *Alisporites* sp., trisaccate. (G) *Klausipollenites schaubergeri*, tetrasaccate dyad. (H) *K. schaubergeri*, fused pollen including a trisaccate. (I–P) Pollen of modern pine (*Pinus mugo* 'Columnaris') irradiated with modeled end-Permian UV-B regimes. (I) Bisaccate. (J) Trisaccate grain with enlarged saccus. (K) Trisaccate grain with enlarged saccus. (L) Trisaccate grain with fused sacci. (M) Trisaccate grain. (N) Tetrasaccate grain. (O) Tetrasaccate dyad. (P) Fused grains, one trisaccate. (A–H) Accession notation: *Sample-slide; England finder coordinate*. (A) 6403373-8; H35. (B) 6403369-8; W40. (C) 6403361. (D) 6403373-8; L34. (E) 6403400-2; T18/3. (F) 6403400-12; N24/3. (G) 6403381-11; Y24/2. (H) 4748/36; N33. Specimens with accession number starting with 640– are housed at Geoscience Australia while 4748– are housed at the Palaeontological Institute, Moscow. Fossilized pollen images courtesy of S. Afonin. Grains published: (A, E–G) Fig. 4 in (Foster and Afonin, 2005). (H) (Foster and Metcalfe, 2002). (I–P) Notation: *Specimen-slide; England finder coordinate, treatment*. (I) 200778-200505; T45-3, 93 (kJ m-2d-1)$_{BE}$. (J) 200779-200684; P47-3, 54 (kJ m-2d-1)$_{BE}$. (K) 200780-200715; L47, 75 (kJ m-2d-1)$_{BE}$. (L) 200781-200746; P45, 75 (kJ m-2d-1)$_{BE}$. (M) 200782-200714; L45-2, 75 (kJ m-2d-1)$_{BE}$. (N) 200783-200743; M40, 75 (kJ m-2d-1)$_{BE}$. (O) 200784-200661; N42-4, 54 (kJ m-2d-1)$_{BE}$. (P) 200785-200568; N44, 54 (kJ m-2d-1)$_{BE}$. *P. mugo* pollen was collected from cones under accession 200281. Extended depth of field (EDF) images were generated using CombineZP by J.P.B.

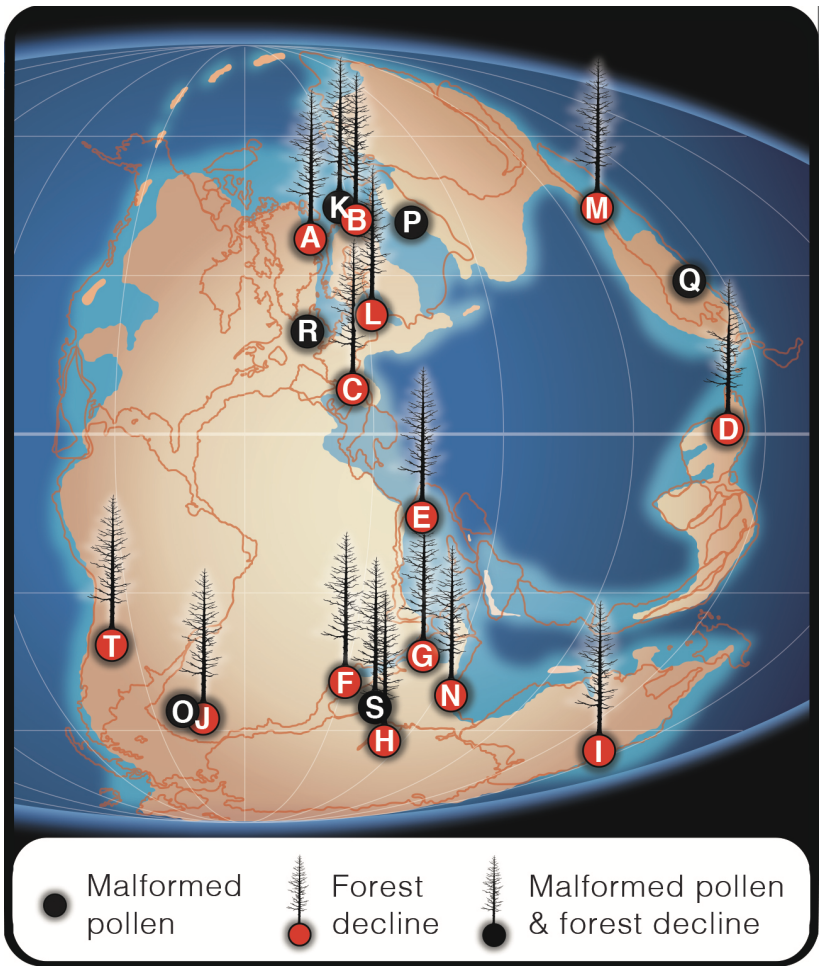


**Figure 2.** Paleogeographic distribution of Permian-Triassic palynomorph sequences featuring forest decline and/or pollen malformations. Gymnosperm turnover documented directly (A–K, S) and indirectly through sequences displaying gymnosperm recovery following lycopsid spore spikes (L–N, T). (A) East Greenland (Looy et al. 2001). (B) Southern Barents Sea (Hochuli et al. 2010). (C) North Italy (Cirilli et al. 1998). (D) Southwest China (Peng et al. 2006; Yu et al. 2015). (E) Israel (Eshet et al. 1995). (F) Madagascar (Wright and Askin, 1987). (G) Pakistan (Schneebeli-Hermann et al. 2015; Hermann et al. 2011). (H) West Antarctica (Lindström, S. McLoughlin, 2007). (I) Australia (Retallack, 1995). (J) South Africa (Aitkin, 1998). (K) Norway and Central Barents Sea (Hochuli et al. 2017, Galfetti et al. 2012). (L) Western Poland (Orlowska-Zwolinska, 1984). (M) North China (Zi-qiang, 1996). (N) South Tibet (Schneebeli-Hermann et al. 2012). (O) South Africa (Prevec et al. 2010). (P) Nedubruvo, Russia (Foster and Afonin, 2005). (Q) North China (Foster and Afonin, 2005). (R) Ireland (Visscher, 1971). (S) South India (Mishra et al. 2017), (T) Argentina (Gutiérrez et al. 2017), Late Permian paleogeographic reconstruction adapted from (Scotese, 1997).

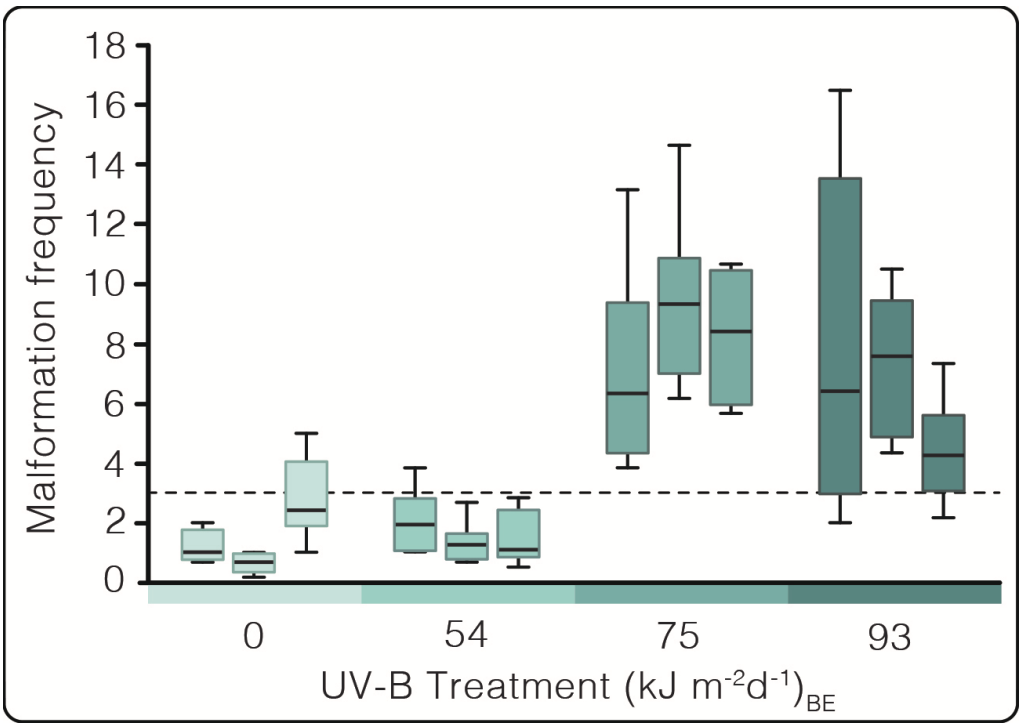


**Figure 3.**
Boxplots represent individual tree specimen pollen yields. Tree specimens in the following order–left to right. Notation: species-specimen number. Species: *Pinus mugo* (PM). (Control [0 (kJ $m^{-2}d^{-1})_{BE}$]): PM03, PM17, PM24. (54 (kJ $m^{-2}d^{-1})_{BE}$): PM15, PM36, PM44. (75 (kJ $m^{-2}d^{-1})_{BE}$): PM38, PM52, PM54. (93 (kJ $m^{-2}d^{-1})_{BE}$): PM10, PM28, PM44. Lower and upper limits of the boxes correspond with first and third quartiles (based on interpolation), the horizontal line in each box represents the median, and whiskers give minimum and maximum values in the data. See results in table S1 and summary in table S2 for two-mixed-factor nested ANOVA.

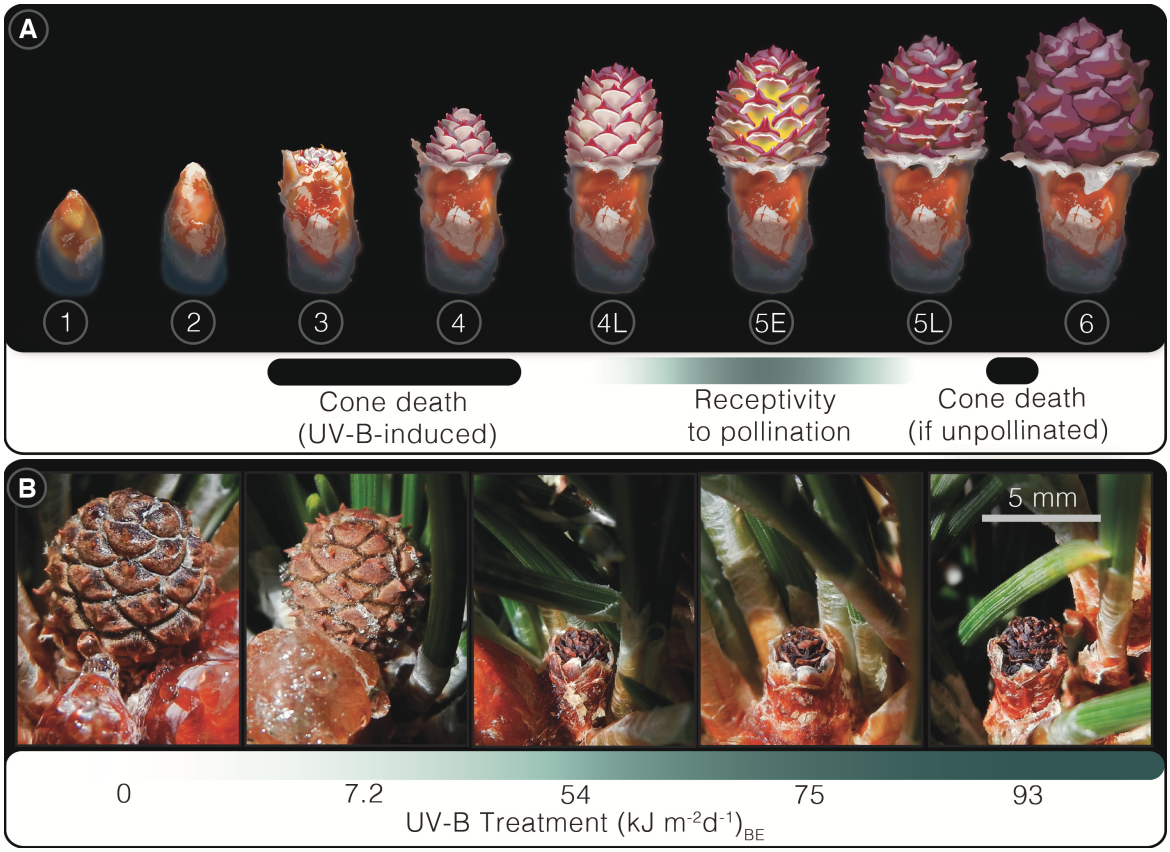


**Figure 4.** Ovulate cone developmental stages in (*Pinus mugo*). (A) Schematic of ovulate cone developmental stages in *Pinus mugo*. Stage descriptions: (1–2) Bud enclosing cone expands. (3) Cone emergence from bud scales. (4) Cone extends. (4L) Extension is completed, but ovuliferous scales (purple) are not fully opened. (5E) Ovuliferous scales perpendicular to cone axis—enabling pollen access to ovules. (5L) Ovuliferous scales swell, intercepting pollination. (6) Ovuliferous scales swollen completely, blocking pollen access to ovules ( Bramlett and O'Gwynn 1980). (B) Images of select ovulate cones from each treatment showing a typical developmental stage ~70–76 days following emergence. Treatments correspond to growth chamber control [0], outdoor ambient [7.2] and end-Permian modeled [54, 75, 93] UV-B regimes. Stages in (A) compiled based on controlled pollination studies of *Pinus* (Cumming and Righter, 1948; Bramlett and O'Gwynn 1980; Bramlett and O'Gwynn 1981) amended with substages of 4 and 5 (Williams, 2009; Owens et al. 1981). Digitally vectored illustrations rendered by J.P.B. using Adobe Illustrator® CS6 (San Jose, CA, US).

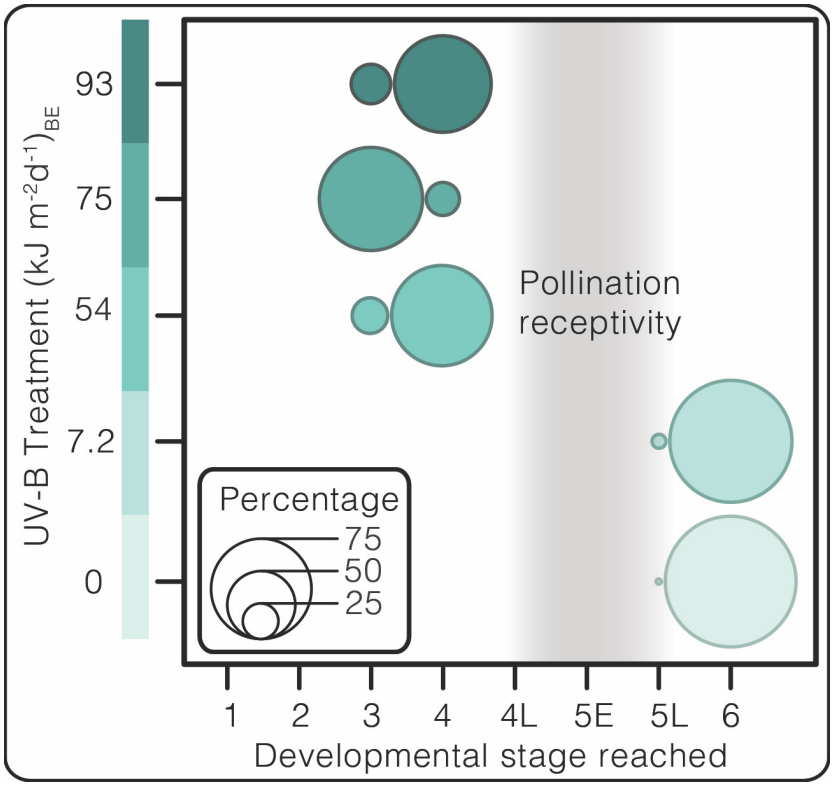


**Figure 5.** UV-B impacts on ovulate cone survivorship in pine (*Pinus mugo*). Bubble chart displaying *P. mugo* 'Columnaris' ovulate cone survivorship by displaying the percentages of cones reaching their furthest developmental stage per treatment population (n= 48 to 60). See table 4 for ovulate cone data.

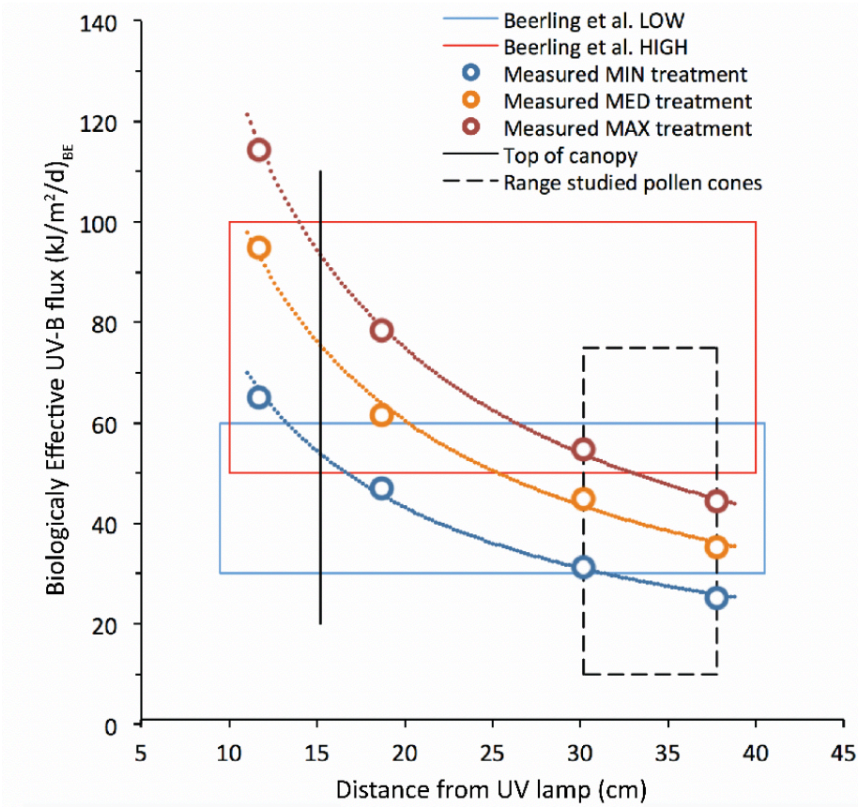


**Fig. 6.** Biologically effective UV-B fluxes versus distance from UV-B lamps in growth chamber experiments. MIN, MED and MAX refer to the three treatment levels of enhanced UV-B irradiation. Red and blue boxes indicate the range of fluxes in the highest and lowest irradiation scenarios modeled for the end-Permian (Beerling et al. 2007). The vertical black line indicates the position at the average top of tree canopies while the black dashed box represents the distance range from the lamp from which pollen cones were analyzed. Open circles give the measured BE UV-B flux values, dotted curves represent the modeled relation between BE UV-B flux and distance ($y = 485\ x^{-0.807}$, $y = 678\ x^{-0.807}$ and $y = 840\ x^{-0.807}$ for MIN, MED and MAX, respectively).

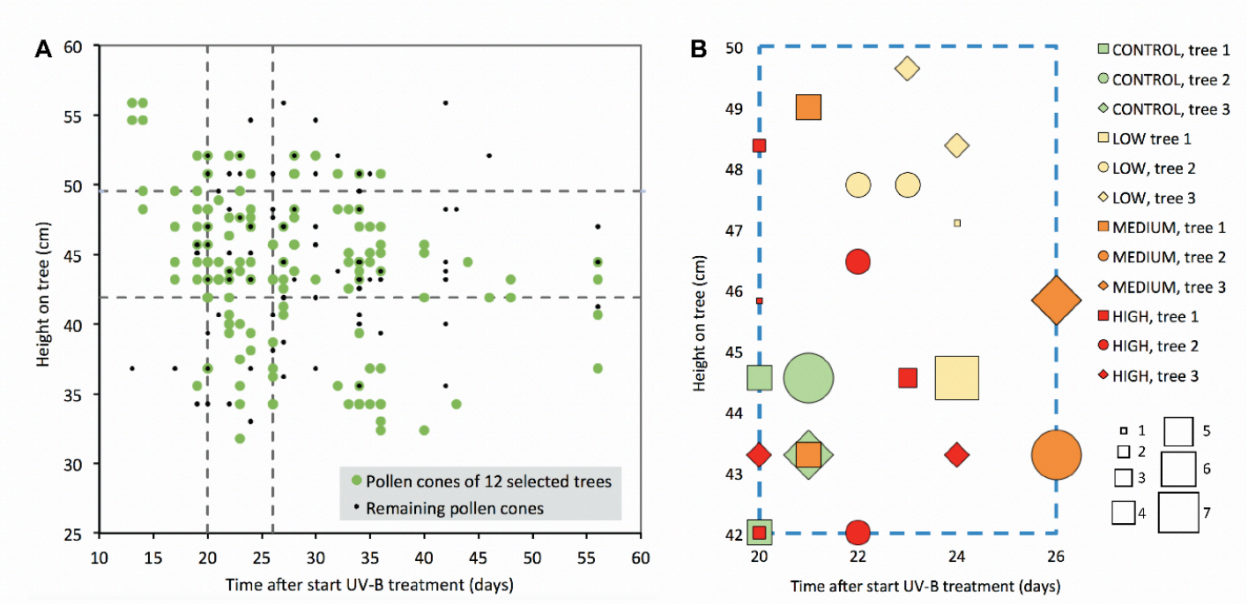


**Fig. 7.** Pollen cone subsampling strategy. (A) Collection timing and canopy height of the 634 pollen cones that developed during the experimental period. Several cones were harvested on the same day and from the same height on the tree resulting in overlapping data points. (B) Collection timing and canopy height of the 96 pollen cones selected for further study. The symbol size refers to the number of cones of a particular tree harvested on the same day and canopy height.

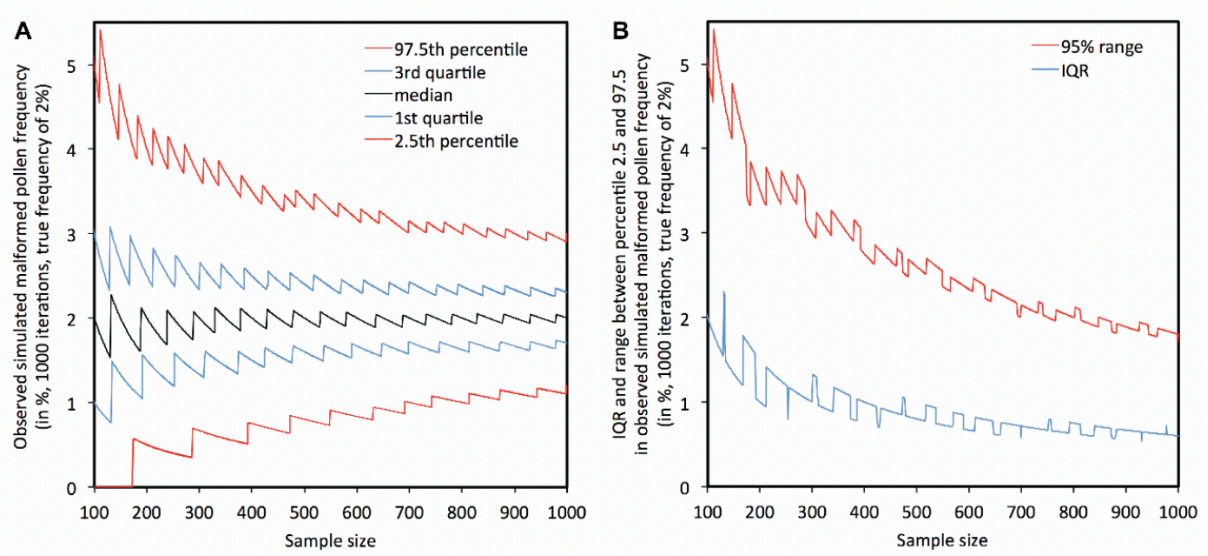


**Fig. 8.** Sample size and accuracy of malformed pollen frequency determination. During *in silico* simulations we simulated pollen subsamples of various sizes (100–1000 grains), in which each grain had 2% chance of being malformed. Each of the 901 different sample sizes was replicated 1000 times. (A) Frequency summary of observed malformation frequencies in simulated pollen subsamples. Various percentiles of observed simulated pollen malformation frequencies versus sample size are indicated. (B) Difference between the first and third quartile (interquartile range, or IQR) and between the 2.5$^{th}$ and 97.5$^{th}$ percentile (95% range) versus sample size.

# CHAPTER 2

## Growth responses of *Isoëtes howellii* Engelmann to elevated UV-B exposure


## ABSTRACT

During the largest extinction event in Earth history, the end-Permian biotic crisis, palynological records show intervals of widespread gymnosperm pollen decline and a concomitant increase in the otherwise rare spores of isoetalean lycopsids. These floral turnovers coincide with widespread appearance of abnormal palynomorphs from both receding gymnosperms and the isoetaleans that rise to dominance. It is hypothesized that these signals indicate elevated ultraviolet-B (UV-B) radiation exposure resulting from volcanogenic deterioration of the stratospheric ozone layer. However, it is unknown whether elevated UV-B levels have adverse effects on lycopsid survival and fitness during ozone weakening events. We experimentally tested whether elevated UV-B exposure affected survivorship, as well as vegetative and reproductive growth responses in *Isoëtes howellii* Engelmann under three UV-B regimes modeled for the end-Permian. Elevated UV-B regimes did not impact survivorship of *I. howellii* but resulted in a greater reduction in corm area (i.e. use of stored reserves) and fewer sporophylls/sporangia produced when compared with non-irradiated control specimens. In addition, irradiated plants tended to produce more megasporangia and fewer microsporangia than the control specimens. In all sporangia sampled, phenotypically normal mega- or microspores were recovered. Heightened UV-B is therefore an environmental challenge that can impose acute reproductive selective pressures on gymnosperms, but not necessarily isoetaleans—although it does seem to represent a greater source of ecological stress for isoetaleans.

## INTRODUCTION

The stratospheric ozone layer plays a vital role in intercepting harmful biologically effective ultraviolet-B radiation (BE UV-B; 280–320 nm; see: Caldwell, 1971) from reaching the Earth's surface. However, anthropogenic influences have caused its strength to fluctuate over the last century (Farman et al. 1985), and, long-term consequences of elevated UV-B exposure on global vegetation are unclear. The fossil record may provide examples of such UV-induced vegetation responses. Paleoatmospheric modelling studies coupled with geochemical investigations in Siberia have shown that organohalogen release from sediments heated during massive flood basalt emplacement within the Siberian Traps large igneous province likely caused global deterioration of the stratospheric ozone layer during the end-Permian crisis (Beerling et al. 2007; Svensen et al. 2009; Black et al. 2014; Broadley et al. 2018). Besides disappearance of several seed plant lineages (e.g. McElwain and Punyasena, 2007), direct signals of environmental stress experienced by plants are recorded as increased presence of seed plant pollen malformations (Foster and Afonin, 2005) and unseparated tetrads of lycopsid spores (Visscher et al. 2004; Looy et al. 2005). Independent of the of the paleoatmospheric and geochemical research, both Visscher et al. (2004), and Foster and Afonin (2005) proposed increased UV-B radiation exposure as a potential cause of pollen malformations and unseparated spore tetrads. These signals are interpreted to reflect reproductive distress in end-Permian floras as abnormal morphology is associated with pollen viability reduction in modern conifers (Wilson, 1965; Sirenko, 2001). Furthermore, in an experimental setting, elevated UV-B regimes modeled for the end-Permian by Beerling et al. (2007) have been found to induce increased production of pollen malformations as well as premature death of ovules in the modern conifer *Pinus mugo* 'Columnaris' (Benca et al. 2018).

While pollen malformations are a potential indicator of reduced fertility in the fossil record (Benca et al. 2018), the wall ultrastructure of lycopsid spores isolated from end-Permian tetrads indicates that they were mature and, besides being clustered in tetrad arrangement, show no sign of abnormal development (Looy et al. 2005). Spores in these unseparated tetrads were produced by members of the family Pleuromeiaceae, a lineage of the heterosporous isoetalean clade—known from dispersed cavate microspore genera *Densoisporites* and *Lundbladispora*, and by a less known lycopsid lineage that produced the microspore *Uvaesporites* (Looy et al. 2005). *Lundbladispora* species have been found *in situ* in the fossil genera *Pleuromeia* (Lugardon et al. 1999), *Annalepis* (Lugardon et al. 2000; Grauvogel-Stamm and Lugardon, 2001) and are also associated with fossil remains of *Viatcheslavia* Zalessky 1936 (Naugolnykh, 2001; Naugolnykh and Zavialova, 2004). During the global biotic crisis these early Mesozoic isoetaleans were widely distributed across Euramerica, Cathaysia and Gondwana (e.g., Wang 1996, Retallack, 1997; Grauvogel-Stamm, 1999; Grauvogel-Stamm and Ash, 2005). In palynological assemblages from shallow marine sediments, the first change from pollen to spore dominated assemblages corresponds with the collapse of marine ecosystems at the end of the Permian (e.g., Twitchett et al. 2001; Looy et al., 2001). Subsequent records show similar declines and/or turnover in gymnosperm pollen diversity and abundance. Study of this

widespread pattern of lycopsid dominance accompanying gymnosperm recessions suggested that isoetalean members of this lineage may have had a number of physiological and life history traits that gave them an advantage under environmental challenges during the crisis and its aftermath (Looy et al. 2001).

The Early Triassic *Pleuromeia sternbergii* is the best-known taxon within the lineage (Grauvogel-Stamm, 1999). This species had an unbranched, erect shoot with a cormose base, helically-arranged lanceolate succulent leaves, and a terminal strobilus (Grauvogel-Stamm, 1999). Despite difference in size, fossilized *P. sternbergii* specimens bear remarkably similar foliar anatomical and morphological functional traits to the last living members of this group today; the quillworts (genus *Isoëtes*; Looy, 2000). *Isoëtes* is also the only living plant group to have a spore wall ultrastructure nearly identical in complexity and organization to that of members of the Pleuromeiaceae (e.g., Tryon and Lugardon, 1991; Lugardon et al. 1999; Looy et al. 2005).

Understanding how modern isoetaleans respond to elevated UV-B regimes in the present could help determine whether past ozone weakening events restructured plant communities through imposing environmental challenges that Pleuromeiaceae were better-equipped to handle than gymnosperms. However, it is unknown whether living isoetaleans are capable of surviving and producing spores under elevated UV-B exposure. In this study, we addressed this knowledge gap by using the terrestrial species *Isoëtes howelii* Engelmann as an extant counterpart to the extinct Pleuromeiaceae. We grew *I. howelii* under control [non-irradiated] conditions and three UV-B radiation regimes modeled for the end-Permian (Beerling et al. (2007). This experiment was designed to test whether elevated UV-B exposure has an effect on (1) survival and vegetative growth- and (2) the production of megasporophylls and microsporophylls (sporangium-bearing leaves) in *I. howellii*.

## METHODS

### Rationale for species selection

Our experimental set-up aimed to address whether extinct isoetaleans may have been capable of surviving and reproducing under UV-B regimes modelled for the end-Permian biotic crisis. *Isoëtes howellii* was selected as a suitable modern counterpart to extinct Permian and Triassic members of the Pleuromeiaceae, being a readily-accessible, large (up to 60 cm-diameter rosette) terrestrial species that naturally grows under bright, full sunlight in seasonally dry vernal pools. Similarly, *in situ* deposits of *Pleuromeia sternbergii* show that this extinct isoetalean occupied semi-arid to wetland habitats in basinal lowlands across their range (Zi-Qiang, 1996; Retallack, 1997; Grauvogel-Stamm,1999; Grauvogel-Stamm and Ash, 2005).

**Experimental design**

Source plants for the experiment were collected from Hidden Lake in the Mount Burdell Open Space, Marin County, CA. Eighty *Isoetes howellii* specimens were collected as dormant subterranean corms from the dried lakebed on 21 August 2016. Specimens were excavated from the lakebed using a garden trowel. Corms were placed in 2-gallon plastic bags (Ziploc®, Dow Chemical Co., Midland, MI, US), left open to dry in a ~22 ˚C laboratory for two days. Specimen bags were then sealed shut and kept under dark conditions for 163 days in a 5 ˚C cold-room. After the cold-treatment, corms were assigned specimen numbers (IH01–IH80). Apart from the central-most, scale-like leaves sheathing the shoot apex, all senesced leaves and roots from previous years were removed. Being circular to elliptic when viewed from the apical pole, defoliated corm diameter was measured in two axes using stainless steel electronic digital calipers (01407A, Neiko Tools, US). The maximum corm area was estimated by standardizing the measured surface to an oval using the following equation:

$$\mathrm{A} = \pi\left(\tfrac{1}{2}d_1 \times \tfrac{1}{2}d_2\right)$$

Where A is the corm area standardized to an oval, $d_1$ is the diameter perpendicular to the corm furrow, and $d_2$ is the diameter parallel to the corm furrow. 64 corms were selected for the experiment, and assigned randomly to 32 15.5 cm wide × 13 cm tall terra cotta pots (Pennington, NorCal, Italy). Two corms were planted in each pot, assigned randomly on the basis of corm area via a randomized number generator in Microsoft Excel (Microsoft). Prior to planting, pots were labelled with a designated number using a #2 pencil on the lower exterior of each pot side. The pot number was also written on the outer surface of the pot lip using either black or red oil paint marker pens (Sharpie®). Pots were partially filled to 9 cm deep with fine-grained mineral substrate (sandy loam; American Soil and Stone, Richmond, CA, US).

Each corm was rinsed with industrial tap water (pH 8.4–8.9) to remove spores from previous growing seasons and detritus, then placed on the sandy loam surface and misted with tap water. Each corm was oriented upward (so that the shoot apex would initiate negatively geotropic growth), toward one side of the pot. The outer periphery of each corm was spaced 2 cm from the pot rim at the substrate surface. Two corms were planted per pot, aligned on sides opposite one another, perpendicular to the pot label axis. Plastic plant labels with specimen number were inserted into the substrate against the pot wall closest to each specimen. Each pot was then filled with an additional 4 cm of dry sandy loam, ensuring both corms and labels were completely buried. Specimen labels were buried to prevent UV-B-induced degradation of plastic and associated volatile release.

Four groups of eight pots were assigned to a control (non-irradiated) group, and three groups supplemented with biologically effective (BE) UV-B radiation [54 (kJ $m^{-2}d^{-1})_{BE}$, 75 (kJ $m^{-2}$ $d^{-1})_{BE}$, and 93 (kJ $m^{-2}$ $d^{-1})_{BE}$] respectively. These UV-B fluxes correspond with increased

near-surface UV-B irradiance deviating from a modeled Late Permian baseline of 10–20 (kJ m-2 d-1)BE under various reductions in stratospheric ozone column thickness. Specifically, the lowest UV-B regime corresponds with a paleo-atmospheric modeling scenario in which the total estimated volume of Siberian trap and organohalogen emissions was released over a longer time span [over 400 kyr]. In contrast, the two higher UV-B regimes correspond with modeling scenarios in which the same total volume of Siberian Trap and organohalogen emissions was released into the atmosphere over a shorter time interval [<200 kyr], resulting in greater reduction in stratospheric ozone column thickness (Beerling et al. 2007). These UV-B fluxes were recorded from the potted substrate surface height (13 cm above the chamber floor, 31.5 cm from the UV-B-emitting lamp surface). UV-B measurements were conducted using a UV-B sensor and handheld radiometer calibrated before the experiment in Fall, 2016 (SKU 430; Apollo Display Meter; Skye Instruments Ltd., United Kingdom). These three BE UV-B regimes correspond with 2.5×, 3.5× and 4.3× the estimated mean biologically effective (Caldwell-adjusted sum; Caldwell, 1971) daily outdoor UV-B fluxes for the source locality [Hidden Lake, Marin Co. CA] from February through September—21.6 (kJ $m^{-2}$ $d^{-1}$)$_{BE}$ (UVMRP). However, this growing season mean BE UV-B estimate is considerably higher than the estimated spring BE UV-B fluxes experienced by *I. howellii* during sporogenesis in its natural habitat [~7 kJ $m^{-2}$ $d^{-1}$)$_{BE}$], because of the influence of substantially higher fluxes estimated for the summer and early autumn months in the calculation.

The experiment was conducted in a custom-constructed growth chamber at the Oxford Tract Research Facility, University of California Department of Plant and Microbial Biology, Berkeley, California. The rectangular chamber interior measured 9.8 $m^2$ [2.49 m long × 1.28 m wide × 1.36 m tall], was outfitted with four cool white fluorescent light tubes (Sylvania 25248: P48T12/CW/VHO) transversely-oriented in pairs on opposite sides of the chamber, and 32 longitudinally-oriented fluorescent tubes (Sylvania OCTRON 3500k F096/735/HO). The chamber was equipped with four service doors, facilitating access to each of the four sample groups.

Pots in the non-irradiated control and three irradiated treatment groups were arranged in two rows [four pots per row] placed in 65.4 cm long × 45.1 cm wide × 7.6 cm tall molded fiberglass dough trays (870008 5136; MFG Tray Co., Linesville, PA, US) filled to 3 cm deep with industrial tap water (pH 8.4–8.9). The plants were therefore sub-irrigated throughout the experiment and the substrate surface was never touched nor top-watered to prevent disturbance or exposure of buried corms to light. The water level of basins was maintained twice weekly using a hose. The chamber control group was provided no supplemental UV-B radiation (0 (kJ $m^{-2}$ $d^{-1}$)$_{BE}$). The three treatment groups were each provided two parallel 120 V fluorescent UV-B lamps; each containing two broadband tubes with a 312 nm emission peak and 281–405 nm spectral output (XX-15B; Spectronics Corporation, Westbury, NY, USA). Emitting surfaces of the lamps were suspended 43.5 cm above the chamber floor (31.5 cm above the substrate surface) from frames constructed of bolted galvanized steel slotted angles (G2195803; Zoro Tools®, Buffalo Grove, IL, US). The sides of the steel frame for each treatment group were

shielded by four panels of 3 mm-thick clear UV-B-resistant acrylic panels (Acrylite®, TAP Plastic, CA, US). These Acrylite Acrylic panels prevented escape of direct and reflected UV-B radiation from each treatment group to neighboring specimen groups in the chamber.

The UV-B-emitting surface of each lamp was covered by a 0.003 mm-thick fresh sheet of clear, cellulose acetate (Grafix™; Ohio, USA) to intercept UV wavelengths shorter than the spectrum reaching Earth's surface (< ~295 nm) (Williamson et al. 2001). These filters were replaced biweekly [Wednesdays and Sundays], to avoid UV-induced degradation of the cellulose acetate. UV-B intensity was attenuated in the 54 and 75 $(kJ\ m^{-2}\ d^{-1})_{BE}$ treatments by covering emitting surfaces of lamps with aluminum mesh screen (1.5 $mm^2$ mesh size) (Phifer Inc., Alabama, USA). Two sheets of mesh were stacked offset for the 54 $(kJ\ m^{-2}\ d^{-1})_{BE}$ treatment, and one sheet for the 75 $(kJ\ m^{-2}d^{-1})_{BE}$ treatment. Lamps in the 93 $(kJ\ m^{-2}\ d^{-1})_{BE}$ treatment therefore were only shielded by cellulose acetate.

Treatments ran for 204 photoperiods [13 February 2017 to 5 September 2017]. Photosynthetically Active Radiation [PAR] and UV-B photoperiod were gradually adjusted over the months to simulate natural photoperiod and average February through September temperatures at the source locality (Novato, CA, US; Table 1). Photoperiods were programed to occur at night to minimize interference with radiation treatments by daily rotations. Chamber day and night temperatures were programmed to simulate climatic conditions recorded near the source locality from January–August, 2017, [the last growth season specimens experienced in the field prior to the experiment] rather than typical greenhouse conditions. These settings were chosen because *Isoëtes* spp. do not produce spores consistently under static climatic conditions typical of greenhouses (J. Benca, pers. obs.). Day temperatures were therefore adjusted each month of the experiment to simulate monthly average high temperatures-, while night temperatures were set to simulate monthly average low temperatures for Novato, CA (Table 1). However, night temperatures were programmed to 10°C throughout the experimental duration because all monthly average low temperatures recorded in Novato were <10°C and the environmental chamber in which the experiment was conducted could not sustain temperatures below 10°C. Both day and night temperatures were increased at the end of the experiment to expedite drying of the substrate and induce annual drought dormancy in the plant specimens (Table 1).

Plants emerged from dormant corms during the treatment. Their first leaf tissues to emerge therefore experienced control or treatment conditions. Emergence date was recorded for nearly all specimens. Each growth chamber group and individual specimens were photographed weekly throughout the experimental duration. Pigmentation of plants throughout the study was captured by photographing treatment groups alongside a visual color reference card (43232102 ColorChecker Classic; X-Rite, Inc., Grand Rapids, MI, US) using a digital camera (Coolpix S8100; Nikon Corp., Minato, TKY, JP).

On 20 August 2017; 16 days before the treatment ended on 5 September 2017, no more water was added to the basins and a drying period was initiated to stimulate seasonal dormancy as would occur in the ephemeral pool habitat of *I. howellii*. After the UV-B treatment ended, plants were left in the growth chamber for five days [6 September 2017 to 11 September 2017] under the same PAR photoperiod, but increased day and night-time temperatures to speed drying and discourage fungal establishment on corms going into dormancy (see Table 1).

**Harvesting specimens and sporangia**

Plants were excavated using a trowel on 11 September 2017. Specimens were removed carefully by carving a 5–6 cm deep plug of dried substrate ~1–2 cm outside the circumference of each subterranean corm and levered out of the substrate. The surrounding substrate plug was removed, excess substrate manually brushed off, and placed in a 1 qt sealed plastic bag (Ziploc®). The bag was labeled with specimen number, pot number and specimen orientation [left or right side of pot] using a permanent marker (Sharpie®). Specimens were transported from growth chamber facilities to the lab, removed from their bags and left exposed on a lab bench to dry for four days. Drying was necessary to prevent fungal infection of sporangia. After drying, all dried roots were removed from the corm and sporophylls clipped to ~2–4 cm from the sporangium base [ensuring sporangia remained intact on the plant] using straight blade, sharp-pointed dissecting scissors (Fisherbrand™) to aid in maneuverability of specimens during leaf and sporangium extraction.

All leaves but those sheathing living leaves at the plant center were removed and counted. *I. howellii* typically produces four types of leaves throughout a growing season in two forms: sterile lycophylls, and sporangia-bearing sporophylls; (1) the outermost whorls of black, non-photosynthetic subterranean scale lycophylls that sheath the earliest-emerging leaves at the beginning of the growing season, (2) the earliest-emerging sterile photosynthetic lycophylls, (3) megasporophylls [with megasporangia at the base] produced during the early to mid- growth season, and (4) microsporophylls [with microsporangia at the base] produced at the end of the growth season. Aborted mega- and microsporangia (indicated by flattened, shriveled sporangia with little to no visible contents), were also enumerated when present.

Megasporangia and microsporangia were sampled sequentially from the outermost to innermost whorls and counted as separate chronologies, since megasporangia usually were produced earliest in the season followed by a later zone of microsporangia toward the interior of the leaf spiral. Sequential labeling in order of acropetally successive (older to younger) sporophylls enabled subsequent selection of sporangia toward the beginning, middle and end of the spore-production window in each treatment group for future micro- and megaspore viability assessment. Since the outermost whorls of sporophylls [and sporangia] yield the most mature spores (Taylor and Luebke, 1986) the earliest sporophylls in collection sequence had the greatest chance of yielding spores that were viable at harvest. The leaves, corm, and bags containing microcentrifuge tubes of isolated sporangia were placed in a larger specimen bag, labeled with specimen number, pot number, orientation within the pot, and date extracted using a permanent

marker (Sharpie®). Specimen bags were then stored dry at 4.0 °C in a walk-in cold room so that future micro- and megaspore viability experiments could be pursued.

**Analyses**

Thirteen traits comparisons were observed between I. howellii specimens in the control and three elevated UV-B regimes: (1) corm area before the experiment, (2) corm area following the treatment, (3) percent reduction in corm area during treatment, (4) number of days between hydration and corm (leaf) emergence, (5) number of sterile scale lycophylls producted, (6) number of sterile photosynthetic lycophylls produced, (7) total number of sterile lycophylls (scale + photosynthetic lycophylls) produced, (8) number of megasporangia produced, (9) number of microsporangia produced, (10) total number of sporophylls produced, (11) percentage of sporophylls within specimens that are megasporophylls, (12) percentage of sporophylls within specimens that are microsporophylls, and (13) the number of sporophylls with aborted sporangia. One-way ANOVAs and combined box- and jitterplots were generated using the ggplot2 package (Wickham, 2016) in R (R Development Core Team, 2010).

**RESULTS**

In total, 60 of 64 dormant specimens collected from the field emerged from dormancy under growth chamber settings at the start of the experiment. The first leaves emerged from the substrate 8–18 days after being hydrated under experimental settings. There are significant ($p < 0.05$) differences in emergence time between the sample groups ($p = 0.033$; Table 2), with specimens in irradiated treatments generally emerging several days later than control group specimens (Fig. 1A). 59 of the 60 specimens that emerged survived the experiment, the only mortality being specimen IH16 in the 75 $(kJ\ m^{-2}\ d^{-1})_{BE}$ treatment. Therefore, *I. howellii* experienced low mortality rates under the control and all three end-Permian modeled UV-B regimes respectively.

Prior to the experiment, specimens across the sample groups did not display significant differences in corm diameter ($p = 0.985$) (Table 3; Fig. 1B;). In contrast, following one growth season of culture in an environmentally-controlled chamber, all *I. howellii* specimens studied (including the control treatment) exhibited a marked reduction in corm diameter. However, the diameter of the actively growing zone of corms was significantly different across the sample groups ($p = 7.04 \times 10^{-8}$; Table 4, Fig. 1C), with associated corm reduction being higher in specimens of the irradiated treatment groups (Fig. 1D, $p < 2 \times 10^{-16}$; Table 5).

There was no significant difference in scale and photosynthetic lycophyll production between the sample groups ($p = 0.375$; Table 6; Fig. 1E), though the largest number of sterile leaves produced per specimen occurred within the 54 and 75 $(kJ\ m^{-2}\ d^{-1})_{BE}$ UV-B treatments. Therefore,

the UV-B exposure in our treatments does not appear to impact the production of subterranean sheathing and exposed photosynthetic lycophylls in *I. howellii*. In contrast, heightened UV-B exposure did negatively influence sporophyll production. A significant difference ($p = 6.8 \times 10^{-4}$) was observed between the sample populations, with a generally negative correlation between the intensity of BE UV-B exposure and the number of microsporophylls produced (Table 7; Fig. 2A). Significant differences were also observed in the number of megasporophylls between sample groups ($p = 8.06 \times 10^{-3}$; Table 8), with greater variability in the number of megasporophylls produced and lower medians in the 54, 75, and 93 $(kJ\ m^{-2}\ d^{-1})_{BE}$ UV-B treatments than the control group (Fig. 2B).

Overall, there were significant differences between the total number of sporophylls produced between the sample groups ($p = 8.1 \times 10^{-3}$), with more sporophylls produced in the control group than the three irradiated treatment groups (Table 9; Fig. 2C). Although no significant difference was detected between the groups in the proportion of sporophylls that are megasporophylls ($p = 0.92$; Table 10) and microsporophylls ($p = 0.06$; Table 11), there appears to be a positive correlation between the proportion of sporophylls that are megasporophylls and UV-B dosage (Figs. 2D). Additionally, although no significant difference in the number of sporophylls with aborted sporangia was observed between the sample groups ($p = 0.12$; Table 12), there appears to be a positive correlation between the number of sporangia aborted and UV-B dosage (Fig. 2E). Therefore, elevated UV-B exposure not only adversely impacts overall vegetative (corm tissue) and sporangia production in *I. howellii,* but also may induce plants to shift toward investing more resources toward megaspore [and in turn, megagametophyte] production. Morphologically, leaf tissues of all specimens in each of the three end-Permian modelled UV-B regimes became deeply pigmented in dark bronze hues, in contrast to the typical green foliage of the control specimens (Fig. 3). Additionally, all mega- and microsporangia observed yielded many phenotypically normal megaspores or microspores respectively.

## DISCUSSION

Previous studies have found that elevated UV-B exposure has an effect on both vegetative growth and reproductive success of plants. Higher levels of UV-B disrupting physiological processes such as photosynthesis (Tevini and Teramura, 1989), but can also induce changes in foliar morphology that can impact biomass production. Examples of such changes range from a reduction in shoot internode- and leaf lamina lengths, increase in axillary shoot production (Barnes et al. 1990), increasing leaf and cuticular thickness (Basiouny et al. 1978), altering leaf shape and/or orientation (Greenberg et al. 1997), as well as changing stomatal density and conductance (Kostina et al. 2001). Elevated UV-B exposure effects on reproductive success in land plants have only been investigated in seed-bearing lineages and include reductions in pollen viability (e.g. *Brassica rapa*; Demchik and Day, 1996), as well as reductions in seed yield and quality (e.g. soybean (*Glycine max*); Teramura et al. 1990).

However, UV-B influences on plant growth and function vary considerably both inter- and intra-specifically (Murali and Teramura, 1986). Generally, plant species and/or populations that naturally occur at lower latitudes and/or higher elevations are more resistant to UV-B than those from higher latitudes and/or lower elevations (Sullivan et al. 1992). Other plant lineages are less susceptible to UV-B because they have certain physiological or morphological traits that help mitigate the effects of increased UV-B exposure. For example, some angiosperms with the $C_4$ photosynthetic pathway appear to be less susceptible to foliar damage than those with the $C_3$ pathway as they have traits such as sclerification of tissues and nearly vertical orientation of leaves that minimize UV-B interception of leaf tissues during midday (Basiouny et al. 1978), when UV-B fluxes are typically highest. Additionally, alpine members of the conifer family Pinaceae have been found to be highly resistant to foliar UV-damage (Sullivan and Teramura, 1988), as they have a thickened epidermis in their leaves that effectively screens out UV-B wavelengths before they can reach the UV-sensitive chromophores and mesophyll cells (DeLucia et al. 1992). Some other seed plants also have ways of acclimating to elevated UV-B exposure, such as the up-regulation and accumulation of UV-B-absorbing compounds (e.g. flavonoids) in foliar tissues exposed to solar radiation (Lois, 1994), for example, in the upper (adaxial) epidermal cell layers of leaf and shoot tissues (Schmelzer et al. 1988). Additionally, Lomax et al. (2008) found that the concentration of two UV-B-absorbing compounds [*p*-coumaric and ferulic acid] increased in the spore walls of herbarium specimens of lycopsids (*Lycopodium* spp.) collected during times of anthropogenic ozone column reduction (and consequently higher UV-B exposure) at high latitude sites.

Most studies addressing the impact of elevated UV-B exposure on plant fitness have been performed on seed plants grown under considerably lower UV-B regimes (e.g. 1×, 2×, to 3× ambient modern conditions; 7.7 $(kJ\ m^{-2}\ d^{-1})_{BE}$ at temperate mid-latitudes; Bassman et al. 2002) than in this study (2.5×, 3.5× 4.3× the estimated ambient sum Caldwell UV-B regimes averaged from February through September at the source locality; 21.6 $(kJ\ m^{-2}\ d^{-1})_{BE}$ (UVMRP)). In a previous experiment, the same UV-B regimes used in this study were found to sterilize entire treatment groups of a dwarf alpine conifer (*Pinus mugo* 'Columnaris'), through inducing death of ovules prior to pollination receptivity (Benca et al. 2018). However—based on visual inspection of specimens—these UV-B regimes did not appear to adversely impact vegetative growth of *P. mugo* (Benca et al. 2018). Therefore, anomalously high UV-B regimes, such as those modeled for the end-Permian, can impose deleterious impacts on the reproductive capacity even in modern gymnosperm lineages that are UV-resistant in nature today.

In our current study, we demonstrate that the UV-B regimes modeled for the end-Permian crisis—as also observed for *Pinus mugo* (Benca et al. 2018)—do not kill individuals of an extant counterpart to the Pleuromeiaceae; *Isoëtes howellii*. However, in contrast with results of the *P. mugo* study, we find that elevated UV-B exposure does adversely impact vegetative growth (in the form of perennial corm growth) in this modern isoetalean. Additionally, although these UV-B regimes did reduce sporophyll production [i.e. the production of spore-bearing organs], they

did not impede the production of megaspores and microspores. This observation contrasts with conifer responses to these same UV-B regimes in that all *P. mugo* ovules (organs evolutionarily derived from- and maintaining the function of megaspores) died off before becoming receptive for fertilization (Benca et al. 2018). Therefore, under the same experimentally-induced UV-B regimes, modern conifers are unable to form viable megagametophytes while isoetaleans are at least capable of producing mature megaspores that appear phenotypically normal. However, germination studies of the spores produced in this experiment will be required to determine whether the irradiated microspores and megaspores in *I. howellii* are viable.

In one growth season, most irradiated *I. howellii* specimens experience a substantially greater reduction in corm area and also produce fewer mega- and microsporangia than non-irradiated specimens. However, sterile leaf [scale and photosynthetic lycophyll] production does not appear to be significantly impacted by elevated UV-B regimes, suggesting these plants are still able to maintain above-ground vegetative growth, even while under stress. The background reduction in corm area in the control specimens may result from energetic costs experienced by *I. howellii* specimens establishing during their first season in cultivation following a period of annual drought dormancy in nature. Additionally, positive correlation between corm area reduction and UV-B dosage may result from plants investing greater energy in photoprotective pigment production and/or increasing cuticle thickness. Ongoing analysis of UV-absorbing pigment concentrations in both spore wall and leaf tissue samples collected at the end of the experiment will help determine whether either condition may have contributed to the greater reduction in corm area observed in irradiated specimens.

The increased use of corm energy reserves observed in irradiated specimens of this experiment suggests that the subterranean corm is a structure that facilitates survival of isoetalean lycopsids under anomalous environmental challenges, as has been previously inferred for the end-Permian crisis survivor *Pleuromeia sternbergii* (Looy, 2000). This growth strategy appears to enable isoetaleans such as *Isoëtes howelii* to invest energy drawn from a subterranean, protected region of the shoot towards megaspore and microspore production throughout the growth season, even while accumulating unusually high foliar UV-B exposure. In contrast, the entire shoot system of conifers like *Pinus mugo* (Benca et al. 2018) are aerially exposed. Therefore, under irradiated conditions, conifers may systemically abort their ovules in order to invest adequate growth resources toward foliar protection as long as high UV-B fluxes are present.

Additionally, extant *Isoëtes* spp. of lacustrine habitats have been found to develop persistent and long-lived spore banks (e.g. several decades in *Isoëtes lacustris* in shallow oligotrophic lakes in the Netherlands; Roelofs, *pers. comm.* 2005). Such spore banks in modern *Isoëtes* may result from the deposition of germination inhibitors promoting dormancy in spores during the final stages of sporogenesis, which has been inferred on the basis of experimental studies of *I. coreana* by Oh et al. (2013) demonstrating reduced germination rates of fully mature megaspores when compared to those surgically extracted from megasporangia prior to maturity.

Given similarities in their spore morphology, it is possible that extinct isoetalean lineages such as Pleuromeiaceae also would be capable of generating long-lived spore banks. Such a capability could serve as an added safeguard for sustaining population growth during crisis intervals by providing more recruitment opportunities under the fluctuating solar climate suggested for the end-Permian crisis (Black et al. 2014).

Even though irradiated specimens in our experiment experienced significant reduction in some forms of vegetative growth and reproductive organ production (sporangia; Figs. 1 and 2), the fact that they displayed only 1.5% mortality and were still able to produce phenotypically normal mega- and microspores suggests *Isoëtes howellii* is more UV-tolerant than would be expected for a predominantly semi- to fully aquatic plant lineage. If vegetative growth and generation of sporangia were reduced in latest Permian and early Triassic Pleuromeiaceae under elevated UV-B regimes, plants in this lineage likely would have experienced reduced fitness. Nevertheless, these lycopsids may have been able to produce both viable mega- and microspores even under intense degradation of the stratospheric ozone layer, thereby sustaining their populations through crisis intervals. Such a scenario would contrast with steep fitness declines exhibited in the modern conifer *Pinus mugo* under such conditions (Benca et al. 2018). In other words, if UV-B stress intervals were to occur recurrently over multiple centuries, populations of conifers such as modern *P. mugo* may experience regional extirpation due to lack of recruitment, despite little to no adverse impact on vegetative growth in individual trees. Conversely, populations of isoetaleans such as modern *I. howellii* may persevere—despite incurring higher costs to vegetative growth from environmental stress—because decreased competition resulting from progressive seed plant extirpations in their habitats could have compensated for their slower growth rate. If our experiments with nearest living equivalents of end-Permian gymnosperm and isoetalean taxa are indeed indicative of physiological and life history traits of their ancestors (and note that our comparisons are drawn from conservative characters within those plant groups), then our results may explain how Permian and early Triassic isoetaleans may have gained dominance in plant fossil records worldwide in the near absence or at the expense of gymnosperms and other seed plant lineages.

Given that our experiment was conducted on one species over a single growth season in an environmentally-controlled growth chamber, there are certainly limitations to extrapolations that can be made from our study system. **(1)** Our results apply to only one species, and therefore it is not possible to determine whether other *Isoëtes* species share the same growth, developmental and reproductive responses to elevated UV-B regimes. **(2)** Our specimens did not have a chance to fully establish in cultivation prior to the treatment, meaning a substantial portion of corm reduction witnessed [i.e. in the non-irradiated control group], may have resulted from resource allocation towards generating new roots, while growing in a nutrient-limited mineral substrate (sandy loam). **(3)** Prolonging the experiment by several growth seasons would yield more discernable patterns of UV-B stress and/or acclimation (Teramura and Sullivan, 1990; Bassman et al. 2002), **(4)** Growing plants under natural sunlight outdoors would better

ensure that specimens experienced the full solar spectrum that would be present in nature, which is not possible under artificially-lit environmentally-controlled chamber conditions.

Additional work is required to determine whether stress signals expressed by *I. howellii* eventually culminate in mortality and/or sterility if specimens are grown for subsequent years under high UV-B conditions. Further study of the megaspores and microspores as well as chemical composition of the pigments, cuticle thickness, and stomatal distribution and density of leaf tissues produced during this experiment will also help clarify how *I. howellii* can survive anomalously high UV-B dosages. Germination experiments of the spores produced will determine whether irradiated plants are reproductively viable. Until then, these observations of growth responses suggest modern *Isoëtes* and possibly extinct isoetaleans could continue to persist and possibly even reproduce under conditions that have been demonstrated to sterilize modern conifers.

This study represents the first investigation of the effects of elevated UV-B exposure on growth and the production of vegetative and reproductive organs in a seed-free vascular plant. We demonstrate that a modern isoetealean lycopsid (a member of a lineage that is the closest living sister-group to members of the extinct Pleuromeiacae that were ecologically dominant during end-Permian and early Triassic crisis intervals) is not only capable of surviving elevated UV-B regimes modeled for the end-Permian, but also of developing mega- and microsporangia yielding phenotypically normal megaspores and microspores. However, in the modern species studied, *Isoëtes howellii*, elevated UV-B exposure significantly reduced vegetative and reproductive organ production and corm growth relative to the non-irradiated control group. Results of this study suggest that modern isoetaleans (and potentially Pleuromeiaceae) could have a fitness advantage (or rather: less of a fitness disadvantage) during ozone weakening events over gymnosperms such as conifers. However, further investigations into mega- and microspore morphology and viability will be needed to determine fitness impacts on *I. howellii* in order to infer responses of the most prominent plant lineage worldwide during the largest extinction event in Earth history.

**WORKS CITED**


Barnes, P. W., S. D. Flint and M. M. Caldwell. 1990. Morphological responses of crop and weed species of different growth forms to ultraviolet-B radiation. American Journal of Botany 77: 1354–1360.

Basiouny, F. M., T. K. Van and R. H. Biggs. 1978. Some morphological and biochemical characteristics of $C_3$ and $C_4$ plants irradiated with UV-B. Physiologia Plantarum 42: 29–32.

Bassman, J. H., G. E. Edwards and R. Robberecht. 2002. Long-term exposure to enhanced UV-B radiation is not detrimental to growth and photosynthesis in Douglas-fir. New Phytologist 154: 107–120.

Benca, J. P., I. A. P. Duijnstee and C. V. Looy. 2018. UV-B–induced forest sterility: Implications of ozone shield failure in Earth's largest extinction. Science Advances 4: p.e1700618.

Beerling, D. J., M. Harfoot, B. Lomax and J. A. Pyle. 2007. The stability of the stratospheric ozone layer during the end-Permian eruption of the Siberian Traps. Philosophical Transactions. Series A, Mathematical, Physical, and Engineering Sciences 365: 1843–1866.

Black, B. A., J.-F. Lamarque, C. A. Shields, L. T. Elkins-Tanton and J. T. Kiehl. 2014. Acid rain and ozone depletion from pulsed Siberian Traps magmatism. Geology 42: 67–70.

Broadley, M. W., P. H. Barry, C. J. Ballentine, L. A. Taylor and R. Burgess. 2018. End-Permian extinction amplified by plume-induced release of recycled lithospheric volatiles. Nature Geoscience 11: 682–687.

Caldwell, M. M. 1971. Solar UV irradiation and the growth and development of higher plants. Photophysiology 6: 131–177.

DeLucia, E. H., T. A. Day and T. C. Vogelmann. 1992. Ultraviolet-B and visible light penetration into needles of two species of subalpine conifers during foliar development. Plant, Cell and Environment 15: 921–929.

Demchik, S. M. and T. A. Day. 1996. Effect of enhanced UV-B radiation on pollen quantity, quality, and seed yield in *Brassica rapa* (Brassicaceae). American Journal of Botany 83: 573–579.

Farman, J. C., B. G. Gardiner and J. D. Shanklin. 1985. Large losses of total ozone in Antarctica reveal seasonal $ClO_x/NO_x$ interaction. Nature 315: 207–210.

Foster, C. B. and S. A. Afonin. 2005. Abnormal pollen grains: an outcome of deteriorating atmospheric conditions around the Permian-Triassic boundary. Proceedings of the Geological Society of London 162: 653–659.

Grauvogel-Stamm, L. 1999. *Pleuromeia sternbergii* (Münster) Corda, eine charakteristische Planze des DeutchenBuntsandsteins, In: Hauschke, N. and V. Wilde. Eds. Trias - Eine ganz andere Welt, Verlag Dr. Friedrich Pfeil, München 271–282.

Grauvogel-Stamm, L. and B. Lugardon. 2001. The Triassic lycopsids *Pleuromeia* and *Annalepis*: relationships, evolution, and origin. American Fern Journal 91: 115–149.

Grauvogel-Stamm, L. and S. R. Ash. 2005. Recovery of the Triassic land flora from the end-Permian lifecrisis. Comte Rendus, Palevol 4: 593–608.

Greenberg, B. M., M. I. Wilson, X. D. Huang, C. L. Duxbury, K. E. Gerhardt and R. W. Gensemer. 1997. The effects of ultraviolet–B radiation on higher plants. In: Wang, W., J. Gorsuch and J. S. Hughes, eds. Plants for Environmental Studies. CRC Press pp. 1–35.

Kostina, E., A. Wulff and R. Julkunen-Tiitto. 2001. Growth, structure, stomatal responses and secondary metabolites of birch seedlings (*Betula pendula*) under elevated UV-B radiation

in the field. Trees 15: 483–491.
Lois, R. 1994. Accumulation of UV-absorbing flavonoids induced by UV-B radiation in *Arabidopsis thaliana* L. Planta 194: 498–503.
Lomax, B. H., W. T. Fraser, M. A. Sephton, T. V. Callaghan, S. Self, M. Harfoot, J. A. Pyle, C. H. Wellman and D. J. Beerling. 2008. Plant spore walls as a record of long-term changes in ultraviolet-B radiation. Nature Geoscience 1: 592–596.
Looy, C. V. 2000. The Permian-Triassic biotic crisis: collapse and recovery of terrestrial ecosystems. LPP Foundation.
Looy, C. V., R. J. Twitchett, D. L. Dilcher, J. H. Van Konijnenburg-Van Cittert and H. Visscher. 2001. Life in the end-Permian dead zone. Proceedings of the National Academy of Sciences 98: 7879–7883.
Looy, C. V., M. E. Collinson, J. H. A. van Konijnenburg-van Cittert, H. Visscher and A. P. Brain. 2005. The ultrastructure and botanical affinity of end-Permian spore tetrads. International Journal of Plant Sciences 166: 875–887.
Lugardon, B., L. Grauvogel-Stamm and I. Dobruskina. 1999. The microspores of *Pleuromeia rossica* Neuburg (Lycopsida; Triassic): comparative ultrastructure and phylogenetic implications. Comptes Rendus de l'Académie des Sciences-Series IIA-Earth and Planetary Science 329: 435–442.
Lugardon, B., L. Grauvogel-Stamm and I. Dobruskina. 2000. Comparative ultrastructure of the megaspores of the Triassic lycopsid *Pleuromeia rossica* Neuburg. Comptes Rendus de l'Académie des Sciences-Series IIA-Earth and Planetary Science 330: 501–508.
Lyddon, J., A. H. Teramura and C. B. Coffman. 1987. UV-B radiation effects on photosynthesis, growth and cannabinoid production of two *Cannabis sativa* chemotypes. Photochemistry and Photobiology 46: 201–206.
McElwain, J. C. and S. W. Punyasena. 2007. Mass extinction events and the plant fossil record. Trends in Ecology & Evolution 22: 548–557.
Murali, N. S. and A. H. Teramura. 1986. Intraspecific differences in *Cucumis sativus* to ultraviolet-B radiation. Physiologia Plantarum 68: 673–677.
Naugolnykh, S. V. 2001. The morphology, systematics and paleoecology of the lycopsid *Viatcheslavia vorcutensis*. Paleontological Journal 35: 204–210.
Naugolnykh, S. V. and N. E. Zavialova. 2004. *Densoisporites polaznaensis* sp. *nov*. with comments on its relation to *Viatcheslavia vorcutensis* Zalessky. Palaeobotanist 53: 21–33.
Oh, M. J., C. Kim, H. R. Na, H. Shin, J. R. Liu, H. K. Choi and S. W. Kim. 2013. High frequency sporophytes regeneration from the spore culture of the endangered aquatic Fern *Isoetes coreana*. American Journal of Plant Sciences 4: 14–20.
R Development Core Team. 2010. *R: a language and environment for statistical computing*. R Foundation for Statistical Computing, Vienna, Austria. ISBN 3-900051-07-0.
Retallack, G. J. 1997. Earliest Triassic origin of *Isoetes* and quillwort evolutionary radiation. Journal of Paleontology 71: 500–521.
Schmelzer, E., W. Jahnen and K. Hahlbrock. 1988. *In situ* localization of light induced chalcone synthase mRNA, chalcone synthase, and flavonoid end products in the epidermal cells of parsley leaves. Proceedings of the National Academy of Sciences of the United States of America. 85: 2989–2993.
Sirenko, E. A. 2001. Palynological data from studies of bottom sediments in water bodies of 30-km Chernobyl Zone. In: Proceedings of the First International Seminar, Pollen as Indicator of Environmental State and Paleoecological Reconstructions. VNIGRI, St. Petersburg (pp. 189–190).

Sullivan, J. H. and A. H. Teramura. 1988. Effects of ultraviolet-B irradiation on seedling growth in the Pinaceae. American Journal of Botany 75: 225–230.
Sullivan, J. H., A. H. Teramura and L. H. Ziska. 1992. Variation in UV-B sensitivity in plants from a 3,000-m elevational gradient in Hawaii. American Journal of Botany 79: 737–743.
Svensen, H., S. Planke, A. G. Polozov, N. Schmidbauer, F. Corfu, Y. Y. Podladchikov and B. Jamtveit. 2009. Siberian gas venting and the end-Permian environmental crisis. Earth and Planetary Science Letters 277: 490–500.
Taylor, W. C. and N. T. Luebke. 1986. Germinating spores and growing sporelings of aquatic *Isoëtes*. American Fern Journal 76: 21–24.
Teramura, A. H., J. H. Sullivan and J. Lydon. 1990. Effects of UV-B radiation on soybean yield and seed quality: a 6-year field study. Physiologia Plantarum 80: 5–11.
Tevini, M. and A. H. Teramura. 1989. UV-B effects on terrestrial plants. Photochemistry and Photobiology 50: 479–487.
Tryon A. F. and B. Lugardon. 1991. Spores of the Pteridophyta: Surface, wall structure and diversity based on electron microscope studies. Springer, New York.
Twitchett, R. J., C. V. Looy, R. Morante, H. Visscher, P. B. Wignall. 2001. Rapid and synchronous collapse of marine and terrestrial ecosystems during the end-Permian mass extinction event. Geology 29: 351–354.
Visscher, H., C. V. Looy, M. E. Collinson, H. Brinkhuis, J. H. Van Konijnenburg-Van Cittert, W. M. Kürschner and M. A. Sephton. 2004. Environmental mutagenesis during the end-Permian ecological crisis. Proceedings of the National Academy of Sciences of the United States of America 101: 12952–12956.
Weather Underground, Weather history for Novato, CA. KCANOVAT59 Personal Weather Station Data. (https://www.underground.com/personal-weather-station/dashboard?ID=KCANOVAT59&cm_ven=localwx_pwsdash#history) Accessed 05 December 2017.
Wickham, H. 2016. *ggplot2: Elegant Graphics for Data Analysis*. Springer-Verlag New York.
Williamson, C. E., P. J. Neale, G. Grad, H. J. De Lange and B. R. Hargreaves. 2001. Beneficial and detrimental effects of UV on aquatic organisms: implications of spectral variation. Ecological Applications 11: 1843–1857.
Wilson, L. R. 1965. Teratological forms in pollen of *Pinus flexilis* James. Journal of Palynology 1: 106–110.
UVMRP, UV irradiance estimator. UV-B Monitoring and Research Program. (http://uvb.nrel.colostate.edu/UVB/da_interactiveMapSums.jsf) Accessed 05 December 2017.
U.S. Naval Observatory, *Berkeley, California; Rise and Set for the Sun for 2013* (http://aa.usno.navy.mil/cgibin/aa_rstablew.pl?ID=AA&year=2013&task=0&state=CA&placeBerkeley). Accessed 05 December 2017.

## CHAPTER 2 TABLES

**Table 1.** Photoperiod settings during growth chamber experiment. Photoperiods based on estimations of sunrise and sunset times for Novato, CA, US (US Naval Observatory). *Chamber photoperiod rounded to the nearest quarter hour. Day temperatures are based on monthly average high temperatures-, while night temperatures are based on monthly average low temperatures from January, 2016 through August, 2016 in Novato, CA recorded by the Hidden Oaks KCANOVAT59 Personal Weather Station (https://www.wunderground.com).

| Chamber treatment (kJ m$^{-2}$ d$^{-1}$)$_{PAR}$ | Tree | Pollen surveyed (n) | Σ Malformation frequency | % Malformed | Malformation index | Malformation classes | | | | |
|---|---|---|---|---|---|---|---|---|---|---|
| | | | | | | 0 Sacci | 1 Saccus | 3 Sacci | 4 Sacci | ≥ 5 Sacci |
| Control [0] | PM03 | 4800 | 58 | 1.2 | 0.8 | 0 | 0 | 49 | 7 | 2 |
| Control [0] | PM17 | 4800 | 30 | 0.6 | 0.4 | 3 | 0 | 22 | 5 | 0 |
| Control [0] | PM23 | 4800 | 131 | 2.7 | 1.8 | 1 | 0 | 116 | 12 | 2 |
| 54 | PM15 | 4800 | 98 | 2.0 | 1.3 | 5 | 0 | 90 | 2 | 1 |
| 54 | PM36 | 4800 | 64 | 1.3 | 0.9 | 3 | 0 | 58 | 3 | 0 |
| 54 | PM44 | 4800 | 69 | 1.4 | 0.9 | 11 | 0 | 50 | 4 | 4 |
| 75 | PM38 | 4800 | 339 | 7.1 | 4.6 | 4 | 0 | 328 | 5 | 2 |
| 75 | PM52 | 4800 | 456 | 9.5 | 6.3 | 0 | 0 | 438 | 16 | 2 |
| 75 | PM54 | 4800 | 395 | 8.2 | 5.4 | 0 | 1 | 371 | 22 | 1 |
| 93 | PM10 | 4800 | 384 | 8.0 | 5.3 | 3 | 0 | 371 | 10 | 0 |
| 93 | PM28 | 4800 | 354 | 7.4 | 4.9 | 4 | 0 | 334 | 14 | 2 |
| 93 | PM42 | 4800 | 213 | 4.4 | 2.9 | 2 | 0 | 205 | 6 | 0 |

**Table 2.** One-way ANOVA comparing the number of days between *Isoëtes howellii* corm hydration and emergence between sample groups. Significance ($p < 0.05$) of differences between control and three irradiated treatments were tested. Listed are degrees of freedom (*df*), sum of squares (*SS*), mean sum of squares (*MS*), F-statistic (*F*), and p-value. Data consisted of a maximum of 16 specimens per treatment; four groups: Control (non-irradiated), 54, 75, and 93 $(kJ\ m^{-2}\ d^{-1})_{BE}$ UV-B treatments.

| | *df* | *SS* | *MS* | *F* | *p*-value |
|---|---|---|---|---|---|
| Treatment | 3 | 40.02 | 13.338 | 3.161 | **0.033** |
| Residuals | 50 | 210.97 | 4.219 | | |

**Table 3.** One-way ANOVA comparing *Isoëtes howellii* corm size prior to experimental treatment between sample groups. Significance ($p < 0.05$) of differences between control and three irradiated treatments were tested. Listed are degrees of freedom (*df*), sum of squares (*SS*), mean sum of squares (*MS*), F-statistic (*F*), and p-value. Data consisted of a maximum of 16 specimens per treatment; four groups: Control (non-irradiated), 54, 75, and 93 (kJ $m^{-2}$ $d^{-1}$)$_{BE}$ UV-B treatments.

| | *df* | *SS* | *MS* | *F* | *p*-value |
|---|---|---|---|---|---|
| Treatment | 3 | 850 | 283 | 0.051 | 0.985 |
| Residuals | 56 | 310223 | 5540 | | |

**Table 4.** One-way ANOVA comparing *Isoëtes howellii* corm size after one growth season in experimental treatment between sample groups. Significance ($p < 0.05$) of differences between control and three irradiated treatments were tested. Listed are degrees of freedom (*df*), sum of squares (*SS*), mean sum of squares (*MS*), F-statistic (*F*), and p-value. Data consisted of a maximum of 16 specimens per treatment; four groups: Control (non-irradiated), 54, 75, and 93 (kJ $m^{-2}$ $d^{-1}$)$_{BE}$ UV-B treatments.

| | *df* | *SS* | *MS* | *F* | *p*-value |
|---|---|---|---|---|---|
| Treatment | 3 | 31647 | 10549 | 16.73 | **$7.04 \times 10^{-8}$** |
| Residuals | 56 | 35322 | 631 | | |

**Table 5.** Results of one-way ANOVA comparing percent reduction in corm area in *Isoëtes howellii* between sample groups over the course of the experiment. Significance ($p < 0.05$) of differences between control and three irradiated treatments were tested. Listed are degrees of freedom (*df*), sum of squares (*SS*), mean sum of squares (*MS*), F-statistic (*F*), and p-value. Data consisted of a maximum of 16 specimens per treatment; four groups: Control (non-irradiated), 54, 75, and 93 (kJ $m^{-2}$ $d^{-1}$)$_{BE}$ UV-B treatments.

| | *df* | *SS* | *MS* | *F* | *p*-value |
|---|---|---|---|---|---|
| Treatment | 3 | 14215 | 4738 | 59.32 | **$< 2 \times 10^{-16}$** |
| Residuals | 56 | 4473 | 80 | | |

**Table 6.** Results of one-way ANOVA comparing the total number of lycophylls [scale and photosynthetic sterile leaves] produced by *Isoëtes howellii* between sample groups. Significance ($p < 0.05$) of differences between control and three irradiated treatments were tested. Listed are degrees of freedom (*df*), sum of squares (*SS*), mean sum of squares (*MS*), F-statistic (*F*), and p-value. Data consisted of a maximum of 16 specimens per treatment; four groups: Control (non-irradiated), 54, 75, and 93 (kJ $m^{-2}$ $d^{-1}$)$_{BE}$ UV-B treatments.

| | *df* | *SS* | *MS* | *F* | *p*-value |
|---|---|---|---|---|---|
| Treatment | 3 | 171.8 | 57.27 | 1.056 | 0.375 |
| Residuals | 56 | 3038.2 | 54.25 | | |

**Table 7.** Results of one-way ANOVA comparing the number of *Isoëtes howellii* microsporophylls [fertile leaves bearing microsporangia] produced between sample groups. Significance ($p < 0.05$) of differences between control and three irradiated treatments were tested. Listed are degrees of freedom (*df*), sum of squares (*SS*), mean sum of squares (*MS*), F-statistic (*F*), and p-value. Data consisted of a maximum of 16 specimens per treatment; four groups: Control (non-irradiated), 54, 75, and 93 (kJ $m^{-2}$ $d^{-1}$)$_{BE}$ UV-B treatments.

| | *df* | *SS* | *MS* | *F* | *p*-value |
|---|---|---|---|---|---|
| Treatment | 3 | 171.8 | 57.27 | 1.056 | 0.375 |
| Residuals | 56 | 3038.2 | 54.25 | | |

**Table 8.** Results of one-way ANOVA comparing the number of *Isoëtes howellii* megasporophylls [fertile leaves bearing megasporangia] produced between sample groups. Significance ($p < 0.05$) of differences between control and three irradiated treatments were tested. Listed are degrees of freedom (*df*), sum of squares (*SS*), mean sum of squares (*MS*), F-statistic (*F*), and p-value. Data consisted of a maximum of 16 specimens per treatment; four groups: Control (non-irradiated), 54, 75, and 93 (kJ $m^{-2}$ $d^{-1}$)$_{BE}$ UV-B treatments.

| | *df* | *SS* | *MS* | *F* | *p*-value |
|---|---|---|---|---|---|
| Treatment | 3 | 1439 | 479.6 | 4.341 | **$8.06 \times 10^{-3}$** |
| Residuals | 56 | 6187 | 110.5 | | |

**Table 9.** Results of one-way ANOVA comparing the total number of *Isoëtes howellii* sporophylls produced between sample groups. Significance ($p < 0.05$) of differences between control and three irradiated treatments were tested. Listed are degrees of freedom (*df*), sum of squares (*SS*), mean sum of squares (*MS*), F-statistic (*F*), and p-value. Data consisted of a maximum of 16 specimens per treatment; four groups: Control (non-irradiated), 54, 75, and 93 $(kJ\ m^{-2}\ d^{-1})_{BE}$ UV-B treatments.

| | *df* | *SS* | *MS* | *F* | *p*-value |
|---|---|---|---|---|---|
| Treatment | 3 | 5677 | 1892.2 | 12.97 | $\mathbf{1.53 \times 10^{-6}}$ |
| Residuals | 56 | 8172 | 145.9 | | |

**Table 10.** Results of one-way ANOVA comparing percent sporophylls that are megasporophylls between *I. howellii* sample groups. Significance ($p < 0.05$) of differences between control and three irradiated treatments were tested. Listed are degrees of freedom (*df*), sum of squares (*SS*), mean sum of squares (*MS*), F-statistic (*F*), and p-value. Data consisted of a maximum of 16 specimens per treatment; four groups: Control (non-irradiated), 54, 75, and 93 $(kJ\ m^{-2}\ d^{-1})_{BE}$ UV-B treatments.

| | *df* | *SS* | *MS* | *F* | *p*-value |
|---|---|---|---|---|---|
| Treatment | 3 | 550 | 183.2 | 0.171 | 0.916 |
| Residuals | 56 | 60084 | 1072.9 | | |

**Table 11.** Results of one-way ANOVA comparing percent sporophylls that are microsporophylls between *I. howellii* sample groups. Significance ($p < 0.05$) of differences between control and three irradiated treatments were tested. Listed are degrees of freedom (*df*), sum of squares (*SS*), mean sum of squares (*MS*), F-statistic (*F*), and p-value. Data consisted of a maximum of 16 specimens per treatment; four groups: Control (non-irradiated), 54, 75, and 93 (kJ $m^{-2}$ $d^{-1}$)$_{BE}$ UV-B treatments.

| | *df* | *SS* | *MS* | *F* | *p*-value |
|---|---|---|---|---|---|
| Treatment | 3 | 5660 | 1886.7 | 2.614 | 0.060 |
| Residuals | 56 | 40422 | 721.8 | | |

**Table 12.** Results of one-way ANOVA comparing the number of *Isoëtes howellii* sporophylls with aborted sporangia between sample groups. Significance ($p < 0.05$) of differences between control and three irradiated treatments were tested. Listed are degrees of freedom (*df*), sum of squares (*SS*), mean sum of squares (*MS*), F-statistic (*F*), and p-value. Data consisted of a maximum of 16 specimens per treatment; four groups: Control (non-irradiated), 54, 75, and 93 $(kJ\ m^{-2}\ d^{-1})_{BE}$ UV-B treatments.

| | *df* | *SS* | *MS* | *F* | *p*-value |
|---|---|---|---|---|---|
| Treatment | 3 | 33.93 | 11.311 | 2.032 | 0.12 |
| Residuals | 56 | 311.80 | 5.568 | | |

## CHAPTER 2 FIGURES

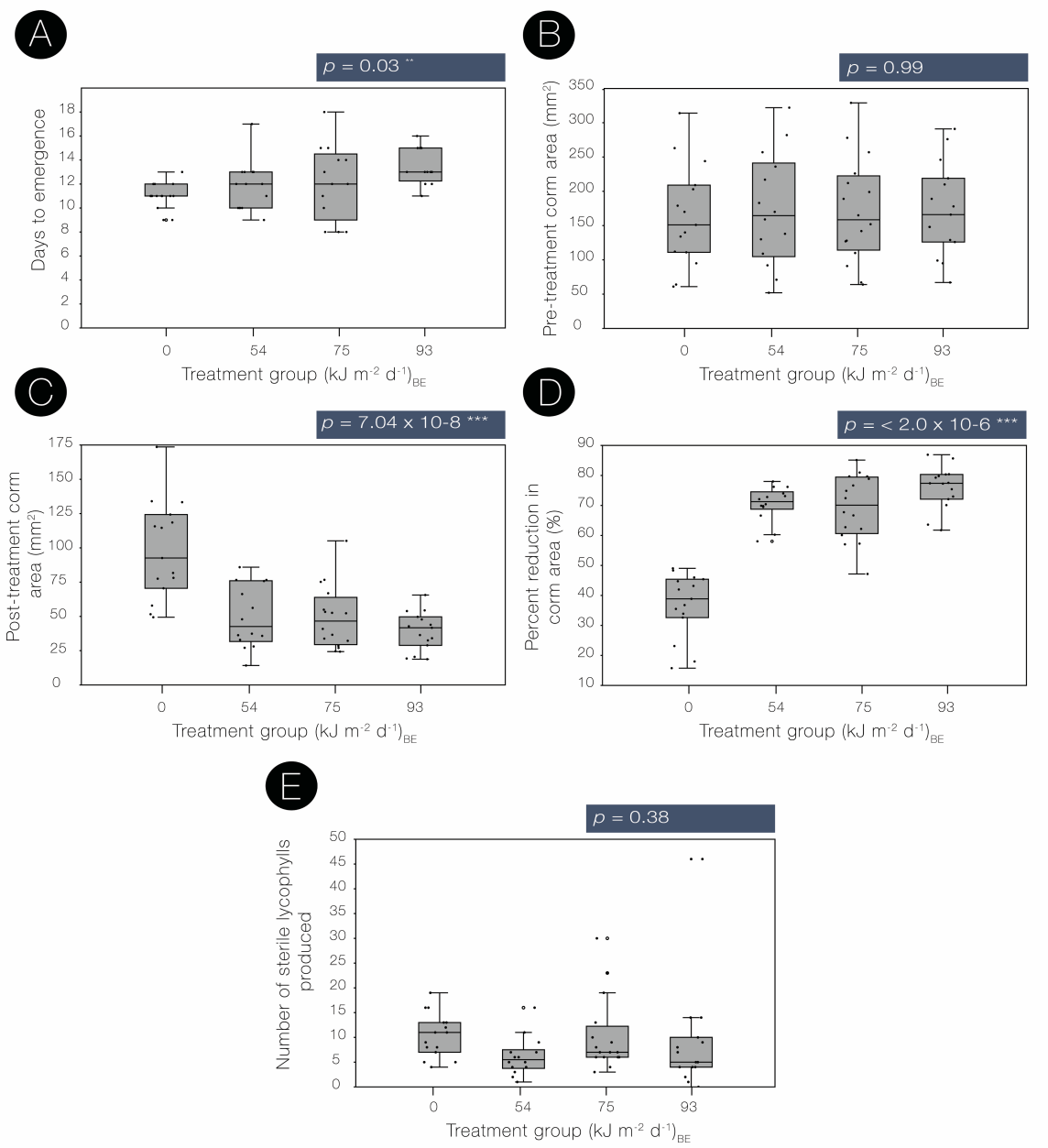


**Figure 1.** Vegetative growth responses of *Isoëtes howellii* to control and three elevated UV-B regimes modeled for the end-Permian. Boxplots show the median and interquartile range (IQR). Whiskers indicate minimum and maximum values within the inner fences (i.e., 1st quartile minus 1.5× IQR, and 3rd quartile plus 1.5× IQR). (A) Days to corm emergence following start of experiment, (B) pre-treatment corm area ($mm^2$), (C) post-treatment corm area ($mm^2$), (D) percent reduction in corm area (%) over the course of the experiment, (E) number of sterile lycophylls [scale and photosynthetic sterile leaves] produced.

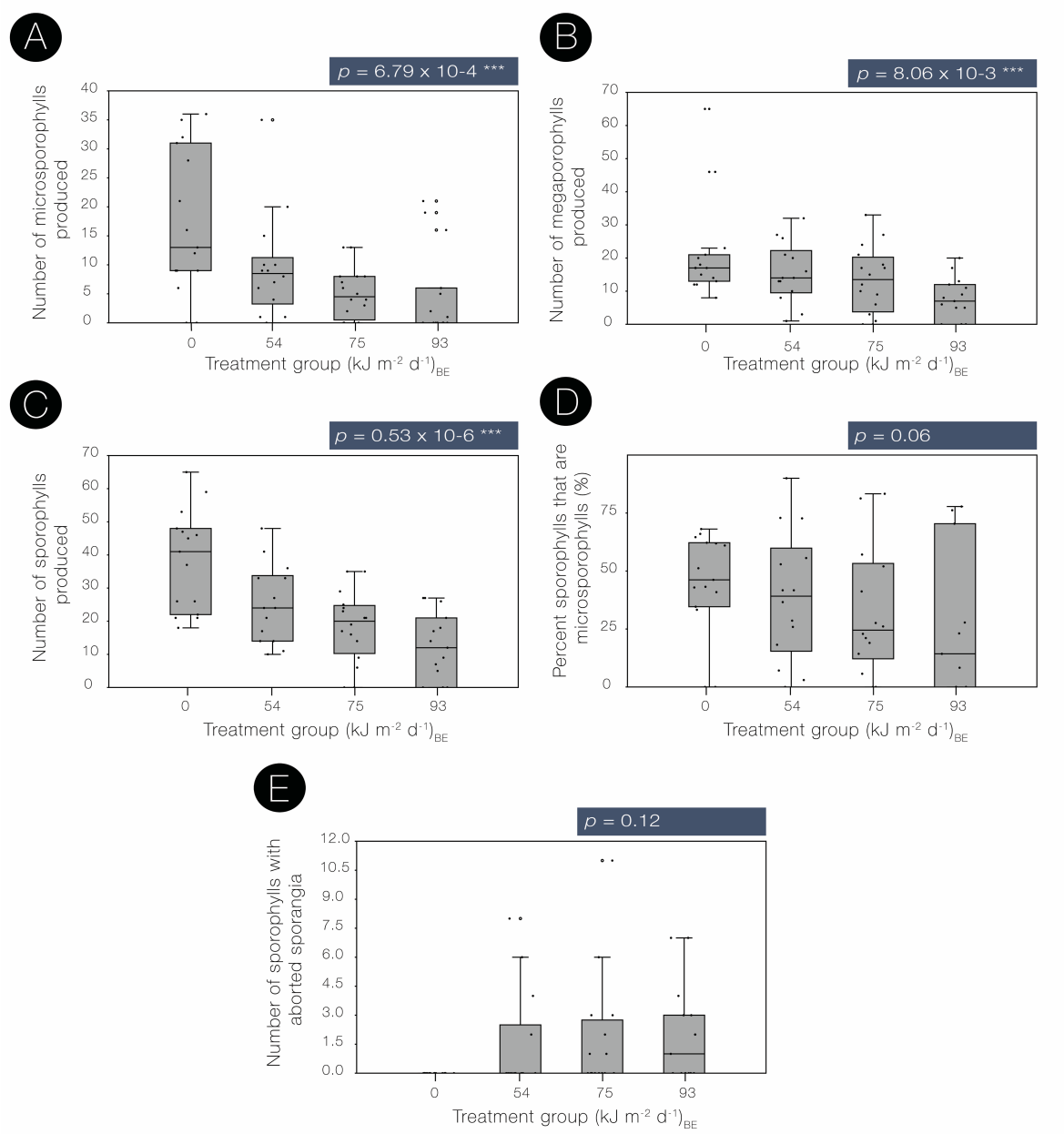


**Figure 2.** Reproductive organ production responses of *Isoëtes howellii* to control and three elevated UV-B regimes modeled for the end-Permian. Whiskers indicate minimum and maximum values within the inner fences (i.e., 1st quartile minus 1.5× IQR, and 3rd quartile plus 1.5× IQR). (A) number of microsporophylls produced, (B) number of megasporophylls produced, (C) number of sporophylls [megasporophylls + microsporophylls] produced, (D) percentage of sporophylls produced that are microphylls, (E) number of sporophylls produced with aborted sporangia.

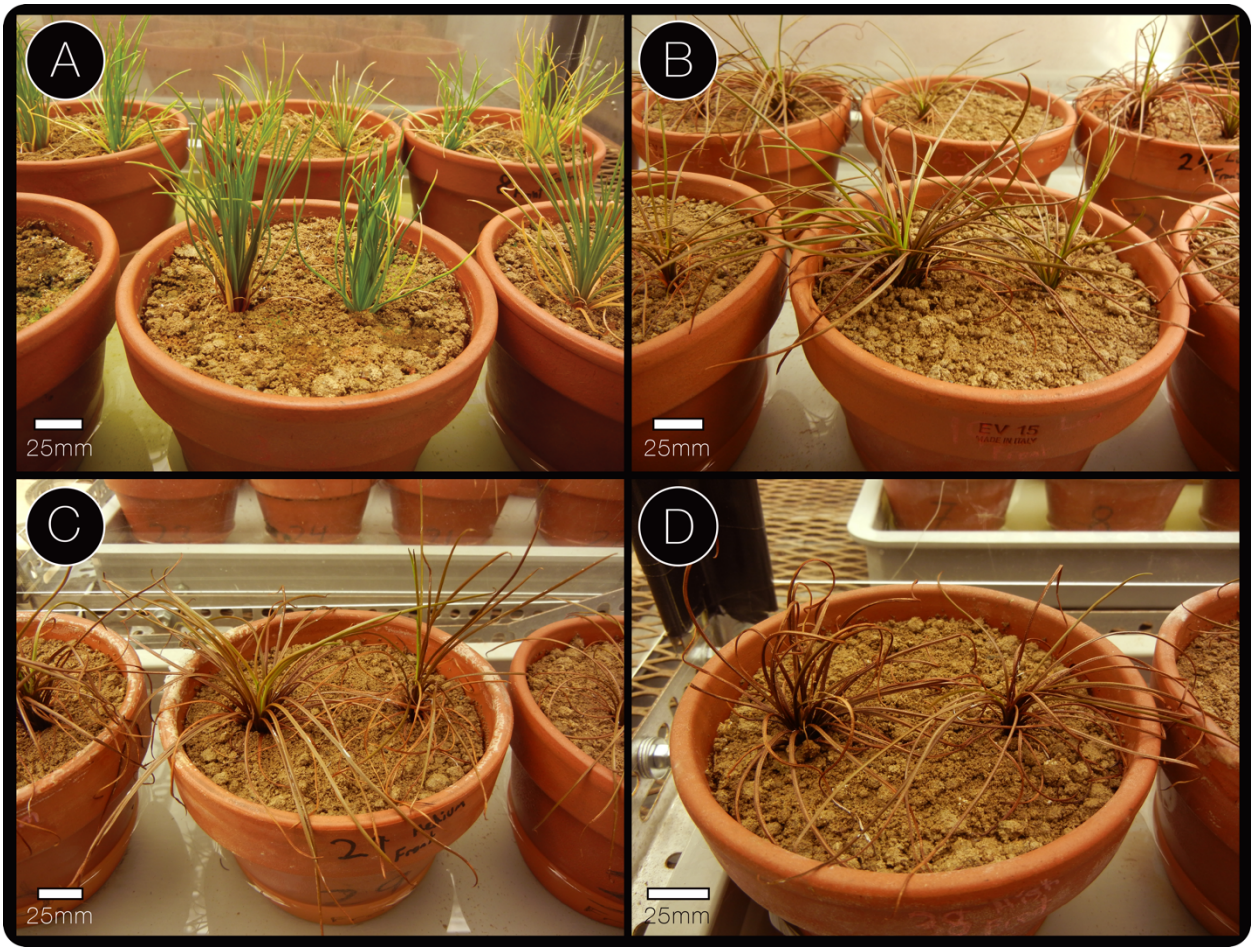


**Figure 3.** *Isoëtes howellii* specimens displaying typical pigmentation of foliage under conditions of each treatment group. Notation: [*pot #: left specimen #, right specimen #*]. (A) Control (non-irradiated) group [pot 3: IH41, IH38], (B) 54 (kJ $m^{-2}$ $d^{-1}$)$_{BE}$ UV-B treatment [pot 19: IH15, IH79], (C) 75 (kJ $m^{-2}$ $d^{-1}$)$_{BE}$ UV-B treatment [pot 29: IH09, IH27], (D) 93 (kJ $m^{-2}$ $d^{-1}$)$_{BE}$ UV-B treatment [pot 38: IH04, IH48].

# CHAPTER 3

## Pollen malformations as indicators of environmental stress: Baselines from a modern biological study


## ABSTRACT

Widespread fossilized malformations in saccate (winged) pollen represent one of the few inferred imprints of a biological stress response during Earth's largest mass extinction, the end-Permian crisis (252 Mya). Since saccate (pre)pollen are characteristic of certain gymnosperm lineages and represent a conspicuous element in the fossil record from the Pennsylvanian to present, deviations in their morphology may provide a unique environmental stress indicator for past ecological perturbations. However, it is unclear how frequently and variably pollen malformations are expressed by gymnosperm lineages during intervals of non-extreme near-optimal conditions. In this study, malformation frequencies were compared between pollen yields of modern species representing 14 genera of two conifer families that produce saccate pollen, Pinaceae and Podocarpaceae, selected from lowland gardens in the United States. Malformations comprise <3% of pollen yields in 12 of the 13 bisaccate genera studied. Conversely, yields of the only trisaccate lineage studied, *Dacrycarpus dacrydioides*, display greater morphological plasticity (>10% of yields). No phylogenetic pattern in the expression of the various malformation types was detected between bisaccate genera or families. These results suggest that bisaccate pollen types usually maintain a high degree of morphological conservatism under present ambient growth conditions irrespective of their phylogenetic affinity, while trisaccate pollen do not. Trisaccate lineages may therefore not be suitable for paleo-environmental stress assessments. The results of this study also indicate malformation frequencies exceeding 3% in bisaccate pollen yields of extant and extinct gymnosperms—as suggested by Foster and Afonin (2005)—holds as potential indicators for environmental stress.

## INTRODUCTION

Environmental stresses—conditions that disrupt metabolic, growth and/or developmental processes of organisms (Lichtenthaler, 1998)—are expected to have influenced biotic turnover during all major Phanerozoic mass extinctions. However, besides the disappearance of certain organism lineages, there are few tangible imprints of environmental stress responses in biota of the fossil record. Increased amounts of spore and pollen malformations are interpreted to be among the few instances of a detectable stress response expressed by plants during both the end-Permian and end-Triassic crises (Visscher et al. 2004; Looy et al. 2005; Foster and Afonin, 2005; van de Schootbrugge and Wignall, 2016). In pollen, these malformations have been observed predominately in saccate forms. These wind-dispersed pollen are comprised of a central body (corpus) and sacci—spongeous, inflated regions of the outermost pollen wall (exine) (Fig. 1). In extant conifers, the sacci primarily function to increase buoyancy of pollen grains, enabling their flotation against gravity through liquid pollination drops exuded by the downward-facing (with respect to gravity) ovules on the seed cone (Salter et al. 2002; Leslie, 2008; 2010), and also may aid in aerial dispersal (Schwendemann et al. 2007).

Saccate pollen are characteristic of several major Paleozoic and Mesozoic seed plant lineages, including conifers, peltasperms, corystosperms, and glossopterids (Clement-Westerhof, 1974; Grauvogel-Stamm, 1978; Millay and Taylor, 1979; Balme, 1995; Lindström et al., 1997). This morphological trait occurs in both prepollen and pollen. Prepollen is characterized by having a proximal aperture and lacking distal features indicative of pollen tube production (Poort et al. 1996). Paleozoic saccate prepollen were usually monosaccate, having one, large saccus (e.g., the late Permian *Nuskosporites*; Poort et al., 1997), although the saccus in several fossil lineages is indented at points, giving the false resemblance of a multisaccate condition (e.g., *Potonieisporites*; Rothwell et al., 2005). Pollen, in contrast, is characterized by having a distal aperture through which a pollen tube emerges and elongates. Saccate pollen are typically bisaccate or trisaccate (having two or three sacci respectively) (Fig. 1).

The saccate morphology first appeared in Late Devonian (383- 372.2 million years ago, Ma) prepollen (Foster and Balme, 1994), diversified in both prepollen and pollen from the Pennsylvanian (323-298 Ma) through the early Mesozoic (Poort et al. 1996; Traverse, 2007) and continue to be widely produced today by ~375 extant species in the conifer families Pinaceae and Podocarpaceae (Leslie, 2010). The bisaccate condition, in which the corpus bears two symmetrical sacci (Fig. 1), first appeared in prepollen (e.g. *Parasporites* Schopf) and pollen (e.g. *Pityosporites* spp. (Seward) Manum) of the Middle to Late Pennsylvanian and became the most abundantly and widely produced form from the early Permian (299-272 Ma) to the present (Kosanke, 1969).

Malformations in the past and present are primarily documented in bisaccate pollen types and include specimens with asymmetrical, reduced, lenticular, fused (confluent, horse-shoe- and/or encircling/ring-like) sacci (Pocknall, 1981; Tretyakova and Noskova, 2004), and/or fewer

or more than two sacci (Wilson, 1965), but also occur as oversized, unseparated and accreted grains (Wilson, 1965; Pocknall, 1981; Foster and Afonin, 2005; Benca et al. 2018; for examples of saccate malformations see Fig. 1). These malformations form during stages of microsporogenesis. Three phases can be distinguished during microsporogenesis namely (1) the microspore mother cell stage, (2) the tetrad stage, and (3) the free spore stage. Normally, the diploid microspore mother cell undergoes two reducing cellular divisions (Meiosis I and II) to produce four haploid microspores in tetrad formation (Blackmore and Crane, 1988). Most malformations in modern saccate pollen-producing conifers are produced in association with meiotic irregularities that occur within microspores prior to or during the tetrad stage (Chira, 1967). For example, unseparated grains (dyads, triads, tetrads) are joined at the polar proximal face of the corpus, preserving their orientation from tetrad configuration. Furthermore, sacci development occurs during meiosis II, when microspores are in the tetrad stage (Ferguson, 1904, Wilson, 1965).

Foster and Afonin (2005) proposed a benchmark of >3% malformations in dispersed fossil and extant pollen yields to indicate environmental stress. However, the observations used to generate this benchmark are difficult to compare as they are drawn from geographically disparate localities lacking environmental controls. These studies also contrast in sampling methods, sample size, and categorizations of malformations (see Foster and Afonin, 2005), and include both members of the Pinaceae and Podocarpaceae. Although saccate pollen of both these conifer lineages is both structurally and functionally similar, and likely ancestral for all extant taxa (Leslie et al. 2015), their microgametophytes are produced by different cellular division patterns (see Sporne, 1965; Fernando et al. 2005). Furthermore, morphological character evolution analyses of saccate pollen in extant and extinct seed plants suggest that the modern saccate pollen morphology may have evolved independently within extant conifer families, as well as in other extinct seed plants (Leslie, 2008).

If members of the Pinaceae and Podocarpaceae—which have been in separate lineages for hundreds of millions of years—develop a similar range of morphological deviations under unstressed, ambient conditions, then malformation expression is more likely to be shared amongst other saccate stem conifers and potentially other extinct seed plant lineages. Also, if pollen yields of both, phylogenetically distant families exhibit low morphological variability under ambient conditions, and high variability under unfavorable conditions, then environmental stress is likely to account for malformations in saccate pollen irrespective of which seed plant group produced them. The purpose of this study is to determine (1) the ratio of phenotypically malformed versus normal pollen in extant members of the Pinaceae and Podocarpaceae grown under ambient, unstressed conditions, and (2) if the range in malformation morphotypes is expressed in a phylogenetically independent manner across and between these lineages. To do this, we conducted a baseline study comparing malformation variability and frequencies in pollen yields from fourteen species representing six genera of the Pinaceae and eight genera of the Podocarpaceae.

## METHODS

### Sample collection

Pollen yields were compared between 14 species representing 14 conifer genera within the Podocarpaceae [8] and Pinaceae [6] (Table 1). Thirteen of these taxa have bisaccate pollen and one has trisaccate pollen (*Dacrycarpus dacrydioides*). Among the bisaccate taxa, two of the species have poorly developed "vestigial" sacci (*Phyllocladus trichomanoides* and *Lagarostrobos franklinii*; Leslie et al. 2015). For each species, five pollen cones were harvested in 2015–2017 from single reproductively mature tree specimens cultivated in lowland (30.8–236 m above sea level) areas of botanical gardens, arboretums, university plantings, and residential zones in the continental United States (Table 2). Pollen cones were collected between 0–2 m above the ground during years in which most trees sampled experienced moderate climatic conditions during microsporogenesis (for details, see Table 3). Twelve out of the fourteen sampled trees were irrigated routinely throughout the year via automated sprinklers or drip irrigation systems. *Cedrus libani* and *Prumnopitys andinus* were not provided supplemental water. While *P. andinus* received sufficient water from rainfall during microsporogenesis, *C. libani* was sampled during a drought year in Berkeley, CA. Additionally, thirteen out of fourteen species were cultivated in open settings while *P. andinus* grew in the understory of a *Pseudotsuga menziesii*-dominated tree stand.

Pollen cones were collected using stainless steel forceps just prior to or after opening (indicated by cone yellowing, expansion and elongation). Each pollen cone was subsequently placed in a plastic 1.7 ml microcentrifuge tube (C2170, Denville Scientific Inc.; Holliston, MA, US) containing a solution of 95% ethanol ($C_2H_6O$; CAS# 64-17-5) to preserve the sample, avoid sample loss, and desiccation-induced grain distortion (Traverse, 2007).

### Sample processing

Microcentrifuge tubes containing individual cones and their dispersed pollen were manually shaken to encourage grain suspension. A disposable soda-lime glass Pasteur pipette and a 3-ml rubber dropper bulb (catalog nos. 13-678-6A and 03-448-26, Fisherbrand) were used to extract and transfer a small subsample of pollen-containing ethanol solution to empty microcentrifuge tubes. The transferred samples were topped with 95% ethanol solution, manually shaken, and centrifuged at 3,800 rpm for 30 s in a microcentrifuge (5415 D, Eppendorf). The ethanol solution was removed using the same pipette, and the tube was filled to 75% volume with 10% potassium hydroxide solution (KOH; CAS #1310-58-3) and placed into wells of a 110-W dry block heater (12621-104, VWR International) set to 131 °C for 6 min. The temperature was measured from the bottom center of wells by a K-type thermocouple sensor probe attached to a liquid crystal display instant-read digital thermometer (HYELEC MS6501). During the KOH treatment, tubes

were removed from wells every 45 s, uncapped to release pressure, manually shaken, and placed back in the well. KOH maceration hydrolyzes cellulose and lyses protoplasts, leaving the exine of pollen grains (that is, the sporopollenin outer layer retained in fossilized palynomorphs) intact but transparent (Traverse, 2007). Following the KOH treatment, the sample tubes were centrifuged, decanted, and filled with 95% ethanol solution. After three further centrifuge/decanting cycles with 95% ethanol solution, two drops of safranin O dye ($C_{20}H_{19}N_4Cl$; CAS #447-73-6) were added, and the tube was topped with 95% ethanol solution, manually shaken, and centrifuged. Eighty-five percent to 90% volume of the dye solution was then decanted via pipette, leaving behind a solution highly concentrated in dyed pollen. One drop of glycerol ($C_3H_8O_3$; CAS #56-81-5) was added and mixed with the sample using a flat toothpick (Diamond, Jarden Corp.).

Sample slides were made using a glass pipette/dropper bulb and transferred to the centers of standard microscope slides on a slide warmer set to 56 °C (XH-2002, Premiere, C&A Scientific Co. Inc.). The subsamples were left on the slide warmer in a fume hood for ~5 min to evaporate residual ethanol. Each sample was gently mixed with one small (diameter, 2 to 3 mm) melted cube of glycerin jelly (7.63% gelatin, 53.4% glycerin, and 0.76% phenol) using a flat toothpick and then enclosed by a 22 mm × 30 mm × 0.16 mm glass cover slip (12-544-A, Fisherbrand). Mounted slides were left for 30 min on the slide warmer (set to 56 °C) to encourage spread of the sample medium under the cover glass. Slides remained in a fume hood at ~22 °C for 2 days after mounting to off-gas residual water and ethanol vapor from under the cover glass. Cover glasses were then sealed by either paraffin embedding or clear nail polish. Five to eight slides were prepared from each pollen cone.

**Sample analysis**

In Excel for Mac (version 16.9), *in silico* simulations (Fig. 2) were used to investigate the effect of pollen subsample size on accurately recognizing background frequencies of pollen malformations (i.e., the chance of each sampled pollen grain exhibiting malformation = 0.02). These simulations showed that subsample sizes exceeding 600 pollen grains do not produce markedly smaller interquartile ranges relative to the increase in effort their analysis requires (Fig. 2). Therefore, 600 pollen grains were morphotyped from each of the 70 sampled cones, yielding a comparison of 3,000 pollen grains per taxon. Pollen grains were morphotyped using a Leica DM2500 microscope fitted with Differential Interference Contrast (to render contrast in transparent pollen) with 20× and 40× Plan Fluor objectives (506503 and 506144, Leica Microsystems Inc.).

Pollen bearing two sacci were counted as phenotypically normal, whereas those having more or less than two sacci and/or fused sacci were scored as malformations (Fig. 1). For each pollen cone sample, the presence of pollen malformation categories were recorded: saccate

malformations: (1) fused sacci [encompassing confluent and horseshoe-shaped sacci], (2) asaccate, (3) unisaccate, (4) trisaccate, and (5) tetrasaccate conditions; unseparated pollen: (1) dyads, (2) triads, and (3) tetrads; and accreted pollen: (1) two accreted pollen, (2) three accreted pollen, and (3) four accreted pollen. Both normal and malformed pollen were tallied using a two key desktop laboratory counter (Clay Adams, Becton, Dickinson and Co.). Additionally, because a single pollen grain can exhibit multiple abnormalities, the occurrence of each malformed trait was scored independently to determine frequency of specific defects within yields. Malformation categories were tallied using a 24-key desktop laboratory counter (Vary Tally, Veeder-Root Inc.). All grains were morphotyped by one individual (J.P.B.) to minimize deviations in protocol.

To limit overlap between malformation categories in individual or joined pollen, only deviations in sacci number and fused sacci were included in this study. While unseparated and accreted pollen were also counted and imaged, they were excluded from most comparisons because they were uncommon in most species studied. Aborted pollen (compacted, often shriveled, grains less than half the size of normal palynomorphs of a species (Saylor and Smith, 1966)) were also excluded from morphological comparisons, as they lack diagnostic features that would be taxonomically assignable in fossil pollen assemblages.

**Imaging**

High-resolution images were taken using the Leica DM2500 microscope using Differential Interference Contrast, a Plan Apo 63× Oil Objective (506187, Leica Microsystems Inc.), and a Nikon Digital Sight DS-Fi1 camera with live feed into a Nikon DS-L2 control unit (Nikon Corp.). Extended depth-of-field images were generated using Adobe Photoshop CS6 (Adobe Systems Inc.). All xx pollen cones (Localities #xxx) and microscope slides (#xx–xx) studied are deposited in the University of California Museum of Paleontology and are available upon request.

**Multivariate analyses**

Multivariate between-species and within-species variation in malformation assemblage type (i.e. counts of various malformation types encountered in 600 pollen studied in each cone) was explored in two ways. First, it was visualized in Canonical Variates Analysis ordination—summarizing the main differences in abnormality assemblage between cones. Second, by calculating pairwise dissimilarity (here: Euclidean distance) between abnormality assemblages of all cones. Both types of analysis were carried out using the statistics software package Past 3.20 (Hammer et al. 2001). In order to reduce a disproportionate influence of rare malformation types in these multivariate analyses, some types were merged (the types used were: Asymmetrical sacci; reduced saccus; enlarged saccus; horseshoe-shaped saccus; no sacci; 1 saccus; 3 sacci; >3

sacci; dyad; >2 pollen clumped; unseparated grains). Only bisaccate-producing taxa were included in the analyses.

The dimension reduction technique CVA is a form of discriminant analysis that examines the structure between multiple, *a priori* defined groups of multivariate data—here 13 species with 5 studied pollen cones each. The multivariate data—here the malformation assemblage of each cone—are ordered and spaced along theoretical axes according to a linear combination of the abundances of all malformation types. The first CVA axis is defined by the linear combination of malformation types that maximizes the separation between the groups (i.e. species); the second axis is the linear combination of malformation types—independent of the first one—that maximizes further species separation; etc.

## RESULTS

Deviations in sacci morphology (fusion, and/or number) represent the most frequently observed form of malformations in most taxa studied, and therefore form the basis of our comparisons. Significant ($p < 0.05$) differences in the total number of malformations occur between Pinaceae and Podocarpaceae ($p = 0.012$), as well as their respective genera ($p = 1.11 \times 10^{-8}$) (Tables 4,5; Fig. 3). Grains with sacci malformations constituted 0 – 2.5 % of total yields in genera within Pinaceae versus 0.2 – 10.9 % in Podocarpaceae. Pollen yields of twelve of the thirteen bisaccate species exhibited < 3% malformations (0 – 2.5 %). A high degree of morphological conservatism was therefore observed in sacci malformation and number, even within two bisaccate genera having vestigial sacci (*Phyllocladus* and *Lagarostrobos*).

Only two members of the Podocarpaceae yielded malformation frequencies of >3%: one bisaccate species, *Nageia nagi* (5.2 – 7.0 % in individual cones, 6.3 % total) and the only trisaccate species studied *Dacrycarpus dacrydioides* (5.2 – 25.5 % in individual cones; 10.9% total). When incorporated into a family-wide comparison, these two outlier genera give Podocarpaceae a substantially higher malformation percentage (~3.0 %, n = 711 of 24,000 grains, 8 genera) than Pinaceae (0.8%, n = 142 of 18,000 grains, 6 genera) (Fig. 3B). In contrast, when *N. nagi* and *D. dacrydioides* are excluded from the Podocarpaceae, the total sacci malformation percentage for the family (1.1 %, n = 195 of 18,000 grains, 6 genera) is similar to Pinaceae.

*Nageia nagi* represents the only geographic outlier to our midlatitudinal sampling on the Pacific coast of the United States (Gainesville, FL, US; 29 °N; Table 2) and displays significantly higher malformation frequency (6.3 %) than all other bisaccate genera (0 – 2.5 %). Although this tree was exposed to higher ambient UV-B regimes than all other taxa studied (Table 3), its heightened malformation frequency could be a stress response to an anomalous below-freezing temperatures (-3.8 °C) experienced during microsporogenesis (Table 3).

Some trees sampled were exposed to seasonal environmental challenges not experienced by the other specimens studied. *Cedrus libani* contrasted from all other taxa sampled in producing its pollen cones during autumn rather than spring and did experience a summer drought in Berkeley, California, US without supplemental irrigation (Table 3). Nevertheless, <3% of pollen yields in this specimen were comprised of malformations. Although many pollen grains produced by this *C. libani* were aborted, all aborted grains were bisaccate and none exhibited morphological deviations apart from being undersized and shriveled.

Although significant differences in saccus malformation percentages per individual cones occur between twelve of the thirteen bisaccate genera (excluding *Nageia nagi*; $p = 0.24 \times 10^{-3}$; Table 6), there is not a substantial difference between the total saccus malformation percentages between these genera (0 – 2.5 %). The significant difference arising from the individual cone comparisons of these bisaccate genera are the result of one outlying cone of *Lagarostrobos franklinii*, which yielded 6% grains with saccus abnormalities, as opposed to 0 – 3.3 % malformations of all other individual bisaccate cones sampled (Fig. 3A). Moreover, there is a significant difference between the malformation frequencies in bisaccate genera (excluding *N. nagi*) and the one trisaccate lineage compared, (*Dacrycarpus dacrydioides*) ($p = 4.74 \times 10^{-13}$; Table 7).

The presence of different malformed pollen sub-categories (fused, asaccate, unisaccate, trisaccate, and tetrasaccate), separated (dyads, triads, and tetrads) and accreted pollen (2, 3, and 4 pollen) were compared between and within cones of each conifer taxon and family. The distribution of abnormal pollen in the different categories varies between genera, however there is no discernable phylogenetic pattern in trait prevalence between genera within the families Pinaceae and Podocarpaceae, both qualitatively, in terms of relative abundance of malformation type (Fig. 4), and quantitatively, in terms of Euclidean distance between malformation assemblages versus the phylogenetic distance between the compared taxa (Fig. 5). The only observed phylogenetic signal, yet unsurprisingly, is that for each taxon the within-species dissimilarities (or rather, within-individual differences even) are mostly smaller than between-species comparisons.

Although the degree of dissimilarity in malformation assemblages does not change consistently with phylogenetic distance, there are some marked differences in malformation assemblage composition between taxa (Fig. 6). In Fig. 6, *Nageia nagi* dominates the 1$^{st}$ CVA axis, not just because of its high incidence of malformations in an absolute sense, but just as much because of a disproportionately high abundance of monosaccate pollen within the malformation assemblage. The latter also distinguishes *Keteleeria evelyniana* from most of the other taxa. A third species with a deviating malformation assemblage is *Cathaya argyrophylla*., with its anomalously high abundance of trisaccate pollen and pollen with asymmetrical sacci. Relatively high numbers of asaccate pollen make *Phyllocladus trichomanoides* stand out, but to a much lesser extent than the other three.

Overall, malformations with saccus deviations comprised 0 – 6.0 % of bisaccate pollen yields per cone, and 0 – 2.5 % of all bisaccate pollen (excluding the potentially cold-stressed *Nageia nagi*). In contrast, saccus deviations represented 5.2 – 25.5% of pollen yields from cones, and 10.9 % total in the only trisaccate species studied, *Dacrycarpus dacrydioides*. Therefore, pollen malformations comprise <3% of pollen in healthy bisaccate pollen-producing trees, >3% in a bisaccate conifer experiencing an environmental stress [anomalously cold temperatures during microsporogensis], and >3% in a healthy trisaccate pollen-producing conifer.

## DISCUSSION

Factors that have been shown to generate pollen malformations include a sharp decrease in temperatures (Christiansen, 1960; Chira, 1967), warming and drying climate (Bazhina et al. 2007a; Noskova et al. 2009), acidified rain, heavy metal, geochemical and photochemical pollution (Rezoni et al. 1990; Mičieta and Murín, 1996; Tretyakova and Noskova, 2004), pathogenic fungal attack/disease (Bazhina et al. 2007a), heightened UV-B radiation (Benca et al. 2018), and nuclear radiation (Sirenko, 2001). Aside from nuclear radiation, these stresses are not limited to anthropogenic activities and therefore could have been experienced by tree populations prior to the industrial revolution. High levels of malformed bisaccate pollen thus could have potential as a biological stress indicator from the Pennsylvanian to the present. Pollen with this morphology are wind dispersed, decay-resistant under anoxic conditions, and deposited in lacustrine, riverine and shallow marine depositional settings (Traverse, 2007). Furthermore, pollen malformations represent an exceptional circumstance in which morphological deviations in fossils can be inferred to result from gene × environmental interactions in the past that result in disruptions to meiosis. For example, Chira, 1967 observed that, in *Pinus edulis* experiencing unseasonably cold temperatures during meiosis, 50% of all pollen malformations observed resulted directly from disruptions to metaphase I and anaphase I, while the other 50% resulted from disruptions to anaphase II and metaphase II. Such morphological signatures could have great potential for assessing environmental stress presence in the distant past because meiosis is among the most vulnerable ontogenetic stages in eukaryotes to perturbations in the external environment (e.g. Bazhina et al. 2007a).

Based on what is known about pollen formation in bisaccate conifers, the observed malformations in our baseline study had their origin either from the spore mother cell or tetrad stage of the microsporogenesis process (e.g., Dickinson and Bell, 1970; Kurmann, 1990). Prior to meiosis, the microspore mother cell isolates itself by secreting a callose wall between its surface coat and plasma membrane (spore mother cell coat; Kurmann, 1990). During the tetrad stage, following meiosis I and II, the microspores secrete a surface wall—a primexine layer comprised solely of early sexine—between the protoplast and enveloping callose wall over the entire grain surface, including regions where future sacci are generated (Dickinson and Bell,

1970). This early microspore surface coat and callose wall together isolate grains from each other while in tetrad arrangement (Blackmore and Crane, 1988; Lugardon, 1995). Dickinson and Bell, (1970) described the formation of sacci in *Pinus banksiana* Lamb., observing that sacci are initiated at the end of the tetrad stage when regionalized spaces develop between the inner primexine (early sexine) and plasma membrane, where polysaccharides released from golgi vesicles accumulate. At the end of the tetrad stage, a nexine wall layer is deposited on the outer face of the plasma membrane, sealing off this space containing accumulated polysaccharides from the microspore protoplast. Following dissolution of the callose wall and separation of the microspores from the tetrad, these accumulated polysaccharides expand considerably, separating the nexine and sexine layers further to form a spongeous hollow saccus. The *P. banksiana* study also shows that sacci appear to be regional modifications of normal exine structure in pollen grains, given that the sexine layer and polysaccharides produced are also produced in lower concentrations throughout the primexine covering the microspore (Dickinson and Bell, 1970).

This study shows that under ambient conditions, pollen malformations, although always present, are infrequently expressed, and their frequencies do not show significant variation between genera in modern bisaccate conifer lineages. Morphological conservatism of bisaccate pollen grains under ambient growth conditions therefore suggests that upticks in their malformation frequencies within fossil (Foster and Afonin, 2005), subfossil and modern assemblages (Wilson, 1965; Pocknall, 1981; Tretyakova and Noskova, 2004; Benca et al. 2018) likely reflect the influence of an environmental challenge on gymnosperm microsporogenesis. For example, the only bisaccate-pollen producing conifer sampled in this study to exceed 3% in overall malformations was *Nageia nagi*, a temperate to subtropical conifer species (Eckenwalder, 2009) that experienced anomalous, below-freezing temperatures in Florida during microsporogenesis. Previous studies have used a benchmark of <3% malformed grains in pollen yields of gymnosperms to infer non-stressed growing conditions (Foster and Afonin, 2005), which is confirmed in this study. We observed <3% pollen malformations in all but two individual cone yields of 12 of the 13 bisaccate pollen-producing genera studied (Fig. 3A).

The assumption that increased frequencies in pollen malformations faithfully record historical and modern environmental stress responses does come with caveats. For example, high morphological plasticity of one of the few remaining conifer lineages producing trisaccate grains (*Dacrycarpus dacrydioides*) indicates that not all saccate pollen (such as trisaccates) are suitable for environmental stress assessments. Additionally, morphological deviations are often diverse and variable within pollen yields of modern conifers regardless of the nature of environmental stress experienced by the tree. Although certain morphological deviations in both fossil and modern pollen walls can be inferred to result directly from certain types of developmental disruptions, traceable to specific stages in meiosis I and II (e.g. Chira, 1967; Bazhina et al. 2007a,b; Noskova et al. 2009), it can be difficult to infer presence of a specific environmental stress using higher frequencies of developmental deviations alone, as they arise from numerous genotype × environmental interactions (Veilleux and Lauer, 1981). However, it is possible to constrain the range of plausible stresses by integrating bisaccate pollen malformation frequencies

with other independent lines of geological evidence, when present. Additional lines of evidence for certain types of past environmental stress may include changes in palynological, paleobotanical and faunal assemblages, pollen wall chemistry, geographic and temporal proximity to point sources of environmental perturbation (e.g. volcanic eruptions), as well as geochemical and geophysical data of associated sediments. Moreover, since this malformation baseline study has shown that differences may exist in the composition of malformation types, it may well be possible that a detailed study the malformation assemblage composition could be used as a tool for narrowing what specific stressor may have caused elevated levels of bisaccate malformations in palynological records.

We determined pollen malformation prevalence in modern conifers on the basis of five cones selected from one specimen of a single species per genus. Of course, there are limitations to conclusions drawn from this sampling structure. First, studying a larger number of cones from each tree sampled would provide greater representation of cone-to-cone variation throughout a tree canopy. Second, more than one specimen sampled per species would provide a greater approximation of intraspecific variability in malformation expression. Third, sampling more than one species per genus would help determine variability within genera compared. Fourth, pollen yields sampled from tree populations in natural ecosystems today would provide a more comparable system to fossil pollen records.

Despite these limitations, we aimed to maximize the phylogenetic scope in comparing malformation expression between different lineages of saccate-pollen producing conifers under ambient environmental conditions. Since most conifers do not produce pollen cones naturally until attaining considerable size, growing most lineages in environmentally-controlled chambers throughout microsporogenesis was not possible nor feasible. Conversely, modern saccate conifer lineages occupy geographically, environmentally, and climatically disparate regions and biomes, which renders comparisons of pollen yields between *in situ* native tree stands unsuitable for baseline comparison. Therefore, only botanical garden and arboretum collections in mild climates could accommodate both boreal and tropical lineages under the same conditions for such a comparison. Given the rarity in cultivation of many southern hemisphere lineages used in this study in northern hemisphere garden holdings, it was not possible to access more than one specimen for several species surveyed, limiting comparisons to one specimen per species in our study. Although a larger number of pollen cones sampled per tree would better approximate intra-canopy variation in malformation frequencies within a single growth season, the number of pollen grains morphotyped per tree and per species would not be feasible to assess due to time constraints without use of machine learning.

The comparison of 600 grains per cone from five cones per tree lineage and one species per genus maximized the phylogenetic extent of our comparison. For this baseline assessment, constraining tree sampling to specimens grown in coastal lowland garden settings within a midlatitudinal range (37–47 °N) (Table 2) minimized variation in solar ultraviolet radiation exposure, as heightened UV-B has been demonstrated to influence malformation frequencies

(Benca et al. 2018). Therefore, this selection of garden-grown trees provided an optimal baseline comparison in which environmental challenges experienced between lineages were minimized—the *Nageia nagi* from Florida being the odd one out in this respect. Furthermore, given that the range of malformations and developmental deviations has been shown to be higher in conifers grown under arboretum conditions than populations in natural ecosystems (e.g. *Abies sibirica* Ledeb; Bazhina et al. 2007b), our results should be viewed as conservative with respect to the rarity of malformations produced by tree populations under ambient conditions in nature.

Differences in morphological plasticity in sacci between bisaccate and trisaccate pollen producing extant conifers may result from contrast in pollen shape and their tetrad configurations during meiosis. For example, pollen grains of bisaccate conifer lineages, such as *Pinus* are bilaterially symmetric, forming in pairs oriented at an angle with respect to each other (0º–90º) during the tetrad stage while those of *Dacrycarpus dacrydioides* are radiosymmetric and form in pairs oriented perpendicularly to each other during the tetrad stage (Huynh, 1968; Huynh and Sampson, 1983). Additionally, changes in sacci arrangement and symmetry (e.g. fusion, asymmetry in size and/or shape) may have less influence on buoyancy and flotation against gravity through micropylar pollination drops in radiosymmetric trisaccate grains than bilaterally symmetric bisaccate grains. Another possibility is that since the bisaccate condition is likely to be ancestral to modern *Dacrycarpus* (Leslie et al. 2015), the plasticity of sacci orientation and shape observed may result from this lineage trending toward a fixed trisaccate character state. Regardless, the observation that a modern seed plant lineage with trisaccate pollen grains displays highly variable sacci morphology should caution against use of similar pollen types in the fossil record for environmental stress assessments.

Deviations in saccate pollen are rare (<3% of pollen yields) in modern bisaccate-pollen-producing conifers grown under ambient growth conditions, but not in trisaccate pollen-producing taxa. Deviations in the morphology of bisaccate pollen types can therefore be used as an indicator for past environmental stresses while trisaccate pollen types are unsuitable for such assessments. Integrating fossilized pollen surveys with isotopic and geochemical proxies could therefore provide a unique opportunity to not only identify perturbations that may have occurred in the distant past, but also confirm they were physically experienced by terrestrial organisms through gene × environmental interactions.

**WORKS CITED**


Balme, B. E. 1995. Fossil in situ spores and pollen grains: an annotated catalogue. Review of Palaeobotany and Palynology, 87: 81–323.

Bazhina, E. V., O. V. Kvitko and E. N. Muratova, 2007a. *Abies sibirica* Ledeb. meiosis during microsporogenesis in disturbed forest ecosystems. Forest Science and Technology 3: 95–100.

Bazhina, E. V., O. V. Kvitko and E. N. Muratova. 2007b. Specific features of meiosis in the Siberian fir (*Abies sibirica* Ledeb.) artificial populations. Russian Journal of Developmental Biology 38: 246–252.

Benca, J. P., I. A. P. Duijnstee and C. V. Looy. 2018. UV-B–induced forest sterility: Implications of ozone shield failure in Earth's largest extinction. Science Advances 4: p.e1700618.

Blackmore, S. and P. R. Crane. 1988. The systematic implications of pollen and spore ontogeny. In: Humphries, C. J. Ed. *Ontogeny and systematics*. Columbia University Press, New York. pp. 83–115.

Chamberlain, C. J. 1935. *Gymnosperms: Structure and evolution*. University Of Chicago Press; Illinois, USA.

Chira, E. 1967. Pollen grains of *Pinus edulis* with more than the haploid number of chromosomes. Silvae Genetica 16: 14–18.

Christiansen, H. 1960. On the effect of low temperature on meiosis and pollen fertility in *Larix decidua* Mill. Silvae Genetica 9: 72–78.

Clement-Westerhof, J. A., 1974. In situ pollen from gymnospermous cones from the Upper Permian of the Italian Alps - A preliminary account. Review of Palaeobotany and Palynology 17: 63–73.

Dickinson, H. G. and P. R. Bell. 1970. The development of the sacci during pollen formation in *Pinus banksiana*. Grana 10: 101–108.

Eckenwalder, J.E. 2009. *Conifers of the World*. Timber, Portland, OR.

Ferguson, M. C. 1904. Contributions to the knowledge of the life history of *Pinus* with special reference to sporogenesis, the development of the gametophytes and fertilization. *In* Proceedings of the Washington Academy of Sciences (Vol. 6, pp. 1-202). Washington Academy of Sciences.

Fernando, D. D., M. D. Lazzaro, and J. N. Owens. 2005. Growth and development of conifer pollen tubes. Sexual Plant Reproduction 18:149–162.

Foster, C. B. and B. E. Balme. 1994. Ultrastructure of *Teichertospora torquata* (Higgs) from the Late Devonian: oldest saccate palynomorph. Ultrastructure of fossil spores and pollen. Royal Botanic Gardens, Kew pp.87–97.

Foster, C. B., and S. A. Afonin. 2005. Abnormal pollen grains: an outcome of deteriorating atmospheric conditions around the Permian-Triassic boundary. Proceedings of the Geological Society of London 162:653–659.

Grauvogel-Stamm, L., 1978. La flore du Grès à *Voltzia* (Buntsandstein súperieur) des Vosges du Nord (France). Morphologie, anatomie, interprétations phylogénique et paléogéographique. Université Louis-Pasteur de Strasbourg Institut de Géologie 50, pp. 1–225.

Hammer, Ø., D. A. T. Harper, and P. D. Ryan. 2001. PAST: Paleontological Statistical software package for education and data analysis. Palaeontologia Electronica 4: 9 pp.

Hirase, S. 1896. Preliminary report on the spermatozoid of *Ginkgo*. Botanical Magazine Tokyo, 10: 325–326.

Huynh, K. L. 1968. Etude de l'arrangement du pollen dans la tétrade chez les Angiospermes sur la base de données cytologiques. Bulletin de la Société Botanique de Suisse 78: 151–179.

Huynh, K. L. and F. B. Sampson. 1983. Tetrad arrangement of the trisaccate pollen of *Dacrycarpus dacrydioides* (Podocarpaceae) and developmental morphology of the triradiate ridge. Grana, 22: 1–9.

Ikeno, S. 1896. Spermatozoid of *Cycas revoluta*. The Botanical Magazine, Tokyo 10: 367–368.

Kosanke, R. M. 1969. Mississippian and Pennsylvanian Palynology. In: Tschudy, R.H. and R. A. Scott. Eds. *Aspects of palynology*. John Wiley & Sons, Inc. New York, NY, US.

Kurmann, M. H. 1990. Exine ontogeny in conifers. In: Blackmore, S. and R. B. Knox, Eds. *Microspores Evolution and Ontogeny: Evolution and Ontogeny*. Academic Press Inc., San Diego, CA.

Leslie, A. B. 2008. Interpreting the function of saccate pollen in ancient conifers and other seed plants. International Journal of Plant Sciences 169:1038–1045.

Leslie, A. B. 2010. Flotation preferentially selects saccate pollen during conifer pollination. New Phytologist 188: 273–279.

Leslie, A. B., J. M. Beaulieu, H. S. Rai, P. R. Crane, M. J. Donoghue and S. Mathews. 2012. Hemisphere-scale differences in conifer evolutionary dynamics. Proceedings of the National Academy of Sciences of the United States of America 109: 16217–16221.

Leslie, A. B., J. M. Beaulieu, P. R. Crane, P. Knopf and M. J. Donoghue. 2015. Integration and macroevolutionary patterns in the pollination biology of conifers. Evolution 69: 1573–1583.

Leslie, A. B., J. M. Beaulieu, G. Holman, C. S. Campbell, W. Mei, L. R. Raubeson and S. Mathews. 2018. An overview of extant conifer evolution from the perspective of the fossil record. American Journal of Botany 105: 1531–1544.

Lichtenthaler, H. K. 1998. The stress concept in plants: an introduction. Annals of the New York Academy of Sciences 851: 187–198.

Lindström, S., S. McLoughlin and A. N. Drinnan. 1997. Intraspecific variation of taeniate bisaccate pollen within Permian glossopterid sporangia, from the Prince Charles Mountains, Antarctica. International Journal of Plant Sciences 158: 673–684.

Looy, C. V., M. E. Collinson, J. H. A. van Konijnenburg-van Cittert, H. Visscher and A. P. R. Brain. 2005. The ultrastructure and botanical affinity of end-Permian spore tetrads. International Journal of Plant Sciences, 166: 875–887.

Lugardon, B., 1995. Exine formation in *Chamaecyparis lawsoniana* (Cupressaceae) and a discussion on pteridophyte exospore and gymnosperm exine ontogeny. Review of Palaeobotany and Palynology 85: 35–51.

Mičieta, K. and G. Murín. 1996. Microspore analysis for genotoxicity of a polluted environment. Environmental and Experimental Botany 36: 21–27.

Millay, M. A. and T. N. Taylor. 1979. Paleozoic seed fern pollen organs. Botanical Review 45, 301–375

Muratova, E. N. 1995. Specific features of meiosis in Scots pine near the northern boundary of its range. Russian Journal of Developmental Biology 26: 128–139.

Noskova, N. E., I. N. Tretyakova and E. N. Muratova. 2009. Microsporogenesis and pollen formation in Scotch pine (*Pinus sylvestris* L.) under modern climatic conditions of Siberia. Biology Bulletin 36: 317–322.

Pocknall, D. T. 1981. Pollen morphology of the New Zealand species of *Dacrydium* Selander, *Podocarpus* L'Heritier, and *Dacrycarpus* Endlicher (Podocarpaceae). New Zealand Journal of Botany 19: 67–95.

Poort, R., J. A. Clement-Westerhof, C. V. Looy, and H. Visscher. 1997. Conifer extinction in Europe at the Permian-Triassic junction: morphology, ultrastructure and geographic-stratigraphic distribution of *Nuskoisporites dulhuntyi* (prepollen of *Ortiseia*, Walchiaceae). Review of Palaeobotany and Palynology 97: 9–39.

Poort, R. J., H. Visscher and D. L. Dilcher. 1996. Zoidogamy in fossil gymnosperms: the centenary of a concept, with special reference to prepollen of late Paleozoic conifers. Proceedings of the National Academy of Sciences 93: 11713–11717.

Renzoni, G. C., L. Viegi, A. Stefani and A. Onnis. 1990. Different *in vitro* germination responses in *Pinus pinea* pollen from two localities with different levels of pollution. Annales Botanici Fennici (pp. 85–90). Finnish Botanical Publishing Board.

Rothwell, G. W., G. Mapes and G. R. Hernandez-Castillo. 2005. *Hanskerpia* gen. nov. and phylogenetic relationships among the most ancient conifers (Voltziales). Taxon 54: 733–750.

Salter, J., B. G. Murray and J. E. Braggins. 2002. Wettable and unsinkable: the hydrodynamics of saccate pollen grains in relation to the pollination mechanism in the two New Zealand 584 species of *Prumnopitys* Phil. (Podocarpaceae). Annals of Botany 89: 133–144.

Saylor, L. C., and B. W. Smith. 1966. Meiotic irregularity in species and interspecific hybrids of *Pinus*. American Journal of Botany 53: 453–468.

Schwendemann A. B., G. Wang, M. L. Mertz, R. T. McWilliams, S. L. Thatcher and J. M. Osborn. 2007. Aerodynamics of saccate pollen and its implications for wind pollination. American Journal of Botany 94: 1371–1381.

Sirenko, E. A. 2001. Palynological data from studies of bottom sediments in water bodies of 30-km Chernobyl Zone. In: *Proceedings of the First International Seminar, Pollen as Indicator of Environmental State and Paleoecological Reconstructions*. VNIGRI, St. Petersburg (pp. 189–190).

Sporne, K. R. 1965. Morphology of gymnosperms; The structure and evolution of primitive seed-plants. Hutchinson & Co. Ltd., London.

Traverse, A. 2007. Paleopalynology. 2nd ed. Springer, Dordrecht.

Tretyakova, I. N. and N. E. Noskova. 2004. Scotch pine pollen under conditions of environmental
stress. Russian Journal of Ecology 35: 20–26.

van de Schootbrugge, B. and P. B. Wignall. 2016. A tale of two extinctions: converging end-Permian and end-Triassic scenarios. Geological Magazine 153: 332–354.

Veilleux, R. E. and F. I. Lauer. 1981. Variation for 2n pollen production in clones of *Solanum phureja* Juz. and Buk. Theoretical and Applied Genetics 59: 95–100.

Visscher, H., C. V. Looy, M. E. Collinson, H. Brinkhaus, J. H. A. van Konijnenburg-van Cittert, W. M. Kürschner and M. Sephton. 2004. Environmental mutagenesis during the end-Permian ecological crisis. Proceedings of the National Academy of Sciences of the United States of America 101: 12952–12956.

Wilson, L. R.1965. Teratological forms in pollen of *Pinus flexilis* James. Journal of Palynology 1: 106–110.

UVMRP, UV irradiance estimator. UV-B Monitoring and Research Program. http://uvb.nrel.colostate.edu/UVB/da_interactiveMapSums.jsf

Zavialova, N. and J. H. A. van Konijnenburg - van Cittert, 2011. Exine ultrastructure of in situ peltasperm pollen from the Rhaetian of Germany and its implications. Review of Palaeobotany and Palynology 168: 7–20.

## CHAPTER 3 TABLES

**Table 1.** *In situ* saccus malformation incidence of taxa within the Podocarpaceae and Pinaceae.

| Species | Family | Total | Abnormal | % Abnormal | Fused sacci | Asaccate | Unisaccate | Trisaccate | Tetrasaccate |
|---|---|---|---|---|---|---|---|---|---|
| *Cathaya argyrophylla* Chun & Kuang | Pinaceae | 3000 | 47 | 1.6 | 8 | 4 | 0 | 29 | 6 |
| *Podocarpus totara* G.Benn. ex D.Don var. *aurea* | Podocarpaceae | 3000 | 18 | 0.6 | 11 | 0 | 0 | 6 | 1 |
| *Phyllocladus trichomanoides* D. Don var. *minor* | Podocarpaceae | 3000 | 44 | 1.5 | 2 | 22 | 12 | 7 | 1 |
| *Pinus parviflora* Siebold & Zucc. var. *pentaphylla* (Mayr) A.Henry | Pinaceae | 3000 | 5 | 0.2 | 0 | 4 | 1 | 0 | 0 |
| *Dacrycarpus dacrydioides* (A.Rich.) de Laub. | Podocarpaceae | 3000 | 327 | 10.9 | 262 | 35 | 0 | 0 | 20 |
| *Keteleeria evelyniana* Mast. | Pinaceae | 3000 | 74 | 2.5 | 62 | 0 | 10 | 2 | 0 |
| *Cedrus libani* A.Rich. | Pinaceae | 3000 | 8 | 0.3 | 7 | 0 | 0 | 1 | 0 |
| *Afrocarpus gracilior* (Pilg.) C.N.Page | Podocarpaceae | 3000 | 42 | 1.4 | 1 | 4 | 36 | 2 | 0 |
| *Manoao colensoi* (Hook.) Molloy | Podocarpaceae | 3000 | 6 | 0.2 | 5 | 1 | 1 | 0 | 0 |
| *Lagarostrobos franklinii* (Hook.f.) Quinn | Podocarpaceae | 3000 | 53 | 1.8 | 0 | 53 | 0 | 0 | 0 |
| *Abies koreana* E.H.Wilson 'Silver Show' | Pinaceae | 3000 | 8 | 0.3 | 0 | 1 | 2 | 5 | 1 |
| *Picea orientalis* (L.) Link 'atrovirens' | Pinaceae | 3000 | 0 | 0.0 | 0 | 0 | 0 | 0 | 0 |
| *Prumnopitys andina* (Poepp. ex Endl.) de Laub. | Podocarpaceae | 3000 | 32 | 1.1 | 23 | 8 | 0 | 1 | 0 |
| *Nageia nagi* (Thunb.) Kuntze | Podocarpaceae | 3000 | 188 | 6.3 | 74 | 46 | 58 | 6 | 1 |

**Table 2.** Locality information of conifer species (Podocarpaceae and Pinaceae) sampled for this study. Location GPS and elevation estimated using satellite image maps in Geoplaner v. 2.8 (http://www.geoplaner.com).

| Species | Family | Specimen | Collection Date | Location | Collector | Degrees Lat. Long. | Elevation (m) |
|---|---|---|---|---|---|---|---|
| *Keteleeria evelyniana* Mast. | Pinaceae | 94.1556 | 8 Apr. 2016 | Berkeley, CA[1] | J. Benca | 37.87447°N -122.23680°E | 237.0 |
| *Dacrycarpus dacrydioides* (A.Rich.) de Laub. | Podocarpaceae | 90.0636 | 8 Apr. 2016 | Berkeley, CA[1] | J. Benca | 37.87355°N -122.23702°E | 235.5 |
| *Pinus parviflora* Siebold & Zucc. var. *pentaphylla* (Mayr) A.Henry | Pinaceae | 88.0146 | 8 Apr. 2016 | Berkeley, CA[1] | J. Benca | 37.87423°N -122.23719°E | 229.1 |
| *Cathaya argyrophylla* Chun & Kuang | Pinaceae | N/A | 11 May 2015 | Boring, OR. | P. Halladin | 45.41331°N -122.35020°E | 191.1 |
| *Cedrus libani* A.Rich. | Pinaceae | N/A | 4 Oct. 2015 | Berkeley, CA[2] | J. Benca | 37.87190°N -122.26208°E | 73.3 |
| *Podocarpus totara* G.Benn. ex D.Don var. *aurea* | Podocarpaceae | 94.1168 | 30 Apr. 2015 | Berkeley, CA[1] | J. Benca | 37.87349°N -122.23695°E | 236.4 |
| *Phyllocladus trichomanoides* D. Don var. *minor* | Podocarpaceae | 61.1598 | 30 Apr. 2015 | Berkeley, CA[1] | J. Benca | 37.87311°N -122.23710°E | 232.8 |
| *Afrocarpus gracilior* (Pilg.) C.N.Page | Podocarpaceae | N/A | 10 Apr. 2017 | Oakland, CA | J. Benca | 37.84122°N, -122.24843°E | 50.3 |
| *Manoao colensoi* (Hook.) Molloy | Podocarpaceae | N/A | 15 Apr. 2017 | Arcata, CA | J. Benca | 40.87466°N, -124.07721°E | 34.4 |
| *Lagarostrobos franklinii* (Hook.f.) Quinn | Podocarpaceae | N/A | 15 Apr. 2017 | Arcata, CA | J. Benca | 40.87476°N, -124.07732°E | 35.7 |
| *Abies koreana* E.H.Wilson 'Silver Show' | Pinaceae | N/A | 15 Apr. 2017 | Boring, OR. | P. Halladin | 45.41266°N, -122.3512°E | 191.5 |
| *Picea orientalis* (L.) Link 'atrovirens' | Pinaceae | N/A | 15 Apr. 2017 | Arcata, CA | J. Benca | 40.87450°N, -124.07757°E | 30.8 |
| *Prumnopitys andina* (Poepp. ex Endl.) de Laub. | Podocarpaceae | N/A | 23 May 2017 | Seattle, WA | K. Possee | 47.65232°N, -122.30719°E | 30.8 |
| *Nageia nagi* (Thunb.) Kuntze | Podocarpaceae | N/A | 12 May 2017 | Gainesville, FL | M. Frank | 29.64627°N, -82.34461°E | 47.9 |

**Table 3.** Temperature, precipitation and estimated biologically effective (BE) UV-B exposure for locality regions during estimated months of pollen cone development.

| Locality | Latitude, Longitude for UV measurement | Pollen collection date | Estimated 90-day pollen developmental window | Highest temperature (°C) | Lowest temperature (°C) | Total precipitation (mm) over developmental window | Average estimated BE UV-B ($kJ\ m^{-2}d^{-1})_{BE}$ |
|---|---|---|---|---|---|---|---|
| Berkeley, CA[1] | 38.089°N, -122.03°E | 30 Apr. 2015 | 30 Jan. – 30 Apr. 2015 | 28.3 | 2.2 | 5.8 | 10.0 |
| | 38.089°N, -122.03°E | 8 Apr. 2016 | 9 Jan. – 8 Apr. 2016 | 27.2 | 2.7 | 427.7 | 10.0 |
| Berkeley, CA[2] | 38.089°N, -122.03°E | 4 Oct. 2015 | 6 Jul. – 4 Oct. 2015 | 37.2 | 10.0 | 4.8 | 26.7 |
| Boring OR* | 45.490°N, -121.87°E | 10 Apr. 2017 | 10 Jan. – 10 Apr. 2017 | 15.6 | -11.1 | 688.8 | 7.3 |
| Arcata, CA** | 40.875°N, -123.69°E | 15 Apr. 2017 | 15 Jan. – 15 Apr. 2017 | 20.0 | -2.1 | 751.3 | 9.3 |
| Oakland, CA*** | 38.089°N, -122.03°E | 10 Apr. 2017 | 10 Jan. – 10 Apr. 2017 | 26.7 | 1.1 | 668.5 | 10.0 |
| Seattle, WA | 47.785°N, -122.16°E | 23 May 2017 | 22 Feb. – 23 May 2017 | 18.9 | -1.6 | 517.7 | 10.3 |
| Gainesville, FL | 29.813°N, -82.07°E | 12 May 2017 | 11 Feb. – 12 May 2017 | 35.0 | -3.8 | 89.7 | 18.3 |

**Table 4.** Pairwise ANOVA comparing sacci malformation frequencies of *in situ* pollen between the conifer families Podocarpaceae and Pinaceae. Significance of family-specific differences in pollen malformation frequencies were tested. Listed are sum of squares (*SS*), degrees of freedom (*df*), mean sum of squares (*MS*), F-statistic (*F*), and p-value. Data consisted of 6 species for Pinaceae and 8 species for Podocarpaceae, 1 tree of each species, 5 cones per tree and 600 pollen grains per cone analyzed for malformations.

| | *df* | *SS* | *MS* | *F* | *p*-value |
|---|---|---|---|---|---|
| Family | 1 | 81.0 | 80.99 | 6.616 | **0.0123*** |
| Residuals | 68 | 832.5 | 12.24 | | |

**Table 5.** Pairwise ANOVA of pollen malformation frequencies of in situ pollen between genera conifer genera within the Podocarpaceae and Pinaceae (trisaccate *Dacrycarpus* included). Significance of genus-specific differences in pollen malformation frequencies were tested. Listed are sum of squares (*SS*), degrees of freedom (*df*), mean sum of squares (*MS*), F-statistic (*F*), and p-value. Data consisted of 14 species, 1 tree of each, 5 cones per tree and 600 pollen grains per cone analyzed for malformations.

| | *df* | *SS* | *MS* | *F* | *p*-value |
|---|---|---|---|---|---|
| All species | 13 | 592.7 | 45.59 | 7.96 | **1.11 e-08*** ** |
| Residuals | 56 | 320.8 | 5.73 | | |

**Table 6.** Pairwise ANOVA comparing sacci malformation frequencies of *in situ* pollen per cone between bisaccate genera within the Podocarpaceae and Pinaceae (excluding *Nageia*). Significance of family-specific differences in pollen malformation frequencies were tested. Listed are sum of squares (*SS*), degrees of freedom (*df*), mean sum of squares (*MS*), F-statistic (*F*), and p-value. Data consisted of 6 species for Pinaceae and 7 species for Podocarpaceae, 1 tree of each species, 5 cones per tree and 600 pollen grains per cone analyzed for malformations.

| | *df* | *SS* | *MS* | *F* | *p*-value |
|---|---|---|---|---|---|
| Bisaccate genera | 11 | 34.82 | 3.165 | 4.218 | **0.224 e-3**** |
| Residuals | 48 | 36.02 | 0.75 | | |

**Table 7.** Results of pairwise ANOVA comparing sacci malformation frequencies of *in situ* pollen per cone between all bisaccate genera within the Podocarpacese and Pinaceae (excluding *Nageia*) and the trisaccate genus *Dacrycarpus*. Significance of family-specific differences in pollen malformation frequencies were tested. Listed are sum of squares (*SS*), degrees of freedom (*df*), mean sum of squares (*MS*), F-statistic (*F*), and p-value. Data consisted of 6 species for Pinaceae and 8 species for Podocarpaceae, 1 tree of each species, 5 cones per tree and 600 pollen grains per cone analyzed for malformations.

| | *df* | *SS* | *MS* | *F* | *p*-value |
|---|---|---|---|---|---|
| Bisaccate vs. trisaccate genera | 1 | 461.3 | 461.3 | 82.42 | **4.74 e-13*** ** |
| Residuals | 63 | 352.6 | 5.6 | | |

## CHAPTER 3 FIGURES

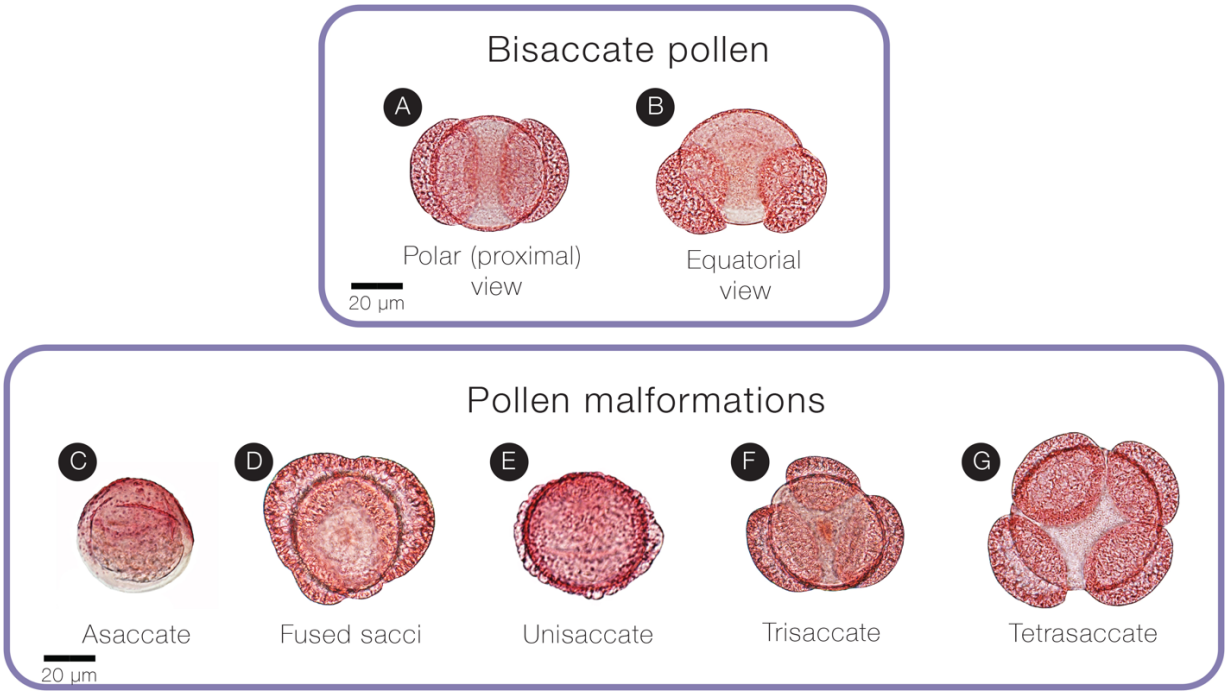


**Figure 1.** Comparison of phenotypical normal bisaccate *Pinus mugo* pollen and observed saccus malformation types in the same species. Specimens photographed from slides of UCMP collection locality number PA134. Grains A, D and F are from Fig. 1 of Benca et al. (2018).

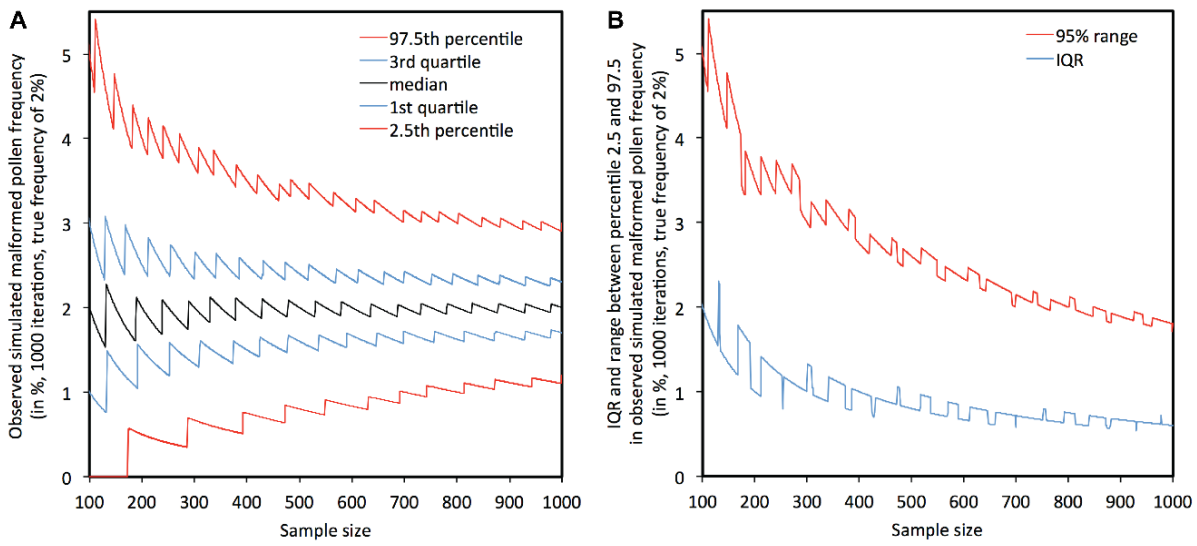


**Figure 2.** Sample size and accuracy of malformed pollen frequency determination. During *in silico* simulations we simulated pollen subsamples of various sizes (100–1000 grains), in which each grain had 2% chance of being malformed. Each of the 901 different sample sizes was replicated 1000 times. (A) Frequency summary of observed malformation frequencies in simulated pollen subsamples. Various percentiles of observed simulated pollen malformation frequencies versus sample size are indicated. (B) Difference between the first and third quartile (interquartile range, or IQR) and between the 2.5th and 97.5th percentile (95% range) versus sample size (from Fig. S3 in chapter 1 of thesis; Benca et al. 2018)

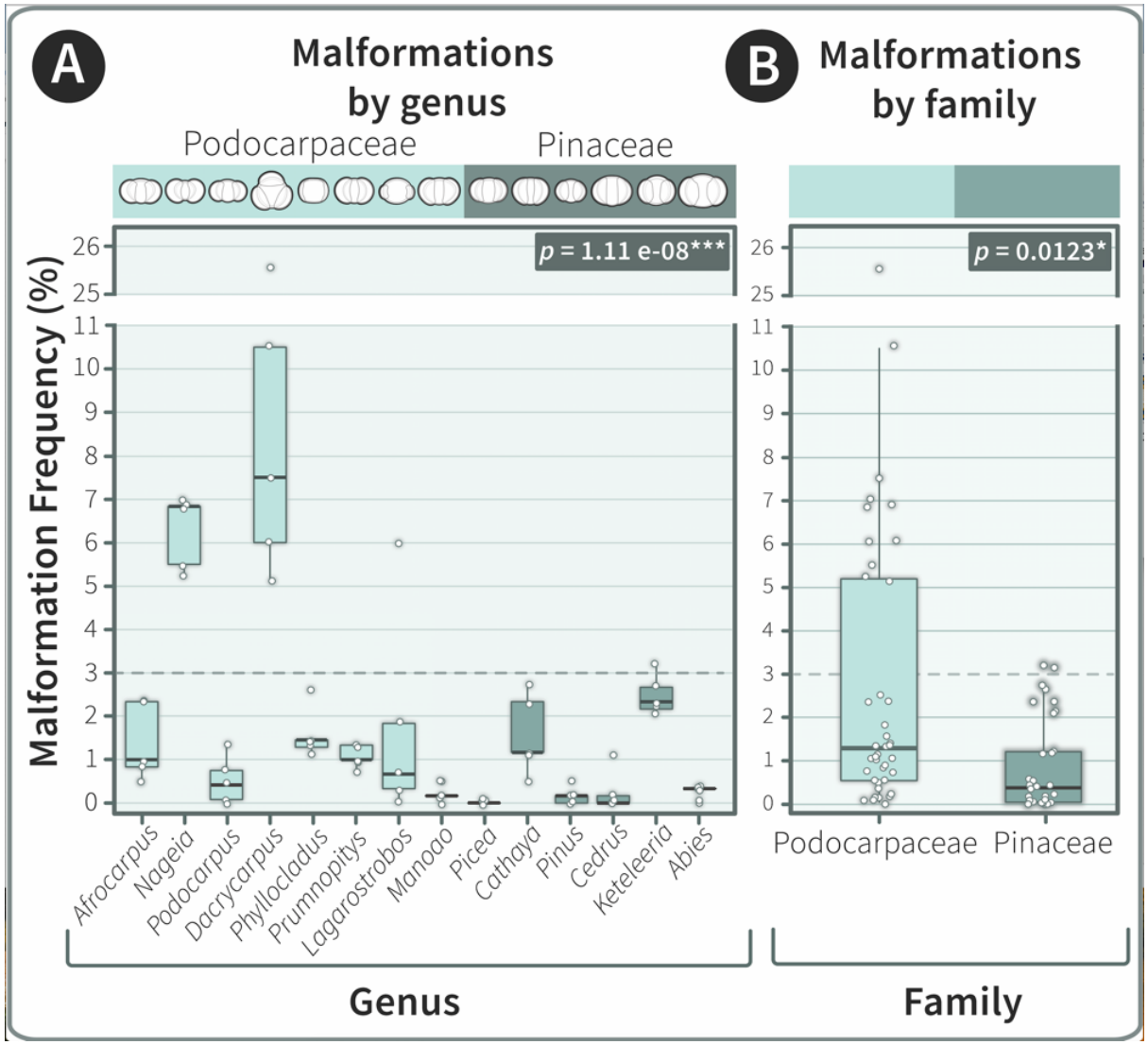


**Figure 3.** *In situ* pollen malformation frequencies in conifer genera Podocarpaceae and Pinaceae by (A) genus, and (B) family. *Y-axis*: Malformation frequency = 100*(no. malformed grains / 600 grains per pollen cone).

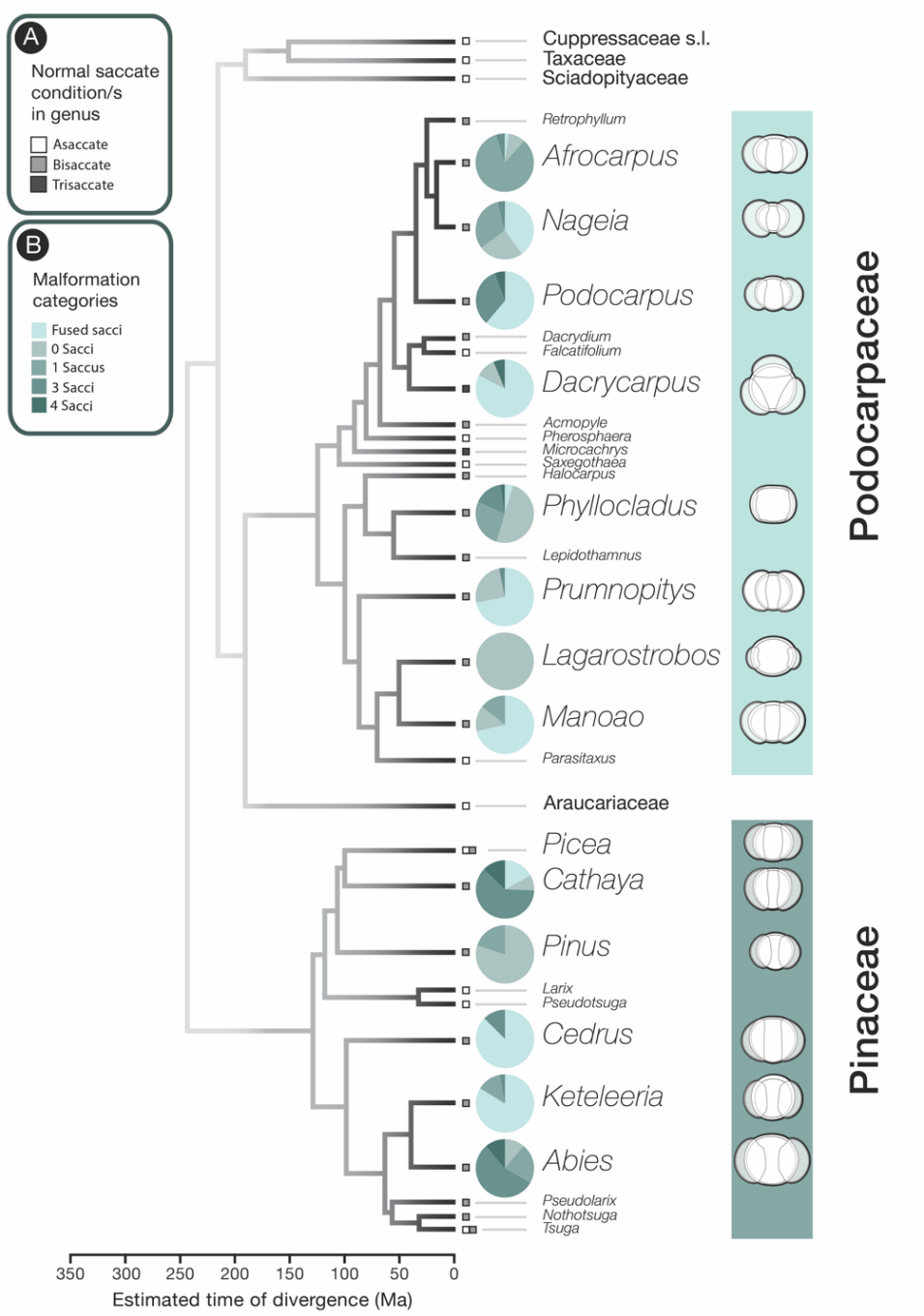


**Figure 4.** Malformation ratios per genus. Extant conifer phylogeny adapted from Leslie et al. (2012). Legend (A) indicates the color of square/s corresponding with normal saccate condition/s in each genus. These squares are indicated to the left of the pie charts and/or genus name. Legend (B) refers to the colors corresponding to specific malformation categories visually represented within the pie charts. Gradient in phylogeny color visually signifies that the conifer phylogeny is in large part generated from molecular techniques influenced heavily by crown

diversity, and that the relationships between these clades in deeper geologic time is less clear (for further discussion, see Leslie et al. 2018).

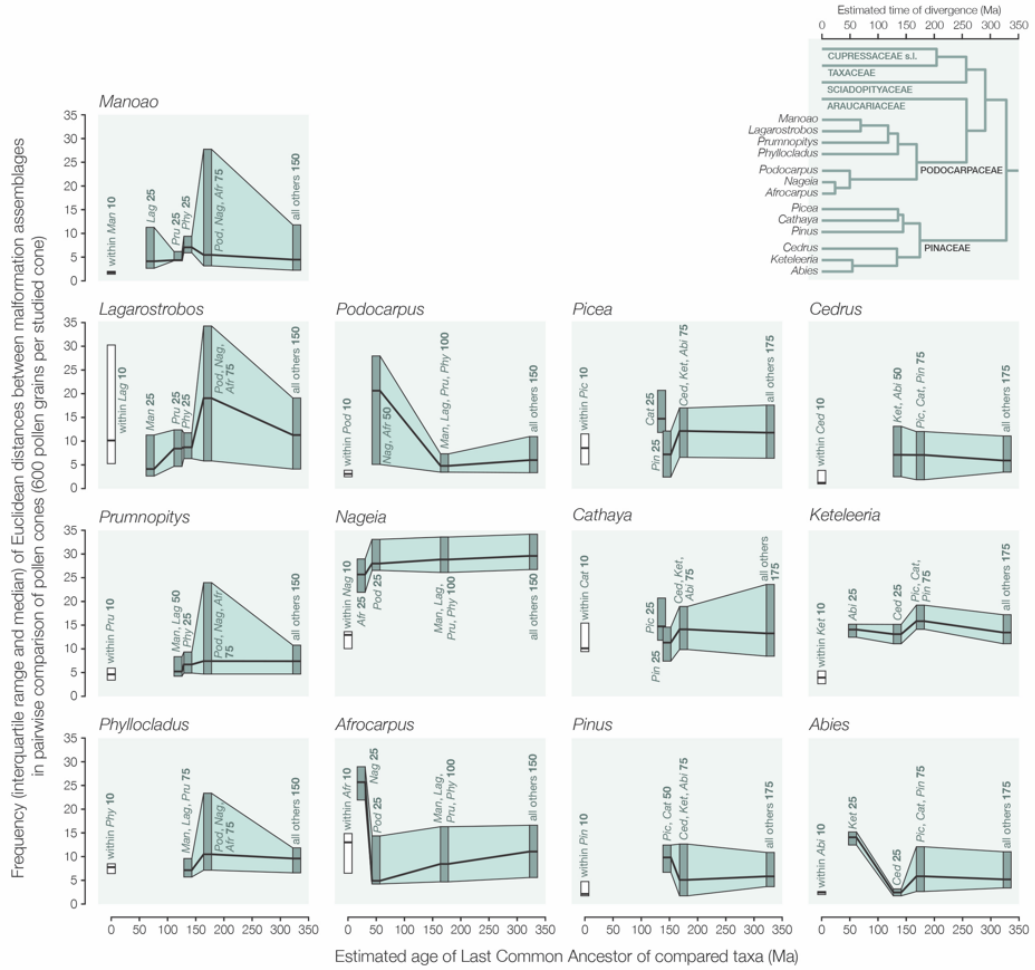


**Figure 5.** Quantified dissimilarity between malformation assemblages (in pairwise comparisons of pollen) versus phylogenetic distance (A-M). Only bisaccate pollen producing species were included. All cones (5 per species) are compared with all other cones, resulting in 10 pairwise comparisons within each species and 1,950 comparisons of cones between taxa. Differences in the types and abundance of malformations are expressed as Euclidean distances. Comparisons are binned based on estimated age of their last common ancestor (0 for within-species comparison), based on the conifer phylogeny by Leslie et al. (2012; see N for a simplified version showing the relation between the genera of the studied species and the extant conifer families), and a distance frequency summary is shown as a box plot for each bin (i.e., interquartile range and median). Bold numbers with each boxplot indicate the number of pairwise comparisons. Trees below A-M show the phylogenetic connection between each species (arrow) and the taxa it is compared with.

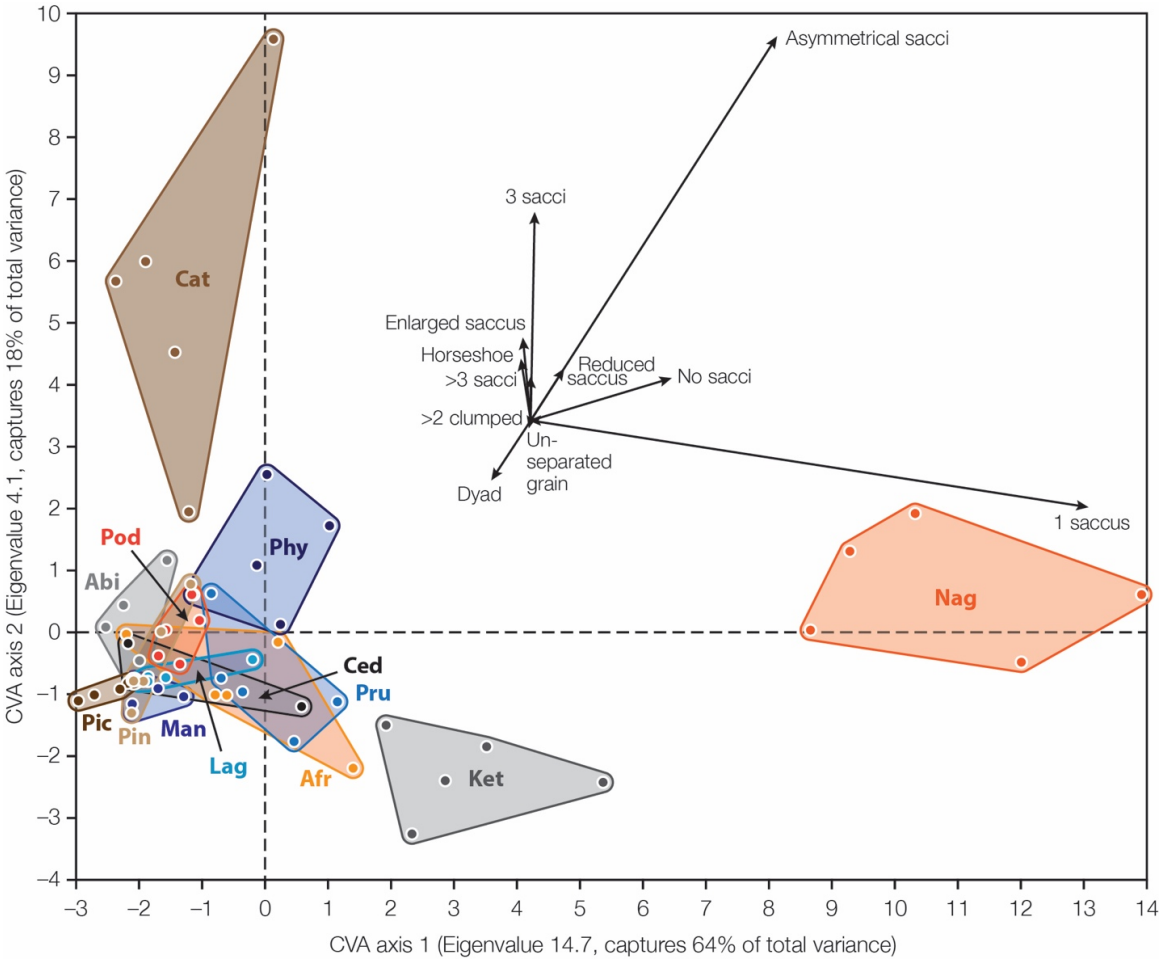


**Figure 6.** Canonical Variates Analysis (CVA) ordination of malformation assemblages. The first two CVA axes capture about 82% of the total variance in malformation assemblage data (i.e. counts of various malformation types encountered in 600 pollen studied in each cone). Only bisaccate-producing taxa were included. Shaded areas indicate convex hulls enveloping data for all 5 cones per species. Note: for clarity, vectors clarifying abnormality type loading on the CVA axes, have been translated away from the origin. Abbreviations: Abi: *Abies koreana*, Afr: *Afrocarpus gracilior*, Cat: *Cathaya argyrophylla*, Ced: *Cedrus libani*, Ket: *Keteleeria evelyniana*, Lag: *Lagarostrobos franklinii*, Man: *Manoao colensoi*, Nag: *Nageia nagi*, Phy: *Phyllocladus trichomanoides*, Pic: *Picea orientalis*, Pin: *Pinus parviflora*, Pod: *Podocarpus totara*, Pru: *Prumnopitys andina*.